Inhibition of Monoamine Oxidase B by substituted coumarin derivatives

BENNIE REPSOLD
(B.Pharm)

Dissertation submitted for the degree Magister Scientiae

in

Pharmaceutical Chemistry

at the

North-West University (Potchefstroom campus).

Supervisor: Prof. S.F. Malan

Co-supervisor: Prof. J.J. Bergh

Assistant Supervisor: Dr. J.P. Petzer

2008

Potchefstroom

This study is dedicated to:

The most admirable person in my life, my dad, Johan Repsold

My dearest, beloved mother, Franci Repsold

My eccentric brother, Johann Repsold

The most unselfish person in the world, Liza van Zyl.

Abstract

Interest in the selective inhibition of monoamine oxidase B (MAO-B) has increased in the last years due to their therapeutic potential in age related neurodegenerative diseases such as Alzheimer's disease and Parkinson's disease. Reversibly inhibiting MAO-B reduces the oxidative deamination of dopamine, increases dopamine levels and, consequently, reduces the production of reactive oxygen species (ROS) which may be the therapeutic intervention that positively affect the tempo and progression of neurodegenerative diseases. Coumarin analogues exhibit a broad spectrum of pharmacological activity, ranging from HIV-1-reverse transcriptase inhibitory properties to competitive, reversible and selective MAO-B and acetylcholinesterase (AChE) inhibition. In this study the stereoelectronic properties of novel coumarin compounds were investigated to optimise a pharmacophore for MAO-B inhibition. This structure was subsequently conjugated to the neuroprotective xanthinyl moieties of caffeine, a specific A_{2A} antagonist and the polycyclic structure, a n-methyl-D-aspartic acid (NMDA) antagonist. Other C-7 substitutents were also considered in this study. These drugs may act via a dual mechanism for the treatment of neurodegenerative disorders.

Coumarin analogues were synthesised *via* etherification, esterification and hydrolysis, and conjugated to the neuroprotective xanthinyl moieties by esterification and amidation using activation chemistry with 1-ethyl-3-(3-dimethylaminopropyl) carbodiimide hydrochloride (EDAC) and N,N-dicyclohexylcarbodiimide (DCC). The final products were obtained as oils or amorphous solids from chromatography and were crystallised from organic solvents. MS and NMR were used to confirm the structures and characterise the compounds.

The synthesised compounds were evaluated *in vitro* as competitive inhibitors of MAO-B, using a spectrophotometric assay that utilised 1-methyl-4-(1-methylpyrrol-2-yl)-1,2,3,6-tetrahydropyridine (MMTP), an analogue of the neurotoxin 1-methyl-4-phenyl-1,2,3,6-tetrahydropyridine (MPTP) as substrate. Baboon liver tissue served as enzyme source. The potency of MAO-B inhibition was expressed as IC_{50} values and the enzyme-inhibitor dissociation constant (K_i value).

Molecular modelling studies were carried out with the published MAO-B crystal structure (PDB: 1oj9) and the proposed inhibitors were prepared in a DS Viewer window using the 'Prepare Ligands' module of Discovery Studios 1.7®. Docking was performed in the 'Dock Ligands'

module (Ligandfit) with minimisation set as smart minimiser. The docking poses were scored with Ligandfit 2 and the consensus Dock Score.

From the molecular modelling studies, it was clear that the inhibitors occupy the entrance and substrate cavities of MAO-B, presenting the coumarin nucleus inside the substrate cavity. *In vitro* MAO-B inhibition assays established that the 7-substituted coumarin derivatives display MAO-B inhibitory properties with K_i values in the low micromolar range. The most potent inhibitor among the analogues was the 4-methyl-2-oxo-2H-chromen-7-yl-(2E)-3-phenylacrylate (BPR 4) while the least potent inhibitor was found to be 3-{4-aza-8-oxoheptacyclo[0.4.1.$0^{2,10}$.$0^{3,14}$.$0^{4,9}$.$0^{9,13}$.$0^{12,15}$] tetradecyl} - [(4'-methyl-2'-oxo-2*H*-chromen-7'-yl)oxy] acetate (BPR 6).

The results of an SAR study established that the potency of MAO-B inhibition by the coumarin derivatives examined is dependent on chain length, lipohilicity, planarity and steric bulk of the substituents on position 7 of the coumarin. These results may be of relevance to diminish or delay the incidence and perhaps the progression of debilitating neurodegenerative diseases.

Opsomming

Belangstelling in die selektiewe remming van monoamienoksidase B (MAO B) het die afgelope aantal jaar toegeneem vanweë hulle terapeutiese potensiaal vir neurodegeneratiewe siektes as gevolg van ouderdom soos Alzheimer en Parkinson se siektes. Omkeerbare remming van MAO-B verminder oksidatiewe deaminering van dopamien, verhoog dopamienvlakke en verminder gevolglik die vorming van reaktiewe suurstofspesies (RSS) wat die terapeutiese intervensie kan wees wat die tempo en vordering van neurodegeneratiewe siektes positief beïnvloed. Kumarienanaloë vertoon 'n breë spektrum farmakologiese aktiwiteit wat van remming van MIV-1-omgekeerde transkriptase tot kompetitiewe, omkeerbare en selektiewe inhibisie van MAO-B en asetielcholienesterase (AChE) strek. In hierdie studie is die stereo-elektroniese eienskappe van nuwe kumariene ondersoek om die farmakofoor vir remming van MAO-B te optimaliseer. Hierdie struktuur is gevolglik met neurobeskermende xantinielgroepe van kaffeïen, 'n spesifieke A_{2A}-antagonis, en die polisikliese struktuur, 'n NMDA-antagonis, gekonjugeer. Ander substituente aan C-7 is ook tydens hierdie studie oorweeg. Hierdie middels kan met 'n dubbele meganisme vir die behandeling van neurodegeneratiewe versteurings werk.

Kumarienanaloë is deur veretering, verestering en hidrolise gesintetiseer en met behulp van aktiveringschemie met 1-etiel-3-(3-dimetielaminopropiel)karbodiimiedhidrochloried (EDAK) en N,N-disikloheksielkarbodiimied (DSK) met die neurobeskermende xantinielgroepe gekonjugeer. Die finale produkte is na chromatografie as olies of amorfe vaste stowwe verkry en is uit organiese oplosmiddels gekristalliseer. MS en KMR is gebruik om die strukture te bevestig en die verbindings te karakteriseer.

Die gesintetiseerde verbindings is *in vitro* as kompetitiewe remmers van MAO-B beoordeel deur 'n spektrofotometriese bepaling met 1-metiel-4-(1-metielpirrool-2-iel)-1,2,3,6-tetrahidropiridien (MMTP), 'n analoog van die neurotoksien 1-metiel-4-feniel-1,2,3,6-tetrahidropiridien (MPTP), as substraat te gebruik. Bobbejaanlewer het as bron van die ensiem gedien. Die sterkte van MAO-B-remming is as die IC_{50}-waardes en die dissosiasiekonstante (K_i-waarde) van die ensiem-remmerkompleks uitgedruk.

Molekulêre modellering is met die gepubliseerde kristalstruktuur van MAO-B (PDB: 1oj9) gedoen en die voorgestelde remmers is met die 'Prepare Ligands'-module van Discovery Studios 1.7® in 'n DS Viewer-venster berei. Passing is met die 'Dock Ligands'-module

(Ligandfit) gedoen met minimisering op "smart minimiser" gestel. Tellings vir die passings is met 'Ligandfit 2' en die 'consensus Dock Score' verkry.

Uit die molekulêre modellering is dit duidelik dat die remmers die ingang en holte vir die substraat van die MAO-B ensiem beset met die kumarienkern in die substraatholte. Bepalings van *in vitro*-inhibisie van MAO-B het getoon dat die 7-gesubstitueerde kumarienderivate remming van MAO-B vertoon met K_i-waardes in die mikromolêre gebied. Van die analoë was die **4**-metiel-2-okso-2H-chromeen-7-iel-(2E)-3-fenielakrilaat (BPR **4**) die kragtigste remmer terwyl 3-{4-asa-8-oksoheptasiklo[0.4.1.$0^{2,10}$.$0^{3,14}$.$0^{4,9}$.$0^{9,13}$.$0^{12,15}$]tetradesiel}-[(4'-metiel-2'-okso-2*H*-chromeen-7'-iel)oksi-asetaat (BPR 6) die swakste was.

Die resultate van 'n SAV-studie het getoon dat die sterkte van MAO-B-remming van die bestudeerde kumarienderivate van die kettinglengte, lipofilisiteit, planariteit en steriese grootte van die substituente in posisie 7 van die kumarien afhang. Hierdie resultate kan van belang wees om die voorkoms en moontlik die vordering van stremmende neurodegeneratiewe siektes te verlaag of te vertraag.

Acknowledgements

First and foremost, I thank God for giving me the opportunity, talent and perseverance to overcome the obstacles during this study and to be able to do what I love. Without Him nothing is possible.

To my study leader and mentor, Prof. Sarel Malan, my greatest appreciation for your guidance and support during this study, and for sharing your valuable knowledge with me. Thank you for all your patience with me.

To my study co-leader, Dr. Jacques Petzer. If everybody has your knowledge and personality, we would be in heaven. Thank you for all your input.

To Prof. Jaco Breytenbach, Dr. D and Lesetja for your support and insights.

To Nellie Scheepers, for your assistance inside and outside the laboratory.

To all my colleagues in the pharmaceutical chemistry department for your friendship and patience. It was a pleasure working with you.

To my lab partners, Ingrid and Jane, thank you for all the humour, 'chats' and lively atmosphere.

To my dearest friend S.G. van Rooy for the motivation. Keep on making that millions!

To my close friends, Jacques, Benno, Gerhard, Dries and Nico – we live life. Thanks for all the socialising

To all my engineering friends, MD, Stef, finish the reactor, you're smart enough.

To my uncle, Leon Repsold, for his logistical support during the annual congress.

To André Joubert and Johan Jordaan for all the structure identifications.

To the National Research Foundation (NRF) for funding.

Table of contents

List of figures

List of tables

Chapter 1 Introduction, aims and objectives

1.1 INTRODUCTION

The most frequent occuring neurodegenerative disorders and cause of disability among western societies are Alzheimer's disease (AD) and Parkinson's disease (PD) (Nussbaum & Ellis, 2003; Janca, 2004). Considering the fact that human life expectancy is increasing (because of better healthcare), and that most neurodegenerative incidents appear at a late age (50-60 years), it is likely that the incidence of PD and AD will increase significantly (Speciale, 2002) over the next years.

1.2 NEURODEGENERATIVE DISORDERS

It has become increasingly clear that the major basic processes involved in neurodegeneration are multifactorial in nature, caused by genetic and environmental endogenous factors (Cavalli, 2007). The neurodegenerative disorders sharing these multifactorial pathogenetic mechanisms are Alzheimer's disease (AD), Parkinson's disease (PD), Huntington's disease (HD) and amyotrophical lateral schlerosis (ALS) - with AD and PD the subject of this study.

Although each disease has its own molecular mechanisms and clinical manifestations, some general pathways can be recognised. They include protein misfolding and aggregation, oxidative stress and free radical formation, metal dyshomeostasis, mitochondrial dysfunction and phosphorylation impairment (Fig. 1.1), all occurring concurrently (Jellinger, 2003).

There is substantial evidence of morphological, biochemical and molecular adnormalities in the mitochondria of various tissues affected by neurodegeneration (Coppede *et al.*, 2006). Moreover, an impressive number of disease-specific proteins that interact with the mitochondria, like the amyloid precursor protein (APP), amyloid beta (Aβ), presenillin in Alzheimer's disease and; α-synuclein, parkin, parkinson disease autosomal recessive early onset 7 (PARK7/DJ-1), PTEN induced putative kinase 1 (PINK1), HtrA serine peptidase 2 (HTRA2) in Parkinson's disease, have recently been described (Lin & Beal, 2006).

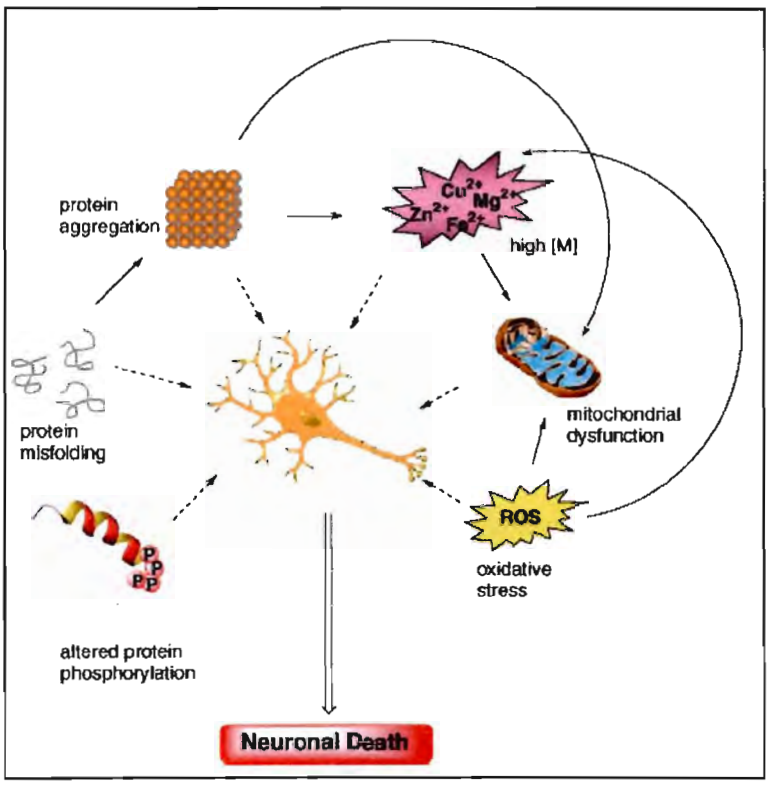

Figure 1.1: Schematic pathways of the multifactorial events leading to neuronal death. General mechanisms, such as protein misfolding and aggregation, oxidative stress, metal (M) dyshomeostasis, mitochondrial dysfunction and altered protein phosphorylation (Cavalli *et al.*, 2007).

Amyloid-β (Aβ) and α-synuclein have been reported to permeabilise both cell and mitochondrial membranes (Caughey & Lansbury, 2003; Kagan *et al.*, 2002). They are, therefore, responsible for membrane depolarisation, calcium dysregulation and impairment of mitochondrial functions (Lin & Beal., 2006).

1.2.1 Alzheimer's Disease (AD)

AD is characterised by progressive loss of cognitive function, short-term memory impairment and gradual loss of judgement and visuospatial skills (Pardo & van Duijn, 2005). Approximately 1% of people aged 65-69 years, up to nearly 30% at the age of 95 years, and a small proportion before the age of 65 (presenile or early onset AD) are at risk (Rocca *et al.*, 1991).

The underlying pathology includes the presence of extra-cellular senile plaques (where amyloid-β protein is the main constituent), neurofibrillary tangles and neuronal loss (Braak & Braak, 1991), which occurs in the cortex and the hippocampus – regions associated with memory and cognition (Braak *et al.*, 1999). Epidemiological and molecular studies suggest multiple etiologies. Genetic mutations in three known genes, the amyloid precursor protein

(APP) and presenilin (PS) 1 and 2 genes (Cruts & van Broeckhoven, 1998; Steele, 2000), and apolipoprotein E (APO E) have been described (Saunders, 2000). Environmental factors, such as aluminium, that promote the formation and accumulation of insoluble amyloid-beta (Aβ) and hyperphosphorylated tau, have also been indicated to play a role (Yokel, 2000).

Currently, acetyl cholinesterase (AChE) inhibitors are the only drugs approved for treatment of cognitive dysfunction in AD. Acetyl choline-enhancing drugs can however, compensate for only part of the neuronal dysfunction in AD. The enhancement of cognition produced by acetyl cholinesterase inhibitors are also transient (Bliss & Collingridge, 1993) and these drugs do not prevent the progressive loss of neurons in AD. No curative treatment is presently available, and cholinesterase inhibitors are implemented for symptomatic relief only (Doody, 1999).

Drugs moving into clinical trials that may modify the progression of AD are anti-inflammatory agents, antioxidants, estrogen, antagonists of APO E4, inhibitors of amyloid-ß production and aggregation and MAO-B inhibitors (Cutler, 2001; Doraiswamy, 2002; Marx, 1996).

1.2.2 Parkinson's Disease (PD)

PD's clinical manifestations are characterised by bradykinesia (akinesia and hypokinesia included), muscle rigidity, tremor, postural abnormalities and freezing phenoma (Nomoto, 2003). It can be caused by genetic aberration and/or environmental toxins (eg. herbicides), which is followed by a sequence of events culminating in the destruction of the dopaminergic neurons of the substantia nigra pars compacta (SNpc) and reductions in their termini within the dorsal striatum and subcortical regions (Hornykiewicz & Kish, 1987; Speciale, 2002). Contributing environmental factors include oxidative stress, mitochondrial dysfunction (Schapira *et al.*, 1993; Mizuno *et al.*, 1994), excitotoxicity with excess nitric oxide formation and glial and inflammatory processes which lead to apoptosis (Matthews *et al.*, 1997; Hunot & Brugg, 1997). The SNpc is not the sole site of neuronal damage and the locus coeruleus, raphe nuclei and the nucleus basalis of Meynert could also be affected (Fahn, 2000).

Dopamine (DA) replacement therapy with levodopa (L-Dopa) in conjunction with systemic decarboxylase inhibitors eg. benserazide and carbidopa (Agid *et al.*, 1999) and/or with reversible and selective catechol-O-methyltransferase (COMT) inhibitors (eg. entercapone and tolcapone) or selective, irreversible MAO-B inhibitors (eg. deprenyl) are the present first-line treatment regime of (Fig. 1.2) Parkinson's disease (Drukarch & van Muiswinkel, 2000).

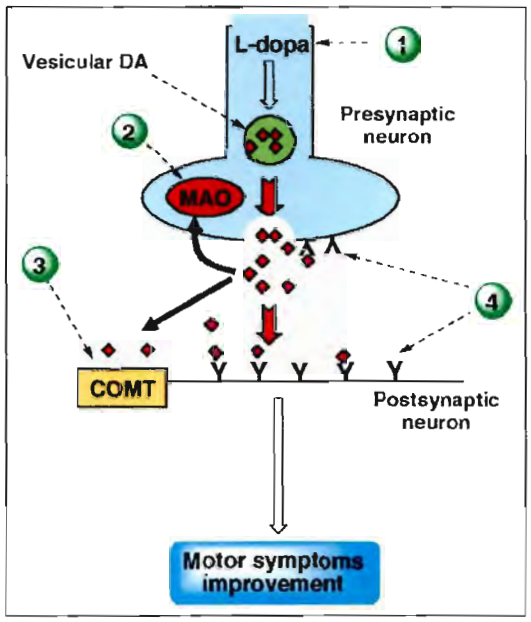

Figure 1.2: Mechanism of action of DA at a dopaminergic synapse. Currently available anti-PD drugs act at points **1-4** as indicated in the picture. L-Dopa (**1**), is presently the main drug used for treatment. The others are MAO (**2**) and COMT (**3**) inhibition as well as dopaminergic receptor agonists (**4**).

1.3 MAO-B INHIBITION

Interest in the selective inhibitors of monoamine oxidase B (MAO-B) has increased in recent years due to their therapeutic potential in age-related neurodegenerative diseases such as Alzheimer's disease and Parkinson's disease. Reversibly inhibiting MAO-B reduces the catalysed oxidative deamination of dopamine, increases dopamine levels and consequently, reduces the production of reactive oxygen species (ROS). This may be the therapeutic intervention that positively affect the tempo and progression of neurodegenerative diseases.

1.4 STRUCTURES OF IMPORTANCE IN THIS STUDY

The one-molecule, one target paradigm has led to the discovery of many successful drugs and ligands endowed with outstanding *in vitro* selectivity. Diseases with a multifactorial nature (eg. neurodegenerative disorders) can however, often find ways to compensate for a protein whose activity is affected by a drug, by taking advantage of the redundancy of the system, ie., the existence of parallel pathways (Frantz, 2005; Mencher & Wang, 2005). Therefore, drugs hitting a single target may be inadequate for treatment of neurodegenerative syndromes, which involves multiple pathogenic factors (Bishop & Sham, 2000). A new strategy is emerging on the

basis of the assumption that a single compound, having multiple biological properties, may be able to hit multiple targets. These molecules are defined as MTDLs (multi-target-directed ligands) and are effective in treating complex diseases because of their ability to interact with the multiple targets thought to be responsible for the disease pathogenesis. (Morphy *et al.*, 2004; Morphy & Rankovic, 2005; Morphy & Rankovic, 2007). The risk of possible drug-drug interactions would be avoided and this approach might lead to a new treatment regime. The compounds illustrated in figure 1.3 served as a favourable basis for a MTDL approach in this study.

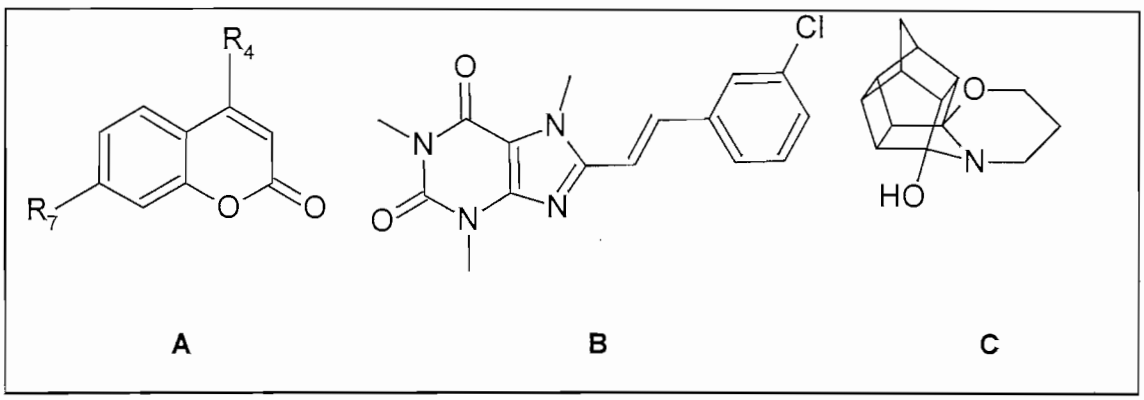

Figure 1.3: Structures of importance in this study. (**A**) coumarin (**B**) (E)-8-(3-chlorostyryl)caffeine (**C**) 3-hydroxy-4-aza-8-oxaheptatetradecane

Coumarins exhibit a broad spectrum of pharmacological activity, ranging from HIV-1-reverse transcriptase inhibitory properties (Naser-Hijazi *et al.*, 1994; Murray *et al.*, 1982; Wenkert & Buckwalter 1972) to competitive, reversible and selective MAO-B and AChE inhibition (Novaroli *et al.*, 2006).

Structure activity relationship (SAR) studies revealed that substitution in position 7 of the coumarin [Fig. 1.3 (**A**)] resulted in high inhibitor activity towards the MAO enzyme (Novaroli *et al.*, 2006), while A/B selectivity are modulated through substitution at position 3 and/or 4 (Gnerre *et al.*, 2000).

A_{2A} antagonists are currently being investigated as possible therapeutic agents for the symptomatic treatment of motor deficits in PD. (E)-8-(3-Chlorostyryl)caffeine [Fig. 1.3 (**B**)] was recently reported to be a potent and selective competitive MAO-B inhibitor (Petzer *et al.*, 2003) and an antagonist of adenosine A_{2A} receptors (Suzuki *et al.*, 1993).

The 3-hydroxy-4-aza-8-oxaheptatetradecane [Fig. 1.3 (**C**)] is thought to possess pharmacokinetic and pharmacological characteristics that may find application in the treatment of neurodegenerative diseases such as blood-brain barrier permeability and antagonism of the NMDA receptor. The latter prevents cytoplasmic Ca^{2+} influx and eventually neuronal cell death.

Conjugation with the polycyclic structure may improve the pharmacokinetic and pharmacodynamic properties of current drugs (Geldenhuys *et al.*, 2005; Randall & Thayer, 1992).

It was reported that AChE might induce Aβ aggregation through the direct interaction of its peripheral anionic site (PAS) with fibrils of the peptide (Alvarez *et al.*, 1995). Ligands having affinity for both the AChE catalytic site and PAS as well as M_2 receptors would potentiate the remaining cholinergic transmission in affected brain regions while antagonising the M_2 autoreceptor would facilitate the release of acetylcholine (ACh), thus preventing ACh breakdown and AChE mediated Aβ fibrils formation (Melchiorre *et al.*, 1998; Melchiorre *et al.*, 2003). AP 2238 (Fig. 1.4) is one such compound that showed evidence of suppressing Aβ aggregation (Piazzi *et al.*, 2003).

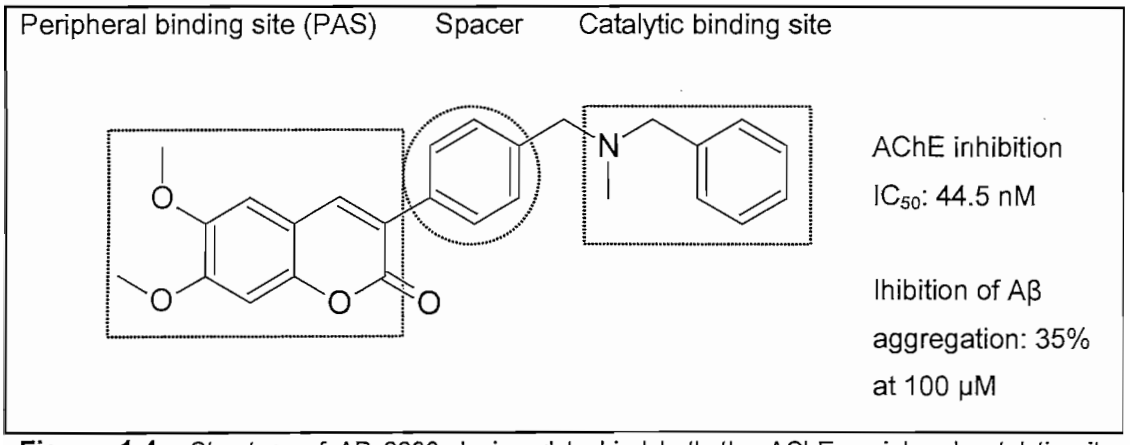

Figure 1.4: Structure of AP 2238 designed to bind both the AChE peripheral catalytic site (green dashed line) and the catalytic binding site (blue dashed line) in order to counteract AChE induced Aβ aggregation as well as increasing ACh content.

Incorporating the coumarin moiety will be the approach of choice for the development of a MTDL to (1) prevent ROS generation through MAO-B inhibition and possibly to (2) counteract Aβ aggregation via AChE inhibition.

1.4.1 Proposed Compounds

In the current study a series of 7-substituted coumarin derivatives (Fig. 1.5) were synthesised, evaluated for MAO-B inhibition and subjected to molecular modelling studies. Compounds **1-3** represent the optimisation of the pharmacophore while compounds **4-6** represents the conjugation of the neuroprotective entities.

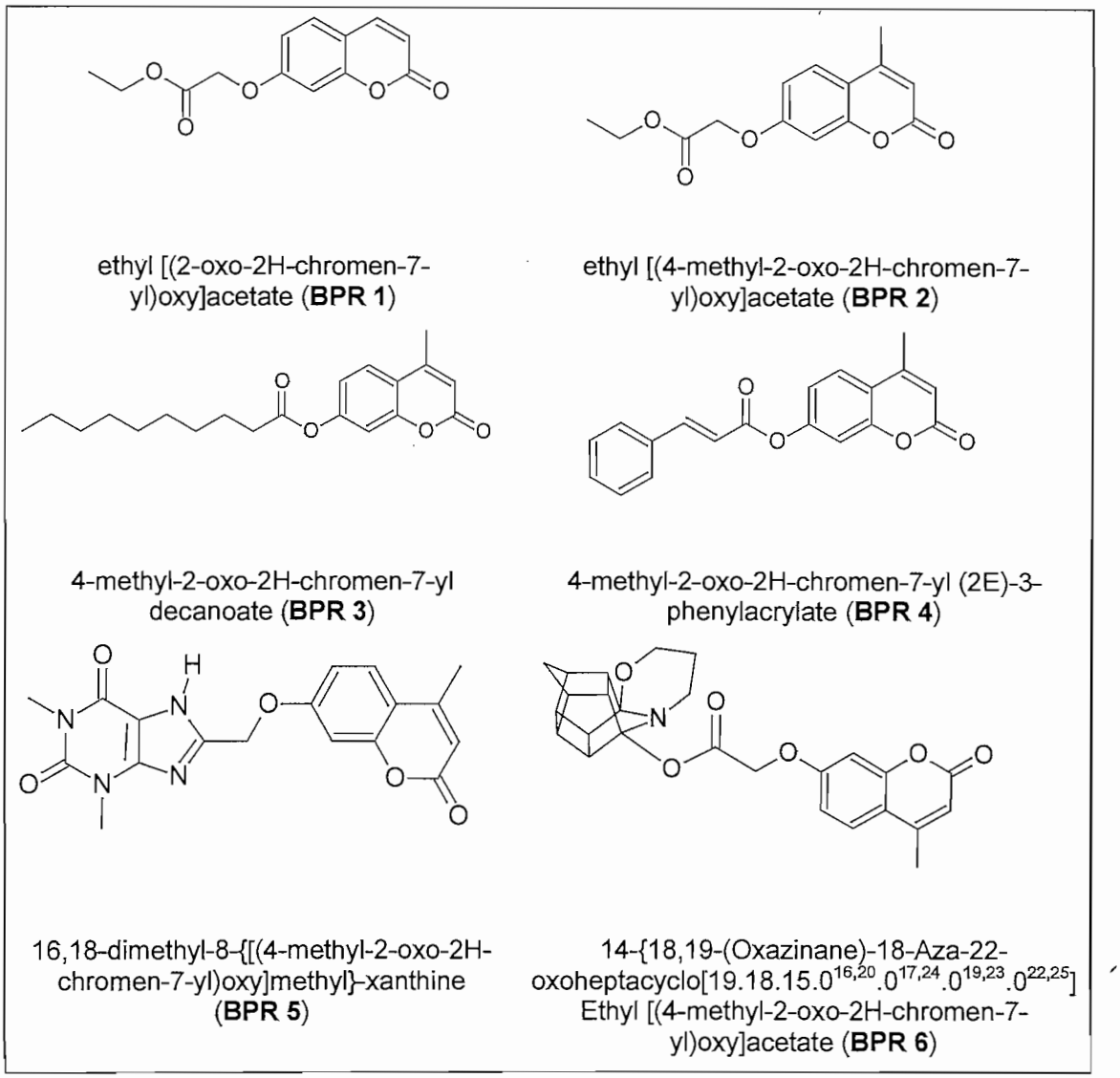

Figure 1.5: The selection of compounds for this study.

1.5 BIOLOGICAL EVALUATION

The synthesised compounds were evaluated *in vitro* as competitive inhibitors of MAO-B using a spectrophotometric assay that utilises MMTP 1-methyl-4-(1-methylpyrrol-2-yl)-1,2,3,6-tetrahydropyridine, an analogue of the neurotoxin MPTP as substrate. The effect of the test inhibitors on the rate of the MAO-B catalysed oxidation of MMTP to the corresponding dihydropyridinium ($MMDP^+$) metabolite was evaluated (Nimkar *et al.*, 1996; Inoue *et al.*, 1999) and expressed as IC_{50} values and the enzyme-inhibitor dissociation constant (K_i values). As enzyme source, the mitochondrial fractions obtained from baboon liver tissue was utilised since it is reported to be devoid of MAO-A activity while exhibiting a high degree of MAO-B catalytic activity. Therefore, even though MMTP is a MAO-A/B mixed substrate, its oxidation by baboon

liver mitochondria can be exclusively attributed to the action of the MAO-B isoform (Inoue *et al.*, 1999).

1.6 MOLECULAR MODELLING

Molecular modelling covers a wide range of molecular graphics and computational chemistry techniques used to build, display, manipulate, simulate and analyse molecular structures. The recent publication of the human MAO-B crystal structure permits modelling and docking of substrates and inhibitors into the active site of the enzyme (Binda *et al.*, 2003). Docking is a useful tool to determine the possibility of a theoretical ligand to bind to a receptor or enzyme and is extensively utilised to determine the properties necessary for high potency. Good correlations between the calculated and experimental inhibition constants (K_i) values were obtained in previous MAO-B studies (Toprakçí & Yelekçi, 2005).

Molecular modelling studies were carried out with the published (www.pdb.org) MAO-B crystal structure (PDB: 1oj9) and the proposed inhibitors were docked with the Ligandfit module of Discovery Studio 1.7® to identify the size and functional groups for optimum binding to the catalytic site of MAO-B.

1.7 AIMS AND OBJECTIVES

The aim of the study was to design and synthesise drugs that act via a dual mechanism for the treatment of neurodegenerative disorders and to serve as models in the manipulation and development of new, potent, selective reversible inhibitors of MAO-B.

This structure was subsequently conjugated to the known neuroprotective xanthinyl moieties, a specific A_{2A} antagonist and the polycyclic tetradecane, a NMDA antagonist. From the molecular modelling studies, it was clear that the inhibitors would occupy both the entrance and substrate cavities, presenting the coumarin nucleus inside the substrate cavity of MAO-B.

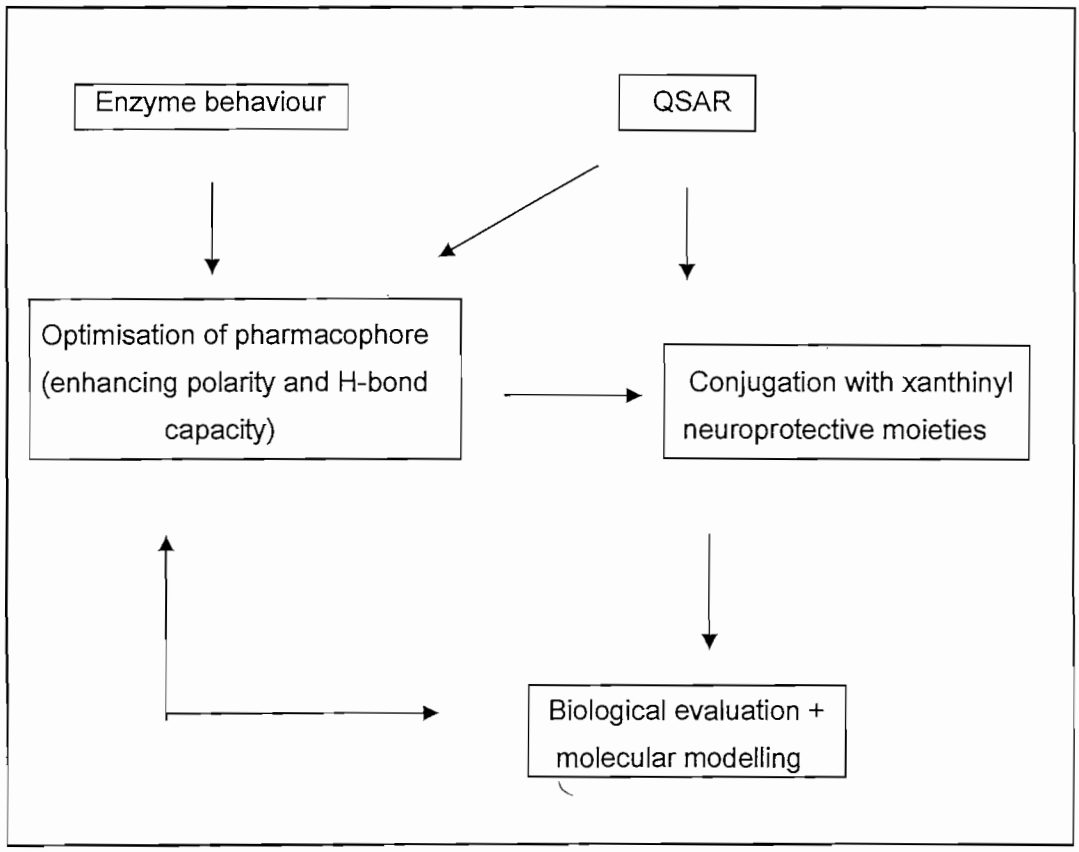

Figure 1.6: General outline of this study.

Chapter 2 Literature overview

2.1 MAO-B IN NEURODEGENERATION

Neurodegeneration occurs in neuropathological conditions such as Alzheimer's disease (AD), Parkinsons's disease (PD) multiple sclerosis (MS), Huntington's disease (HD) and amytrophic lateral sclerosis (ALS) in which the nervous system functionality is decreased owing to the death of neurons (Ekshyyan & Aw, 2004). Morphologically, neuronal death (neurodegeneration) can be divided into two major types: necrosis and apoptosis (Artal-Sanz *et al.*, 2005). There has been a growing interest in the development of drugs that not only provide symptomatic relief for neurodegenerative disorders, but also halt or prevent the neurodegenerative cascades and provide neuroprotection. Since MAO-B inhibitors possess multiple biochemical actions and have protective effects on both vascular and neuronal tissue, they require further consideration in the treatment and prevention of degenerative disease (Riederer *et al.*, 2004). This is confirmed by the mechanism-based inactivator of MAO-B, (R)-Deprenyl (Fig. 2.5), which is frequently used in combination with L-DOPA as dopamine replacement therapy in PD. The purpose of this section is to provide a literature survey in of MAO-B enzyme morphology and behaviour as well as functional moieties of several inhibitors involved in MAO binding.

2.1.1 Relevance of MAO-B

In the brain, MAO-A presents mainly in catecholaminergic neurons, whereas MAO-B is primarily present in glia and in serotonergic neurons (Westlund *et al.*, 1988; Saura *et al.*, 1996). Previous enzymatic assays performed on post-mortem human brain tissue suggest that MAO-B levels in glial cells (Halliwell, 1992; Ekblom *et al.*, 1993) increase with age (Robinson *et al.*, 1971; Fowler & Oreland, 1980; Kornhuber *et al.*, 1989; Sastra & Garcia-Sevilla; 1993; Galva *et al.*, 1995) and in neurodegenerative disease (Adolfsson *et al.*, 1980; Strolin Benedetti & Dostert, 1989).

Catecholamines, (dopamine in particular), are either metabolised by endogenous enzymes such as monoamine oxidases (MAO) or spontaneously degraded by auto oxidation (Fig. 2.1) to yield hydrogen peroxide (H_2O_2) and dopamine–quinones (Sulzer & Zecca, 2000; Graham *et al.*, 1978). The H_2O_2 is fed into the reactive oxygen species (ROS) cycle and the dopamine quinones can modify protein sulfhydryl groups via nucleophilic additions. This leads to exacerbation of inflammation and tissue damage (Graham *et al.*, 1978; Stokes *et al.*, 1999; Tse *et al.*, 1976).

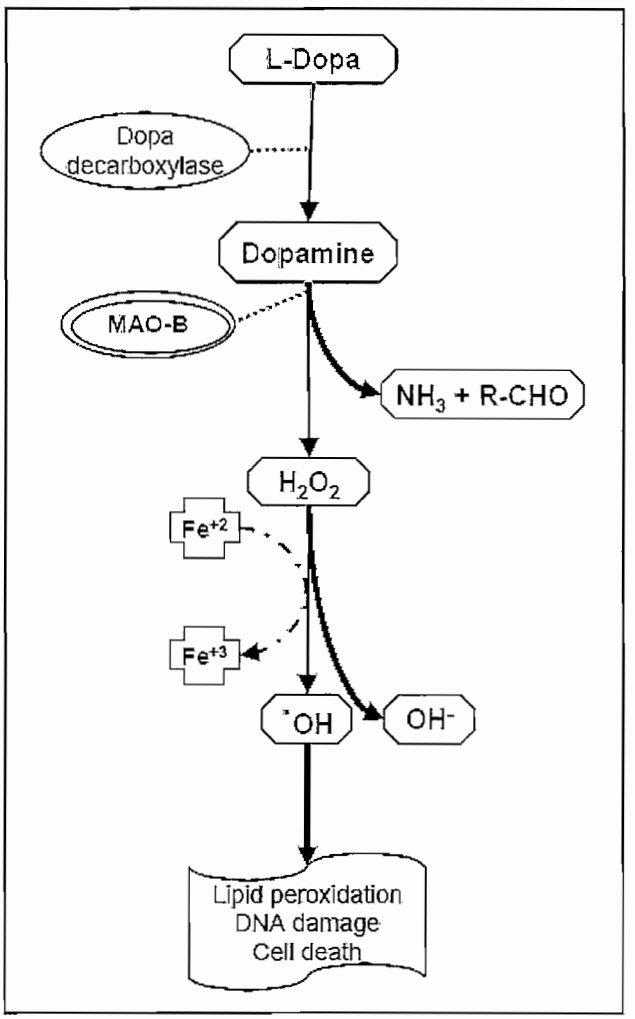

Figure 2.1: MAO-B biochemistry and production of free radicals causing oxidative stress (Riederer *et al.*, 2004).

Free radicals include ROS such as superoxide (O^{2-}), hydroxyl radicals (OH^-), peroxyl radicals (ROO^-) and hydrogen peroxide (H_2O_2), as well as reactive nitrogen species (RNS) such as nitric oxide (NO) and peroxynitrite ($ONOO^-$). Reactive chlorine species

(RCS), such as hypochlorous acid can also be included (Wallace, 1999; Vertuani *et al.*, 2004; Ischiropoulos & Beckman, 2003; Klebanoff, 2005).

Neuronal tissue MAO-B levels increase ~ 4 fold with age, thus leading to enhanced dopamine metabolism and higher hydrogen peroxide formation. This higher MAO-B brain activity contributes to an increase in hydroxyl radicals, and thus the development of Aß plaques (Brühlmann *et al.*, 2001). The increase in brain MAO-B is most likely due to transcriptional elevation of the MAO-B protein (Nakamura, 1990) and is predominant in plaque-associated astrocytes in neuropathologically verified AD brains (Jossan *et al.*, 1991; Saura *et al.*, 1994).

The beneficial effects of (R)-deprenyl may be dependent on the inhibition of the MAO-B catalysed oxidation of dopamine in the CNS, consequently conserving the depleted supply of dopamine and delaying the need for L-Dopa therapy in patients diagnosed with early PD (Rabey *et al.*, 2000). (R)-Deprenyl is also reported to exert a neuroprotective effect by blocking apoptotic cell death (Tatton & Greenwood, 1991).

Return of enzyme activity following treatment with irreversible inactivators such as (R)-deprenyl, requires *de novo* synthesis of the MAO-B protein. (R)-Deprenyl is further metabolised to (R)-methamphetamine, a compound that possess neurotoxic effects (Riederer *et al.*, 2004).

Reversibly inhibiting MAO-B will reduce dopamine catabolism, increase dopamine levels and consequently suppress the generation of ROS (Knoll & Magyar, 1972). The ideal would be to develop safer inhibitors, designed to be reversible while retaining selectivity towards MAO-B and exhibiting a dual mechanism of action for neuroprotection.

2.1.2 The MPTP model and development of neurodegeneration

MPTP (1-methyl-4-phenyl-1,2,3,6-tetrahydropyridine) was discovered after induction of irreversible parkinsonian syndrome in addicts following injection of MPTP as a contaminant of a poorly synthesised meperidine analogue. (Langston *et al.*, 1983; Langston *et al.*, 1999). MPTP structurally resembles a number of known environmental agents such as paraquat (DiMonte, 2006) and rotenone (McNaught *et al.*, 1996) and is useful as a neurotoxin because it mimics the same sequence of degeneration that occurs in man.

Post mortem examination of several patients ranging from 3 to 16 years post-exposure and onset of parkinsonism, revealed not only evidence of progressive neurodegeneration, but also reactive microglial clusters surrounding nerve cells. In animal models of PD, MPTP was found to reproduce many of the characteristics of the disease when administered to mice (Przedborski *et al.*, 2000) and primates (Hurley *et al.*, 2003).

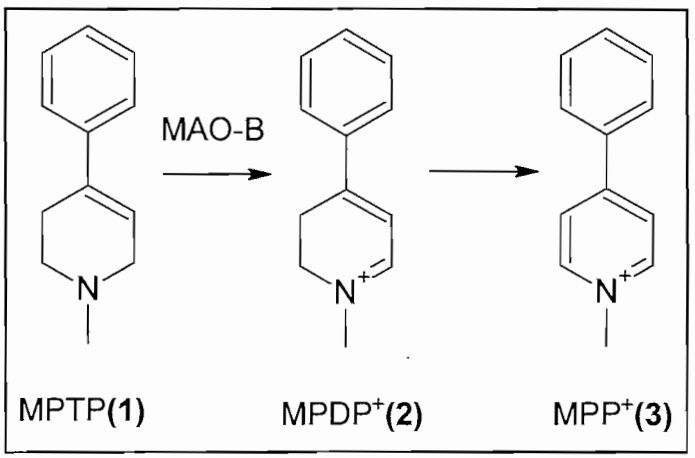

Figure 2.2: The MAO-B dependent bioactivation pathway for MPTP (**1**) via $MPTP^+$(**2**) to MPP^+ (**3**), the active toxin (Chiba *et al.*, 1984).

1-Methyl-4-phenyl-1,2,3,6-tetrahydropyridine [MPTP (**1**)] is an excellent MAO-B substrate, and the neurotoxicity thereof is dependent on its MAO-B catalysed oxidation (Fig. 2.2) to the dihydropyridinium intermediate 1-methyl-4-phenyl-2,3-dihydropyridinium [$MPDP^+$ (**2**)], which undergoes further oxidation to the 1-methyl-4-phenylpyridinium species [MPP^+ (**3**)], the ultimate toxin (Inoue *et al.*, 1999). MPP^+ exits the glia into the extracellular space, and is transported into DA neurons where the neurotoxic events occur (Smeyne & Jackson-Lewis, 2005). The vesicular monoamine transporter (VMAT2) sequesters monoamine neurotransmitters as well as MPP^+ from the cytoplasm space into synaptic vesicles. (Miller & Gainetdinov, 1999; Müller *et al.*, 2003; Beal, 2003).

Within the dopaminergic neuron, MPP^+ inhibits mitochondrial electron transport complex I (Fig. 2.3), resulting in decreased ATP production and cell death (Przedborski *et al.*, 2000).

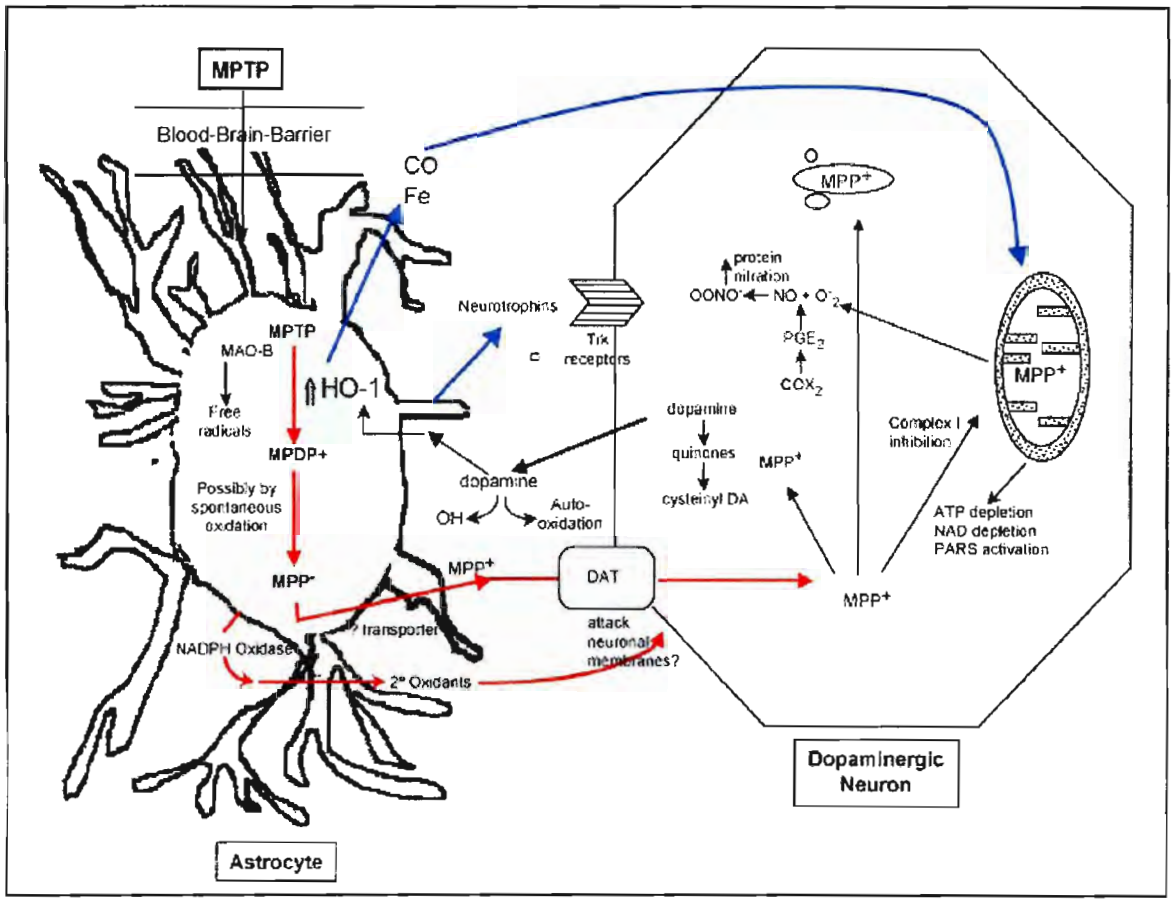

Figure 2.3: Schematic representation of the mechanism of MPTP action in the nigrostriatal system. Red arrows represent the initial (toxification) role of glial cells. Blue arrows represent the second (neuroprotective) role of glial cells (Smeyne & Jackson-Lewis, 2005).

MPTP induces peak microglia activation within 2 days after acute MPTP intoxication and produces a pro-inflammatory environment in the substantia nigra (SN) and striatum with predominant production of TNF-α, interleukin-1ß (IL-ß) and IL-6 (Teismann *et al.*, 2003; Youdim *et al.*, 2002; Hunot *et al.*, 1999). This leads to the upregulation of iNOS (inducible nitric oxide synthase), COX-2 and MMP-9 (Teismann (b) *et al.*, 2003; Hunot *et al.*, 1999; Youdim *et al.*, 2002; Lorenzl *et al.*, 2004; Shen *et al.*, 2005).

iNOS produces large amounts of nitric oxide (NO) which reacts with superoxide radicals to produce peroxynitrite ($OONO^-$), causing neurons to be at risk of possible attack by this glial-derived reactive nitrogen species (Lancaster *et al.*, 1996).

2.2 MONOAMINE OXIDASES

Amine oxidases (AOs) have traditionally been divided into two main groups, based on the chemical nature of the attached cofactor (Fig. 2.4). The flavin adenine dinucleotide (FAD) containing enzymes [monoamine oxidase-A (MAO-A), MAO-B and polyamine oxidases (PAO)] are intracellular enzymes (Shih *et al.*, 1999). The other class of AOs contain a cofactor possessing one or more carbonyl groups, which appears to be topa-quinone (TPQ) in most cases (Klinman & Mu, 1994; Lyles & Chalmers, 1995). These enzymes include diamine oxidases (DAO), lysyl oxidase, plasma membrane bound and soluble MAOs (Salmi *et al*, 2001).

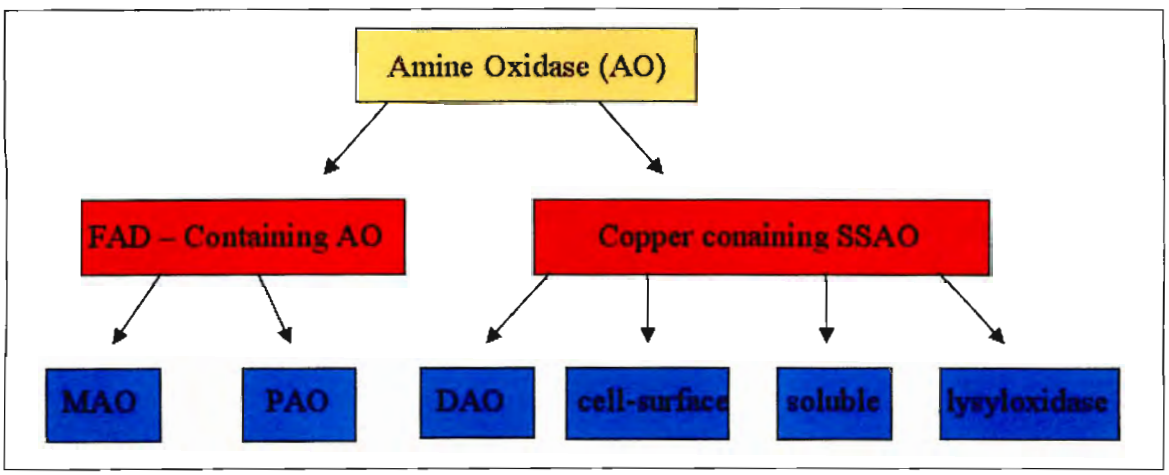

Figure 2.4: Classification of amine oxidases (Jalkanen & Salmi, 2001).

Monoamine oxidase (MAO) is a ~ 60-kDa mitochondrial outer membrane flavin adenine dinucleotide (FAD) cofactor containing enzyme that exists in neuronal, glial and other cells (Bach *et al.*, 1988; Hubálek *et al.*, 2005). According to substrate and inhibitor specificities, it exists as two isoforms, namely MAO-A and MAO-B (Grimsby *et al.*, 1990). MAO-B constitutes about 80% of the total MAO activity in the human brain (Riederer *et al.*, 1978; Sonsalla & Golbe, 1988) and is the predominant form of the enzyme in the striatum (Riederer *et al.*, 1989).

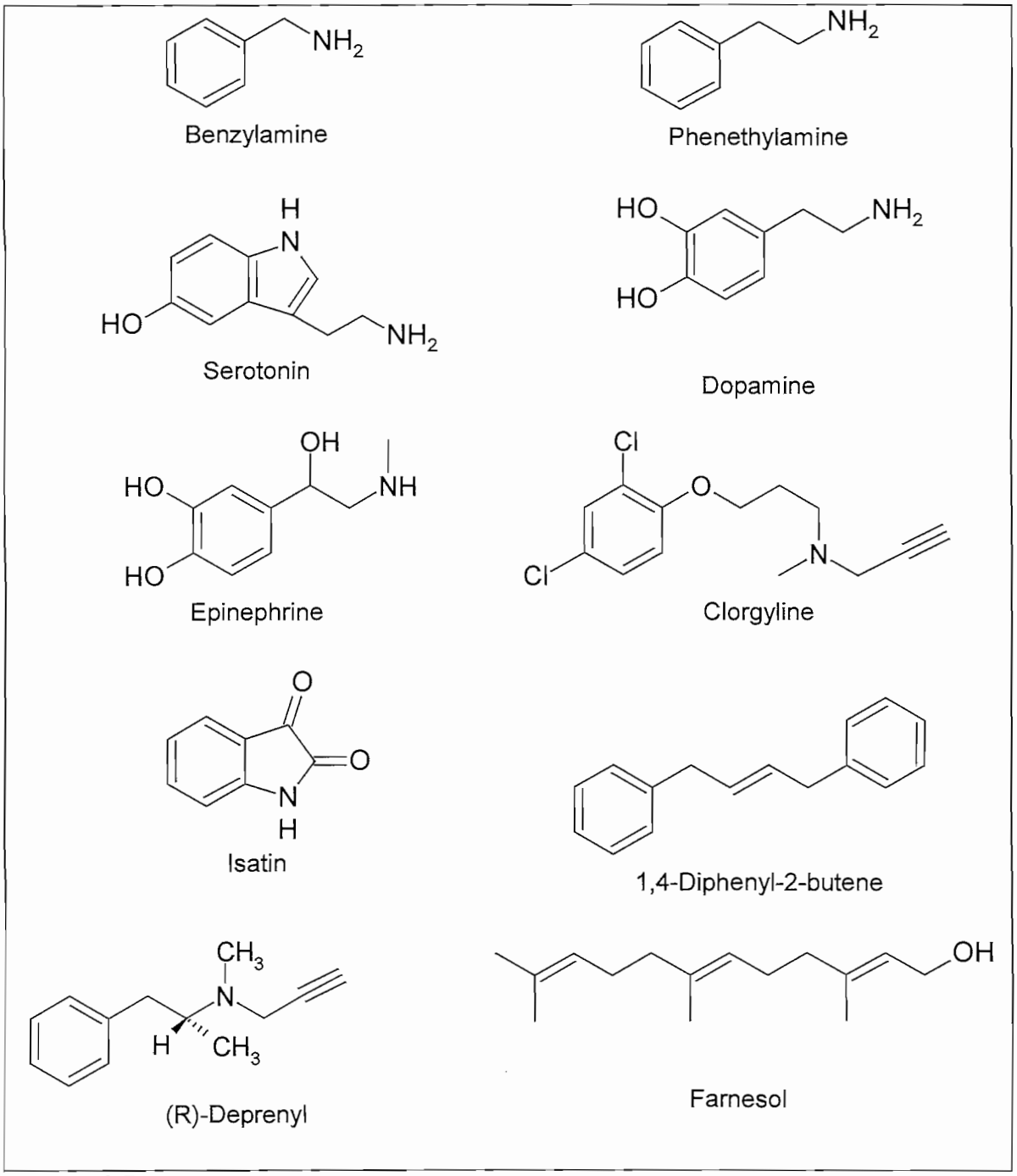

Figure 2.5: Chemical structures of compounds discussed in the text.

MAO-A catalyses the deamination of serotonin (5-HT), norephinephrine and epinephrine (Fig. 2.5) and inhibition (eg. by clorgyline) of this enzyme results in an antidepressant and anti-anxiety effect. MAO-B catalyses the deamination of ß-phenylethylamine and benzylamine (Fig. 2.5) and inhibition (eg. by (R)-deprenyl) of this enzyme results in anti-Parkinson's and anti-Alzheimer's effects, thus its relevance in neuroprotective studies (Ooms *et al.*, 2003).

Although MAO-A and MAO-B are different with regards to substrate specifities, they are similar in that both have the same type of covalent flavin (8α-S-cysteinyl FAD) and they share a ~ 70% sequence identity (Edmondson *et al.*, 2004). A common characteristic of MAOs not found in other outer membrane mitochondrial proteins is the presence of a C terminal non-cleavable targeting signal sequence which is inserted in the membrane without proteolytic maturation (Binda *et al.*, 2004).

2.2.1 Morphology of monoamine oxidase B (MAO-B)

Monoamine oxidase B is a flavin-adenine dinucleotide (FAD) containing enzyme, consisting of 520 amino acids and is located in the outer mitochondrial membranes of neuronal, glial and other cells (Weyler *et al.*, 1990). It exists as a dimer in its membrane bound form. The membrane binding site of each monomer faces the membrane surface (Fig. 2.6 & Fig. 2.8) and partly interacts with it (Binda *et al.*, 2004).

The crystal structure of human MAO-B (EC no.: 1.4.3.2.) at 3 Å reveals that this dimeric enzyme has a C-terminal transmembrane helix protruding from each monomer that anchors it to the membrane. This transmembrane anchoring helix (Fig. 2.6) is formed by the 32 C-terminal amino acids (residues 489-520) and is not only for membrane binding, but for enzyme functionality as well as stability. Additional interactions for this membrane binding are facilitated by apolar loops on the protein surface, located near the C-terminal helix. The suggestion that the membrane has a function in the control of substrate binding, is confirmed by the presence of a loop (residues 99-112), which regulates (opening and closing) the active site cavity of MAO-B (Binda *et al.*, 2004). The solvent exposed hydrophobic sites (Pro109-Ile110, Trp157) are postulated to be involved in membrane binding because of their presence in the MAO-B substrate binding domain (Fig. 2.6 & Fig. 2.8) as well as their close proximity to the C-terminal helix (Binda *et al.*, 2004).

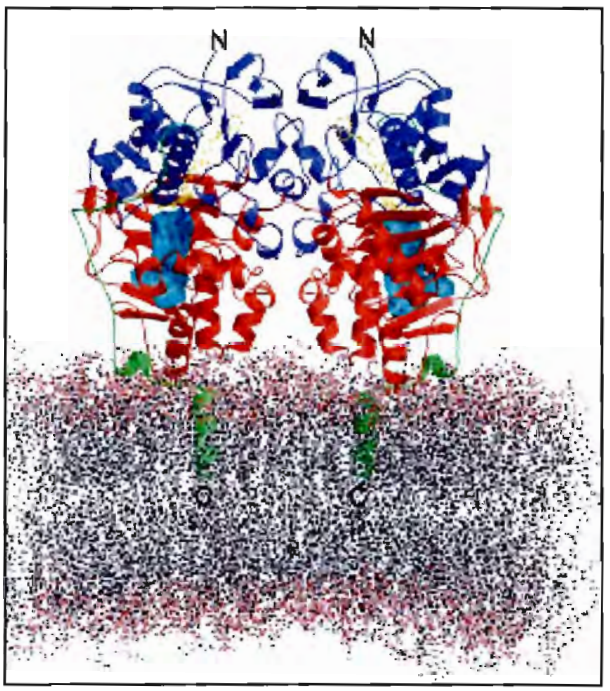

Figure 2.6: Three-dimensional structure of human MAO-B with the dimer bound to the phospholipid bilayer. Each monomer has a two-domain overall topology, consisting of the FAD binding domain in blue and the substrate-binding domain in red. The amino and carboxy termini of each monomer are highlighted as **N** and **C**, respectively. The FAD cofactor is represented in yellow ball-and-stick. The C-terminal membrane-binding region is depicted in green. In each monomer the active site cavity is colored in light blue (Binda *et al.*, 2004).

The entrance from the surface to the active site of the enzyme consists of two cavities (Fig. 2.7 & Fig. 2.8) namely the entrance cavity and the substrate cavity (Hubálek *et al.*, 2005). The entrance cavity occupies a volume of 290 $Å^3$ whilst the hydrophobic substrate cavity is larger and a have a volume of 420 $Å^3$ (Edmondson *et al.*, 2004). The combined 700 $Å^3$ large cavity originates from one side of the protein surface and stretch deep into the protein until it reaches the flavin cofactor. It is this entity that forms the active site of the enzyme (Binda *et al.*, 2004).

The Connolly channel surface in translucent yellow (Fig. 2.7) shows these two distinct cavities inside the binding site; the entrance cavity, which is connected to the outside of the protein, and the substrate cavity, located in the vicinity of the FAD. Ile199 and Tyr326 (Fig. 2.7: carbon atoms in magenta) separate these two cavities (Novaroli *et al.*, 2006). The dots inside the pockets (Fig. 2.7) are coloured according to the molecular lipophilicity potential (MLP) values according to the following decreasing scales: polar

values in red, magenta, orange, and yellow; hydrophobic values in blue, cyan, green-blue and green (Novaroli *et al.*, 2006).

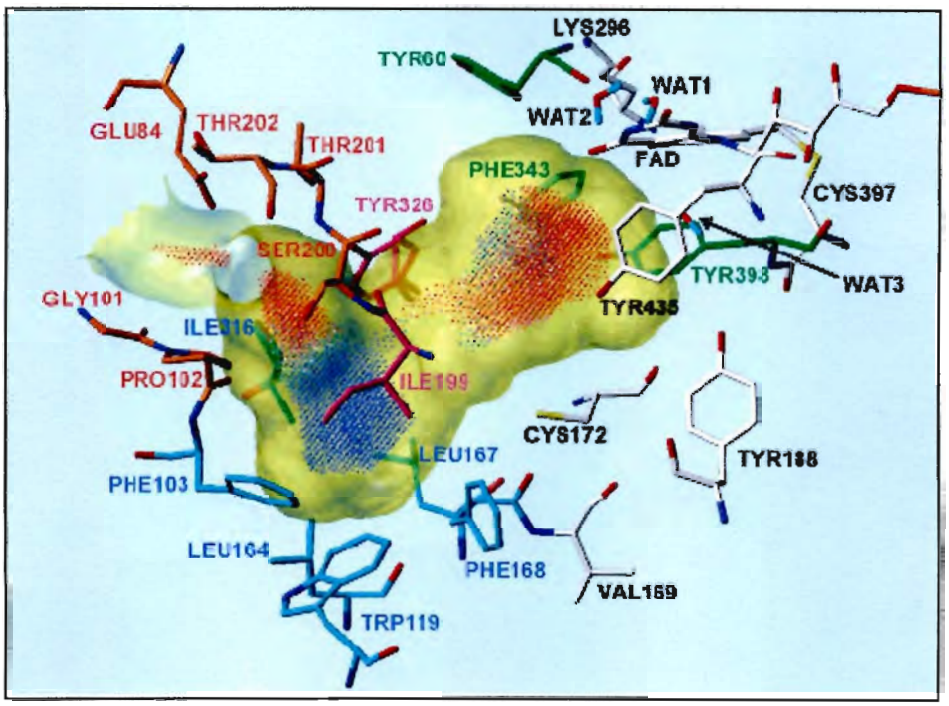

Figure 2.7: Binding site of MAO-B. The Connolly channel surface of the cavities is displayed in translucent yellow. The coloured dots describing the lipophilicity inside the pockets are colour-coded according to their MLP values. The amino acids potentially interacting with the ligands are color-coded following their localization around the binding site. The flavine adenine dinucleotide cofactor (FAD) and the three selected water molecules (WATX) are represented as an integral part of the MAO-B structure model (Novaroli *et al.*, 2006).

The substrate cavity is mainly polar. This is explained by a number of polar side chains (Fig. 2.9), accessible H-bonding groups as well as the presence of the flavin nucleus and the three buried water molecules in the vicinity of this cavity. Only a pocket defined by three apolar residues, Tyr60, Phe343 and Tyr398 (Fig. 2.7: carbon atoms in green), displays a hydrophobic environment. The substrate cavity is also more sterically constrained than the entrance cavity (Novaroli *et al.*, 2006). It is shaped like a flat, elongated disc with the longer axis perpendicular to the flavin ring (Edmondson *et al.*, 2004). The active site cavity gating loop, redidues 99-112, is believed to be partly embedded in the membrane (Fig. 2.8), suggesting that the membrane have a controlling function over this gating loop.

In contrast, various zones displaying opposite lipophilicity are well-defined inside the entrance cavity. The area lined by Phe103, Trp119, Leu164, Leu167, Phe168 and Ile316 results in a highly hydrophobic environment (Fig. 2.7: carbon atoms in cyan), whereas another pocket toward the outside of the protein is surrounded by polar residues like Glu84, Gly101, Pro102, Ser200, Thr201, Thr202 and Tyr326 (Fig. 2.7: carbon atoms in orange), with major hydrogen bonding capacity (Novaroli *et al.*, 2006).

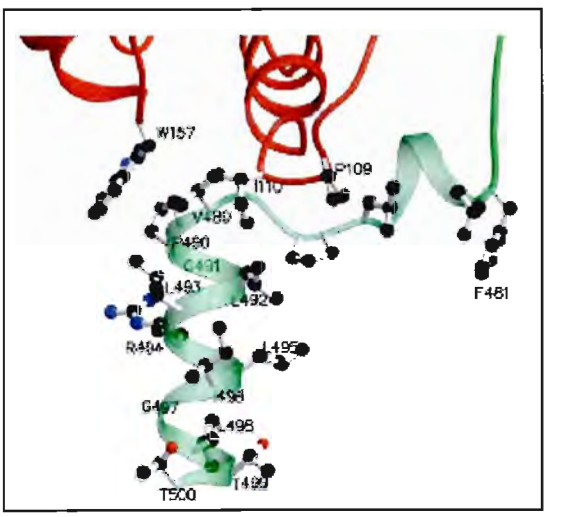

Figure 2.8: Three-dimensional structure of human MAO-B showing the C-terminal transmembrane helix and the neighbouring apolar sites involved in membrane binding. Residue side chains are in ball-and-stick representation, with carbon atoms represented in black, nitrogens in blue, oxygens in red. The gray line is indicative of the upper boundary of the membrane but it is not intended to represent the exact depth of protein insertion into the membrane (Binda *et al.*, 2004).

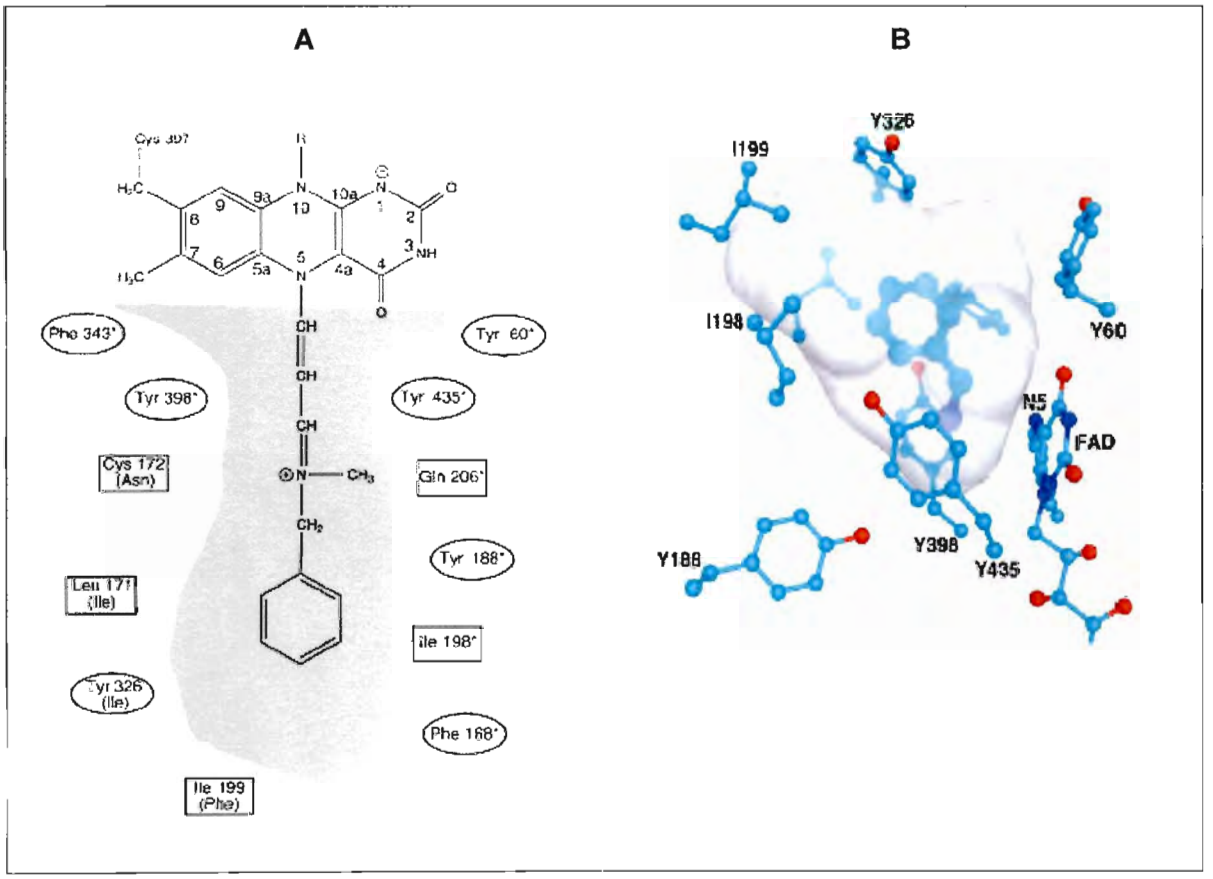

Figure 2.9: The substrate binding site of human MAO-B. (**A**) Schematic representation of the pargyline binding site. MAO-B residues that are conserved in human MAO-A are indicated by an asterisk. For non-conserved amino acids, the replacement side chains of MAO-A are in parentheses. Aromatic side chains are enclosed in ellipsoidal frames and other residues are in retrangular boxes. The atoms of the flavin ring are numbered.

(**B**) A model for the binding of the substrate, benzylamine. Atoms and bonds of the modeled substrate are shown in an increased size. The surface of the solvent inaccessible substrate–binding cavity is semi-transparent. The reactive N5 site on the twisted flavin ring is labeled. Carbons are in cyan, nitrogens in blue and oxygens in red (Binda *et al.*, 2001).

The entrance cavity thus consists of a highly hydrophobic pocket and another pocket surrounded by polar residues and with H-bond capacity. An inhibitor must traverse the entrance cavity in order to gain access to the substrate cavity (Fig. 2.7). This is true for small molecule inhibitors such as isatin (Fig. 2.5) that has been shown to bind within the substrate cavity of the enzyme (Binda *et al.*, 2003). Larger inhibitors, such as 1,4-diphenyl-2-butene and trans,trans-farnesol (Fig. 2.5), appears to exhibit a dual binding mode that involves traversing both the entrance and substrate cavities (Binda *et al.*,

2003). The side chain of Ile199 reveals different rotamer conformations that allow for the fusion of these two cavities. When larger inhibitors occupy the active site, Ile199 is rotated (Fig. 2.7 & Fig. 2.10) out of its normal conformation (Edmondson *et al.*, 2004). Ile199 therefore serves as a 'gating switch', separating the two cavities in order to accommodate these larger inhibitors. The size and chemical nature of the bound inhibitor thus determine separation between the entrance and substrate cavity (Hubálek *et al.*, 2005).

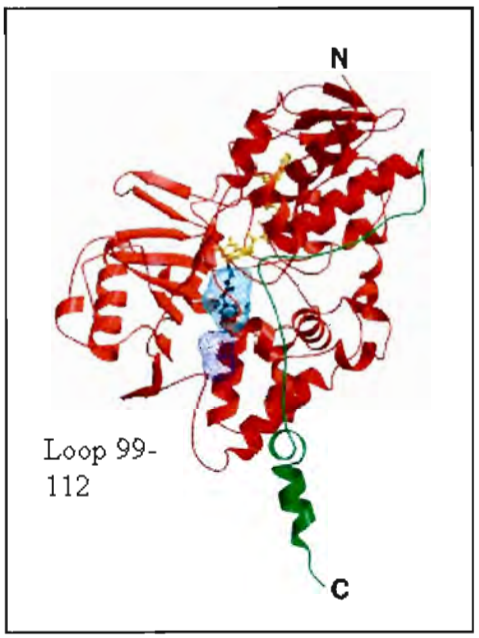

Figure 2.10: Cavities constituting the substrate path from the protein surface to the flavin in the MAO-B monomer. Adjacent to the active site cavity (cyan) is the entrance cavity (blue), which is underneath loop 99-112. The FAD is in yellow and the covalent pargyline is in black inside the entrance cavity (Binda *et al.*, 2001).

The FAD moiety functions as a redox cofactor and is required for catalysis (Edmondson *et al.*, 2004). The oxidation of the amine substrate (Fig. 2.11) leads to the reduction of FAD. The prosthetic group is re-oxidised by molecular oxygen to generate hydrogen peroxide and the imine is hydrolysed in a non-enzymatic process (Binda *et al.*, 2001).

Inhibitors (eg. (R)-deprenyl) form N5 or C4a flavin adducts (Fig. 2.9 & Fig. 2.12) in MAO-B (Edmondson *et al.*, 2004) and electron transfer or polar nucleophillic mechanisms have been proposed for MAO catalysis, implying that polarisibility and hydrophobicity (parameters of electron delocalisations) must be considered for binding (Edmondson *et al.*, 2004; Binda *et al.*, 2004).

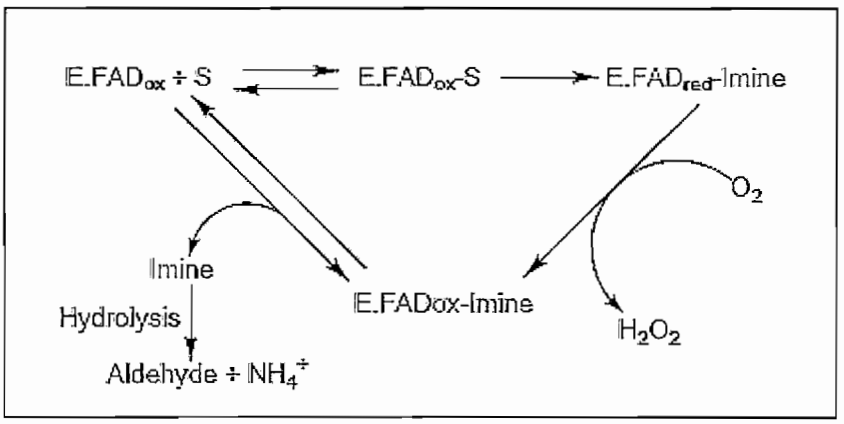

Figure 2.11: Scheme for the overall deamination reaction catalyzed by MAOs (Binda *et al.*, 2001).

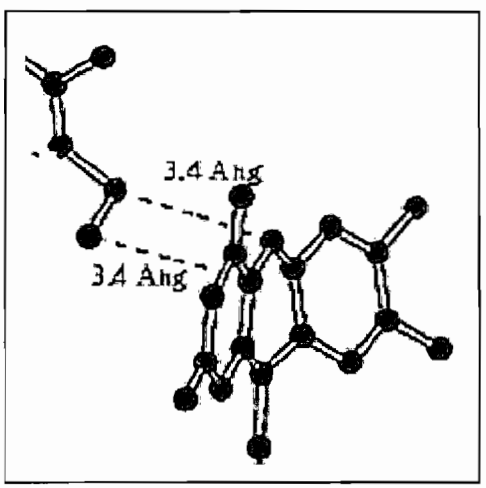

Figure 2.12: Close-up view of the position of bound trans, trans-farnesol with respect to the flavin ring. The dashed lines refer to the distances (3.4 Å) between the farnesol oxygen and the flavin C4a position and between the C1 of farnesol and the flavin N5 position (Binda *et al.*, 2001).

2.2.2 Structural comparison of hMAO-A and hMAO-B

MAO-B mainly acts on small exogenous amines, whereas MAO-A carries out the degradation of bulkier endogenous amine neurotransmitters, such as serotonin (Binda *et al.*, 2001). Both enzymes' active site consists of identical covalent FAD coenzymes (Fig. 2.6 & Fig. 2.10) as well as two tyrosines constituting the aromatic cage (Binda *et al.*, 2002), thus, revealing the same catalytic mechanism (Edmondson *et al.*, 2004). In contrast, the surface area of the active sites opposite to the flavin shows major differences (Fig. 2.13).

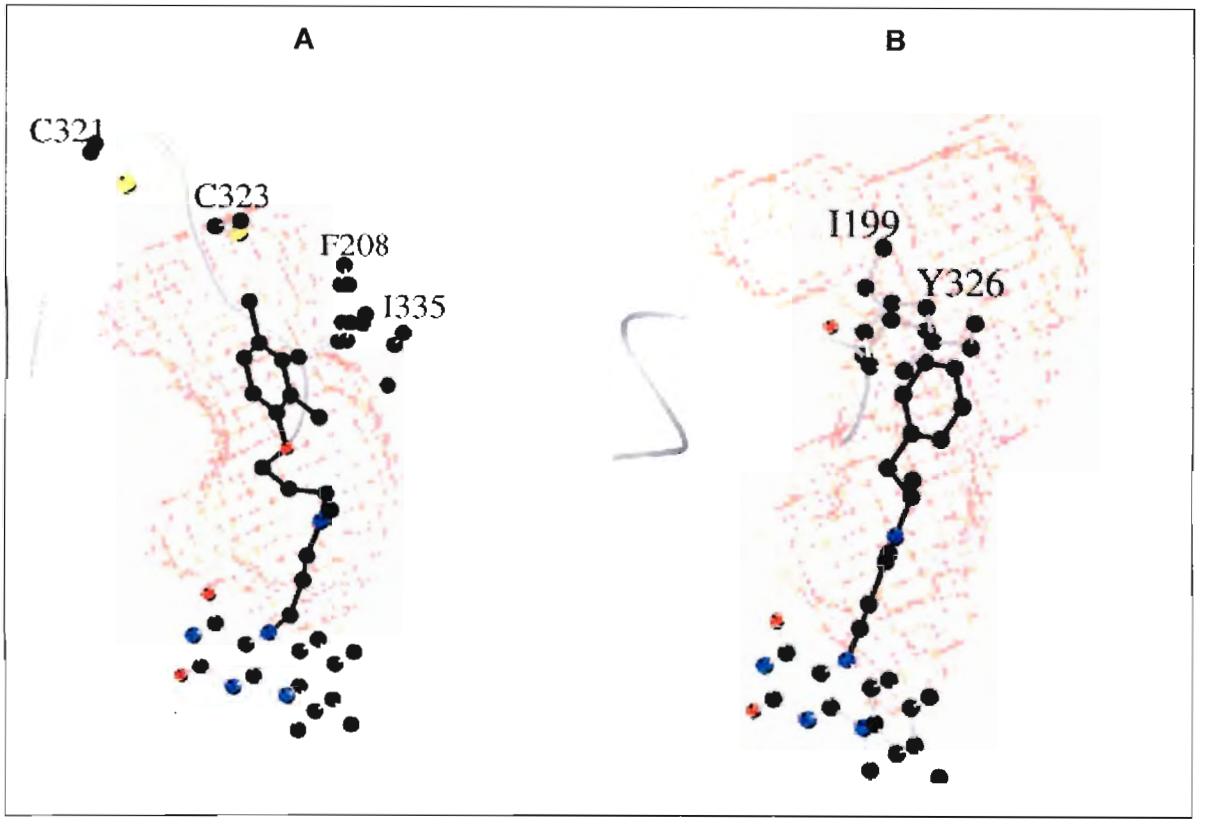

Figure 2.13: The active site cavities in hMAO-A (**A**) and hMAO-B (**B**) in complex with clorgyline and deprenyl respectively. Active site comparison of hMAO-A and hMAO-B with the crucial Phe208 and Ile335 (**A**) residues of hMAO-A superimposed to the corresponding Ile199 and Tyr326 (**B**) residues of hMAO-B (de Colibus *et al.*, 2005).

The differences between human MAO-B and MAO-A in respect to residues lining the substrate cavity include Leu171 (MAO-B)/Ile180 (MAO-A), Cys172/Asn181, Ile199/Phe208 and Tyr326/Ile335. These amino acids are located in the rear of the substrate cavity [Fig. 2.7 & Fig 2.9 (**A**)] and are in Van der Waals contact with the phenyl ring of pargyline. Three of the four residues (Leu171/Ile199 and Tyr326) separate the substrate cavity from the entrance cavity. Side chain changes in these positions thus affect not only steric accommodation of the substrate but may also lead to alterations in the separation of the substrate cavity from the entrance cavity. Therefore, variations in substrate and inhibitor specifities between human MAO-A and MAO-B mainly result from the fine tuning of the size and shape of the hydrophobic substrate cavity and its steric relation with the entrance cavity (Wu *et al.*, 1993; Geha *et al.*, 2001; Binda *et al.*, 2001).

Table 2.1: Replacements of the active site residues in hMAO-A and hMAO-B (de Colibus *et al.*, 2005).

hMAO A	hMAO B
Tyr-69	Tyr-60
Gln-74	Gln-65
Val-91	Val-82
Val-93	Glu-84
Leu-97	Leu-88
Ile-180	Leu-171
Asn-181	Cys-172
Ile-207	Ile-198
Phe-208	Ile-199
Ser-209	Ser-200
Val-210	Thr-201
Glu-216	Glu-207
Cys-323	Thr-314
Ile-325	Ile-316
Ile-335	Tyr-326
Leu-337	Leu-328
Met-350	Met-341
Phe-352	Phe-343
Tyr-407	Tyr-398
Tyr-444	Tyr-435

The active site cavities of the enzymes (Fig. 2.13) are thus different with regards to shape and size. hMAO-A's active site consist of a single hydrophobic cavity of ~ 550 $Å^3$, much shorter in length and wider than that of the longer and narrower ~700 $Å^3$ hMAO-B site (de Colibus *et al.*, 2005). hMAO-B substrate entry therefore requires the entrance and substrate cavities fused for certain inhibitors, where hMAO-A lacks this particular characteristic.

2.3 MAO-B INHIBITION

Reversible, competitive inhibitors are structurally related to MAO substrates and can therefore bind to the active site of the enzyme without any covalent bond formation. Irreversible or "suicide" inhibitors (also known as mechanism based inactivators) are initially bound to MAO-B in a reversible competitive manner, but are then oxidised by the enzyme to the active inhibitor, which covalently binds to the enzyme's active site via the FAD cofactor, thus rendering it permanently ineffective for amine metabolism. This mode of inhibition is more persistent than that achieved by reversible inhibitors (weeks rather than hours), as its effect can only be overcome by *de novo* synthesis of the MAO-B enzyme (Abeles & Maycock, 1976).

In the search for a pharmacophore model for reversible MAO-B inhibition, it was noted that specific hydrogen bonds and hydrophobic interactions were absolute requirements for activity (Ooms *et al.*, 2003). It is believed that these hydrogen bonds within the active cavity of MAO-B (Fig. 2.14) stabilises inhibitors (Wouters *et al.*, 1997). Other inhibitors are stabilised within the MAO-B binding site through hydrophobic interactions between their aryl side chain and the amino acid residues inside the active site (Ooms *et al.*, 2003).

Increased lipophillic interactions result in an increase of MAO-B inhibition as well as selectivity (Ooms *et al.*, 2003). It can clearly be demonstrated that the two parameters, namely hydrogen bonds and hydrophobic interactions, are determining physical factors in inhibition. Hence, confirming a large hydrophobic binding site with polar interactions.

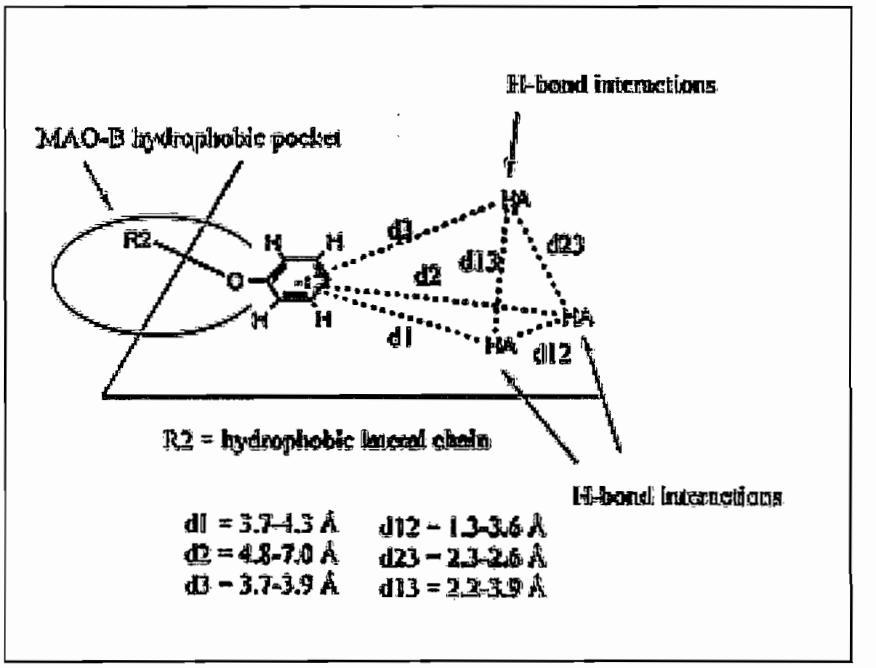

Figure 2.14: MAO-B pharmacophore model. **HA** represents the relative position of the hydrogen accepting group (Ooms *et al.*, 2003).

The fundamental requirements for a MAO inhibitor are that the compound must be lipophillic, have an aromatic ring and contain a nitrogen, sulphur or oxygen atom near the region of the phenyl ring (Wouters *et al.*, 1997). Substrate requirements (eg. benzylamine or phenylethylamine) include larger substituents on the para position of the aromatic ring, which also leads to an increased affinity for MAO-B (Hynson *et al.*, 2003). Natural substrates for MAO-A are mostly ethylamine side chains attached to an aromatic ring (Ravi *et al.*, 2000).

Three types of MAO inhibitors has been classified:

1. Irreversible and non-selective inhibitors;
2. Irreversible but selective inhibitors;
3. In recent efforts – reversible and selective inhibitors (Santana *et al.*, 2006).

2.3.1 Compounds exhibiting MAO-B inhibition activity

Molecular requirements for reversible and selective MAO-A and MAO-B inhibition are only partly understood (Gnerre *et al.*, 2000). Various compounds have been under investigation for MAO-A inhibition, and some also show promise for MAO-B activity (Fig. 2.15 & Fig. 2.16). These include analogues of: propargyl (clorgyline) (**I**), benzamide

(moclobemide) (**II**), phenylethylamine (**III**), indole (**IV**), coumarin (**V**), thioxanthene (**VI**), oxadiazolidone and toloxatone (**VII**) and diazoheterocyclic (**VIII**) derivatives (Santana *et al.*, 2006).

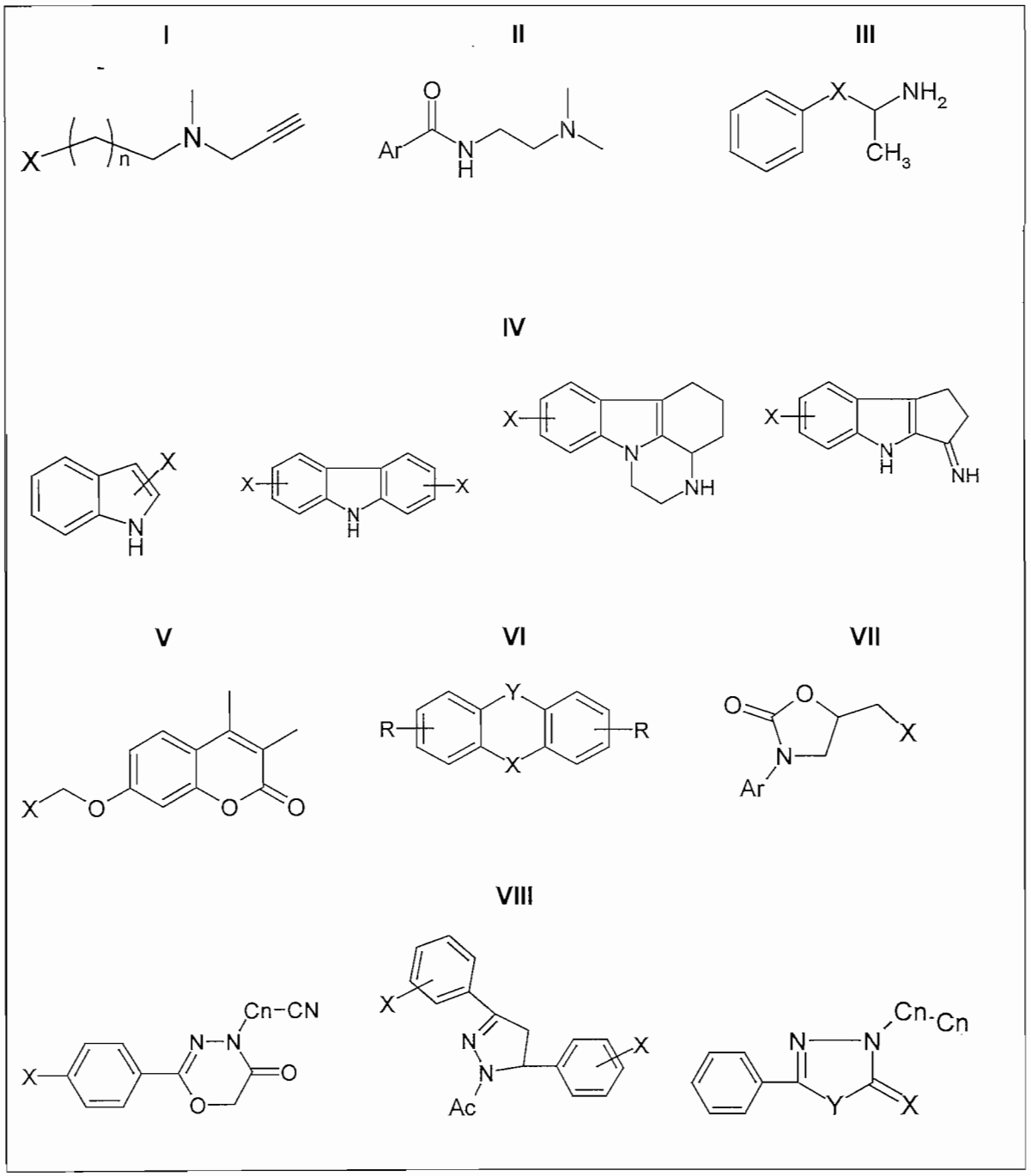

Figure 2.15: Structures of known MAO-A and MAO-B inhibitors (Santana *et al.*, 2006).

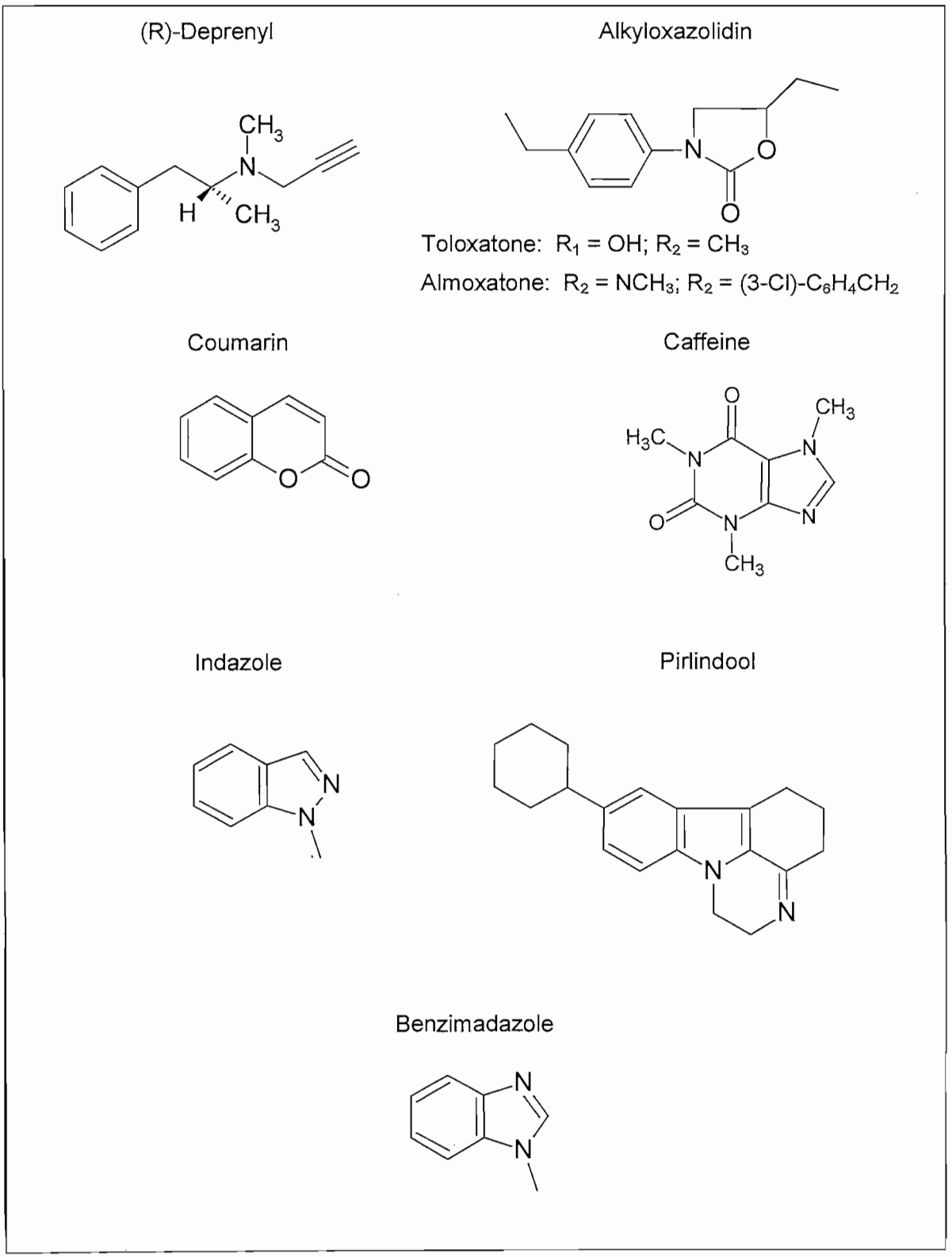

Figure 2.16: Derivatives with selective MAO-B inhibitory activity.

Using SAR and QSAR, several compounds with selective MAO-B activity have been identified (Fig. 2.16) and show promise in the treatment of neurodegenerative disorders (Santana *et al.*, 2006).

2.3.1.1 Coumarin analogues

The coumarins (also known as benzopyrones), exhibit a broad spectrum of pharmacological activity that includes anti-infective, anticancer, antimyotoxic, phytoestrogenic, insecticidal, antifungal and HIV-1-reverse transcriptase inhibitory properties (Naser-Hijazi *et al.*, 1994; Murray *et al.*, 1982; Feuer, 1974; Deana *et* al., 1983; Wenkert & Buckwalter 1972).

Several coumarin derivatives have been shown to act as competitive, reversible and selective MAO-B inhibitors and acetyl cholinesterase (AChE) inhibitors. The coumarin derivatives evaluated (Table 2.3 & 2.4) acted preferentially on MAO-B and IC_{50} values obtained were in the micromolar to low nanomolar range (Gnerre *et al.*, 2000; Novaroli *et al.*, 2006). Coumarins or compounds containing the coumarin moiety can therefore be valuable as lead compounds for the development of new, potent, selective reversible MAO-B inhibitors.

2.3.1.1.1 STRUCTURE ACTIVITY RELATIONS (SAR) OF COUMARINS

Two series of coumarin derivatives (Table 2.2 & 2.3) were synthesised and evaluated to explore MAO-B inhibitory activities and SAR (Gnerre *et al.*, 2000; Novaroli *et al.*, 2006).

Table 2.2: Supersomes and rat brain MAO-B inhibitory activities of coumarin derivatives (Series I).

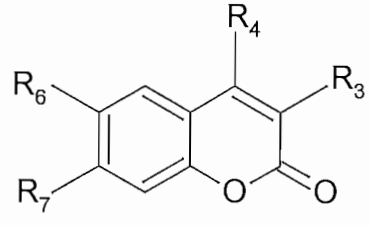

Compound	R_3	R_4	R_6	R_7	pIC_{50} Supersomes	pIC_{50} rat	ΔpIC_{50} [b]
1	H	H	H	$OCH_2C_6H_5$	8.77 ± 0.04	7.26 ± 0.02	1.51
2	H	H	H	$CH_2OC_6H_5$	7.19 ± 0.02	7.07 ± 0.04	0.12
3	H	H	H	$CH_2NHC_6H_5$	7.24 ± 0.06	5.67 ± 0.02	1.57
4	H	CH_3	H	$OCH_2C_6H_5$	8.80 ± 0.06	7.74 ± 0.03	1.06
5	H	CH_3	H	$OCH_2C_6H_4$-3'-NO_2	8.49 ± 0.09	7.88 ± 0.03	0.61
6	H	C_6H_5	H	$OCH_2C_6H_5$	6.59 ± 0.05	5.40	1.19
7	CH_3	CH_3	H	$OCH_2C_6H_5$	8.97 ± 0.13	8.36 ± 0.06	0.61
8	CH_3	CH_3	H	$NHCH_2C_6H_5$	8.86 ± 0.08	6.79 ± 0.02	2.06
9	$(CH_2)_3$		H	$OCH_2C_6H_5$	9.04 ± 0.14	8.46 ± 0.06	0.58
10	$(CH_2)_4$		H	$OCH_2C_6H_5$	8.75 ± 0.04	7.87 ± 0.02	0.87
11	$(-CH=CH)_2$		H	$OCH_2C_6H_5$	8.95 ± 0.09	7.30 ± 0.02	1.64
12	CH_3	CH_3	H	$NHCOC_6H_5$	8.06 ± 0.03	6.72 ± 0.03	1.34
13	CH_3	CH_3	H	$OSO_2C_6H_5$	7.80 ± 0.11	5.28 ± 0.02	2.51
14	CH_3	CH_3	H	$OSO_2C_6H_4$-4-OCH_3	6.70 ± 0.05	4.77 ± 0.01	1.93
15	CH_3	CH_3	H	$OCH_2C_6H_5$	8.41 ± 0.05	7.55 ± 0.03	0.86
16	CH_3	CH_3	H	OH	6.90 ± 0.07	5.51 ± 0.03	1.39
17	H	H	H	$OSO_2C_6H_5$	5.65 ± 0.06	4.26 ± 0.02	1.39

[b] ΔpIC_{50}: pIC_{50} Supersomes - pIC_{50} rat (Novaroli *et al.*, 2006).

Table 2.3: Supersomes and rat brain MAO-B inhibition data for 7-X-substituted benzyloxy-3,4-dimethylcoumarins (Series II).

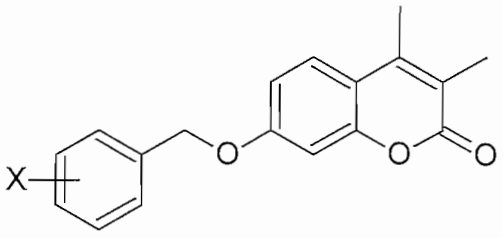

Compound	X	pIC_{50} Supersomes	pIC_{50} rat	ΔpIC_{50}[a]
18	H	8.97 ± 0.13	8.36 ± 0.06	0.61
19	2-CN	8.71 ± 0.06	7.64 ± 0.03	1.07
20	3-CH_3	8.92 ± 0.17	8.36 ± 0.06	0.56
21	3-OCH_3	8.78 ± 0.23	8.44 ± 0.04	0.34
22	3-OCF_3	8.44 ± 0.07	7.94 ± 0.03	0.51
23	3-$NHCOCH_3$	8.10 ± 0.16	6.60 ± 0.03	1.50
24	3-F	9.04 ± 0.15	8.55 ± 0.05	0.49
25	3-Cl	8.67 ± 0.15	8.48 ± 0.05	0.19
26	3-CF_3	8.37 ± 0.11	8.24 ± 0.04	0.13
27	3-CN	8.85 ± 0.02	7.97 ± 0.03	0.88
28	3-NO_2	8.96 ± 0.07	8.59 ± 0.05	0.37
29	4- CH_3	8.86 ± 0.07	8.21 ± 0.03	0.65
30	4-F	8.81 ± 0.13	8.52 ± 0.06	0.29
31	4-Cl	8.83 ± 0.05	8.59 ± 0.03	0.24
32	4-CN	8.63 ± 0.06	8.43 ± 0.05	0.19
33	4-NO_2	8.95 ± 0.06	8.07 ± 0.02	0.88
34	Pentafluoro	8.79 ± 0.07	8.23 ± 0.04	0.56

[a] $\Delta pIC50$: pIC_{50} Supersomes - pIC_{50} rat (Novaroli *et al.*, 2006).

From the above, the SAR of coumarins with MAO-B activity can be summarised as follows:

- For rat MAO-B inhibition, dimethyl substitution at positions 3 and 4 proved to be favourable (Table 2.2: **12-16**) and resulted in one of the most active inhibitors of the rat enzyme (Gnerre *et al.*, 2000).
- Compounds unsubstituted at positions 3 and 4 (Table 2.3: **18**), 4-methyl substituted (Table 2.3: **21**), or bearing cyclo-aliphatic annelation at the 3 and 4 positions (Table 2.3: **26**, **27**, **28**), showed that substitution at these positions has no remarkable influence on human MAO-B inhibitor potency (Novaroli *et al.*, 2006).
- A 7-benzylamino substituent (Table 2.3) revealed lower rat MAO-B affinity, an effect that was not observed for human MAO-B inhibition. Indeed, the 7-benzylamino derivative (**8**) and 7-benzyloxy derivative (**7**) have comparable human pIC_{50} values (Novaroli *et al.*, 2006).
- Although originally underestimated because of their low rat MAO-B inhibitory activity, compounds (Table 2.2: **1**, **4**, **8**, **9**, **10** and **11**) appear to be interesting hits to generate leads for the development of human MAO-B inhibitors (Novaroli *et al.*, 2006).
- All compounds with substitution on the phenyl ring of the 7-benzyloxy group (Table 2.3) showed high activity toward both enzymes, except derivative **23**, which appeared to be much less potent on rat MAO-B (Novaroli *et al.*, 2006).
- Replacing the coumarin nucleus by chromone leads towards a loss in activity for both MAO-A and MAO-B (Brühlmann *et al.*, 2001), thus confirming the fact that the presence of the coumarin nucleus is essential (Gnerre *et al.*, 2000).
- MAO-B inhibition activity and A/B selectivity are modulated through substitution at position 3 and/or 4, where substitutions with methyl groups at these positions increase MAO-B activity (Gnerre *et al.*, 2000).
- Phenyl and trifluoromethyl substitution in position 3 or 4 lead to compounds devoid of MAO-A and MAO-B inhibitory activity. Lipophilic substituents of limited size at position 3 and/or 4 are thus accepted by the MAO B binding site, whilst larger hydrophobic (eg CF_3, phenyl) or hydrophilic (eg. OH groups) are not well tolerated (Gnerre *et al.*, 2000).
- Substitution on position 3 alters AChE and MAO-B inhibitory activity. For example, methyl substitution on position 3 and 4 results in an increases in activity for MAO and AChE. (Brühlmann *et al.*, 2001).
- A decrease in MAO inhibitory activity is achieved through monosubstitution in position 4 with bulky phenyl, trifluoromethyl and hydroxyl groups (Brühlmann *et al.*, 2001).

- Para-substituents (Table 2.3) appeared to be favourable, (Gnerre *et al.*, 2000) while MAO inhibition are decreased through ortho-substitution (Brühlmann *et al.*, 2001).
- Substitution on position 7 of the coumarin nucleus results in an increased MAO-B inhibition activity while selectivity for the MAO-B isomer are modulated through substitution with smaller entities (eg. methyl) at position 3 and/or 4 (Gnerre *et al.*, 2000).

2.3.1.2 Caffeine derivatives

Antagonists of adenosine A_{2A} receptors such as structures **A** and **B** in figure 2.17 were reported to ameliorate motor deficits in MPTP treated animals and therefore may provide symptomatic relief in patients diagnosed with PD.

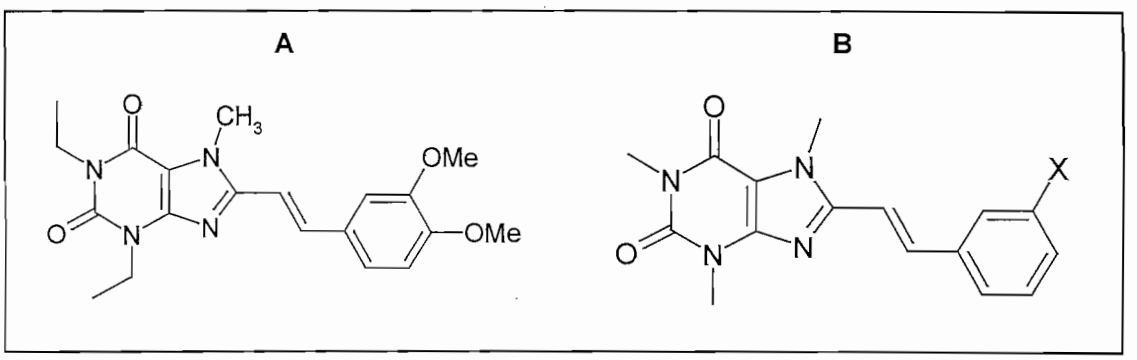

Figure 2.17: Structures of KW-6002 (**A**) and (E)-8-(3-chlorostyryl)caffeine (**B**), X=Cl (Petzer *et al.*, 2003).

Some A_{2A} antagonists also display neuroprotective properties in animal models of PD (Kanda *et al.*, 2000; Ikeda *et al.*, 2002) and are currently being investigated as possible therapeutic agents for the symptomatic treatment of motor deficits in PD (Xu *et al.*, 2005). One such compound, KW-6002 [Fig. 2.17 (**A**)] is currently undergoing clinical trials for this purpose (Shimada *et al.*, 1997; Bara-Jimenez *et al.*, 2003).

2.3.1.2.1 STRUCTURE ACTIVITY RELATIONSHIPS

(E)-8-(3-Chlorostyryl)caffeine [Fig. 2.17 (**B**)] was recently reported to be a potent and selective competitive MAO-B inhibitor (Petzer *et al.*, 2003) as well as an antagonist of adenosine A_{2A} (Suzuki *et al.*, 1993; Müller *et al.*, 1997; Jacobson *et al.*, 1993).

From the available data, the SAR of caffeine analogues for MAO can be summarised as follows:

- While caffeine was found to be a very weak inhibitor of MAO-B, 8-styryl substituted xanthinyl analogues were moderate to potent competitive inhibitors of MAO–B (Petzer *et al.*, 2003).
- Saturation of the styryl double bond (Table 2.4; **48** *vs* **38** and **49** *vs* **45**) led to reduced activity (Petzer *et al.*, 2003).

- The most potent inhibitor among the caffeine analogues was found to be (E)-8-(3,4-dichlorostyryl)caffeine (Table 2.4: **51**). The (E)-8-styrylcaffeine analogue disubstution with chlorine substitution at R_1 and R_2 of the styryl ring (**51**) was found to be a more potent inhibitor than (E)-8-(3-Chlorostyryl)caffeine (CSC) which is monosubstituted with chlorine at R_1 (Van den Berg *et al.*, 2007). This effect of disubstitution on MAO-B inhibition suggests that there exists, possibly within the entrance cavity, an aromatic binding pocket with at least two major interaction sites, one for substituents at C3 (R_1) of the aromatic ring and another for substituents at C4 (Van den Berg *et al.*, 2007).
- The (E)-8-styrylcaffeine analogue that is monosubstituted with chlorine at C4 (R_2) also inhibits MAO-B potently.
- Two other compounds (Table 2.4: **46** and **47**) also proved to be potent inhibitors of MAO-B with K_i values in the nanomolar range. Like CSC, these compounds are (E)-8-styrylcaffeinyl analogues bearing an electronegative group at the C3 position of the styryl ring (Petzer *et al.*, 2003).
- Replacement of the 1,3-dimethyl groups of R_5 and R_6 on the xanthinyl moiety with ethyl groups (Table 2.4: **42** *vs* **43**) impacted negatively on the potency of MAO-B inhibition (Petzer *et al.*, 2003).
- The 7-N-methylxanthinyl analogues (R_4) proved to be more potent inhibitors than the corresponding 7-H-xanthinyl analogues (Table 2.4: **35** *vs* **41**, **42** *vs* **36** and **45** *vs* **38**).

Table 2.4: The K_i values for the inhibition of MAO-B by (E)-8-styrylcaffeinyl analogues.

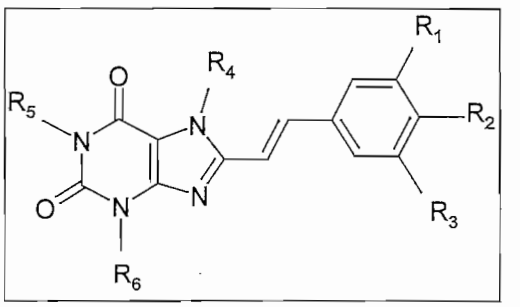

Compound	R_1	R_2	R_3	R_4	$R_{5/6}$	K_i (μM)
35*	OCH_3	OCH_3	H	H	$(CH_2)_3$	63[a]
36*	Cl	H	H	H	CH_3	1.5[a]; 8.0[b]
37*	OCH_3	OCH_3	H	H	CH_3	6[a]
38*	H	H	H	H	CH_3	31[a]
39*	F	H	H	H	CH_3	1.9[a]
40*	NO_2	H	H	H	CH_3	1.7[a]; 9[b]
41*	OCH_3	OCH_3	H	CH_3	$(CH_2)_3$	28[a]; 21[c]; 17[b,d]
42*	Cl	H	H	CH_3	CH_3	0.07[a]; 0.1[c,d]; 0.235[b]
43*	Cl	H	H	CH_3	$(CH_2)_3$	3[a] ; 30[d]
44*	OCH_3	OCH_3	H	CH_3	CH_3	2.7[a]
45*	H	H	H	CH_3	CH_3	3[a]
46*	F	H	H	CH_3	CH_3	0.4[a]
47*	NO_2	H	H	CH_3	CH_3	0.16[a]
48*	H	H	H	H	CH_3	220[b]; 183[a]
49*	H	H	H	CH_3	CH_3	30[b]; 36[a]
50•	Br	H	H	CH_3	CH_3	0.083
51•	Cl	Cl	H	CH_3	CH_3	0.036
52•	CF_3	H	CF_3	CH_3	CH_3	0.239
53•	H	Cl	H	CH_3	CH_3	2.83
54•	H	Br	H	CH_3	CH_3	2.54
55•	H	F	H	CH_3	CH_3	14.95
56•	H	CF_3	H	CH_3	CH_3	0.43
57•	H	CH_3	H	CH_3	CH_3	3.26
58•	H	OCH_3	H	CH_3	CH_3	5.82
59▲	Cl	H	H	CH_3	CH_3	0.07
60▪	CF_3	H	H	CH_3	CH_3	0.133
61▪	CH_3	H	H	CH_3	CH_3	1.431
62▪	H	Cl	H	CH_3	CH_3	0.260
63▪	H	CF_3	H	CH_3	CH_3	0.245
64▪	H	CH_3	H	CH_3	CH_3	0.367
65▪	H	F	H	CH_3	CH_3	1.559

[a] Baboon liver mitochondria.
[b] Human liver mitochondria.
[c] C57BL/6 mouse brain mitochondria.
[d] MPTP was used as substrate.
* Values obtained from Petzer *et al.*, 2003.
▪ Values obtained from Vlok *et al.*, 2006.
• Values obtained from Van den Berg *et al.*, 2007.
▲ Values obtained from Chen *et al.*, 2002

- The *trans* geometry is required because the cis isomer of KW-6002 [Fig. 2.17 (**A**)] was inactive as a MAO-B inhibitor (Petzer *et al.*, 2003).
- MAO-B inhibition activity depends upon the electronic characteristics of the phenyl C3 (R_1) substituent (Table 2.4: **59-61**), since those analogues with electron-withdrawing groups (Table 2.4: **59**, **60**) are significantly more potent as inhibitors than the unsubstituted analogue (Table 2.4: **53-58**) and the analogue bearing an electron-donating methyl group (Vlok *et al.*, 2006).
- MAO-B inhibition activity (Table 2.4: **53** and **54-57**) appears to be dependent upon the size of the C4 (R_2) substituent since inhibitors with relatively bulky substituents (Table 2.4: **53**,**54**,**57**) are more potent than the unsubstituted analogues (Table 2.4: **49**) and the corresponding analogue bearing a C4 fluorine (Table 2.4: **55**) substituent (Vlok *et al.*, 2006).

2.4 CONCLUSION

From the enzyme topology and the SAR of both the coumarin and caffeine derivatives it is clear that compounds with an extended overall topology, sufficient lipophylicity and hydrogen bond capacity should favour MAO-B enzyme interaction. In the series described above, the coumarin compounds exhibited a desirable activity profile and will be conjugated with other neuroprotective moieties such as the caffeine ring and the polycyclic structure for evaluation of MAO-B inhibition.

Chapter 3

Materials and methods

3.1 INTRODUCTION

3.1.1 Rationale of selected compounds

Coumarins exhibit a broad spectrum of pharmacological activity with respect to competitive, reversible and selective MAO-B and AChE inhibition (Novaroli *et al.*, 2006). Structure activity relationship (SAR) studies revealed that substitution in position 7 (Fig. 3.1 **A**) resulted in high inhibitor activity toward the MAO enzyme (Novaroli *et al.*, 2006), while MAO A/B selectivity are obtained through substitution with smaller groups (Table 2.2. **1** *vs.* **4**) at position 3 and/or 4 (Gnerre *et al.*, 2000).

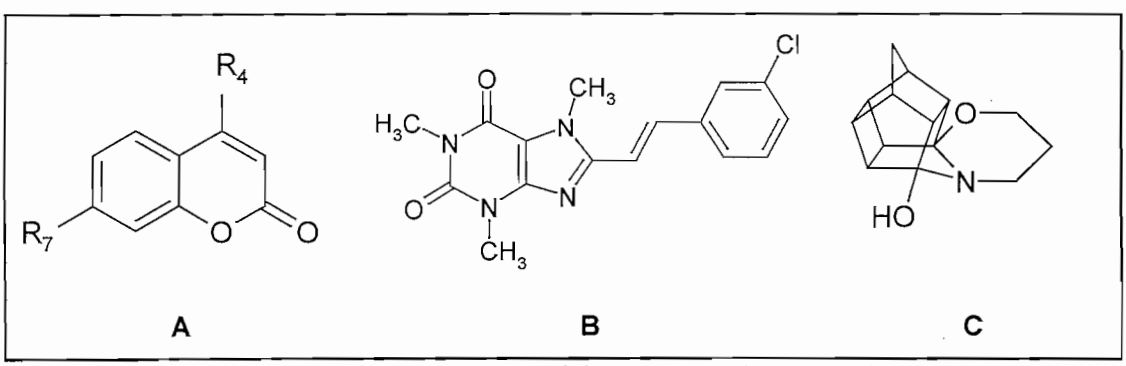

Figure 3.1: Structures of importance in this study. (**A**) coumarin, (**B**) (E)-8-(3-chlorostyryl)caffeine (**C**) 3-hydroxy-4-aza-8-oxaheptacycotetradecane.

Adenosine A_{2A} antagonists are currently being investigated as possible therapeutic agents for the symptomatic treatment of motor deficits in PD. (E)-8-(3-Chlorostyryl)caffeine (Fig. 3.1 **B**) was recently reported to be a potent and selective competitive MAO-B inhibitor (Petzer *et al.*, 2003) and an antagonist of adenosine A_{2A} recptors (Suzuki *et al.*, 1993).

The 3-hydroxy-4-aza-8-oxaheptacyclotetradecane (Fig. 3.1 **C**) possesses promising pharmacokinetic and pharmacodynamic properties that may find application in the treatment of neurodegenerative diseases. This includes favourable blood-brain barrier permeability and antagonism of the NMDA receptor, thus preventing cytoplasmic Ca^{2+} influx and eventually neuronal cell death. These compounds, when conjugated might therefore modify and improve

the pharmacokinetic and pharmacodynamic properties of currently available drugs (Geldenhuys *et al.*, 2005; Randall & Thayer., 1992).

The aim of this study was to conjugate the coumarin moiety with the caffeine and tetradecane structure to obtain MTLs with neuroproptective properties. These drugs should clearly prevent oxidative stress through MAO-B inhibition and possibly counteract Aβ aggregation via AChE inhibition.

3.1.2 Proposed compounds

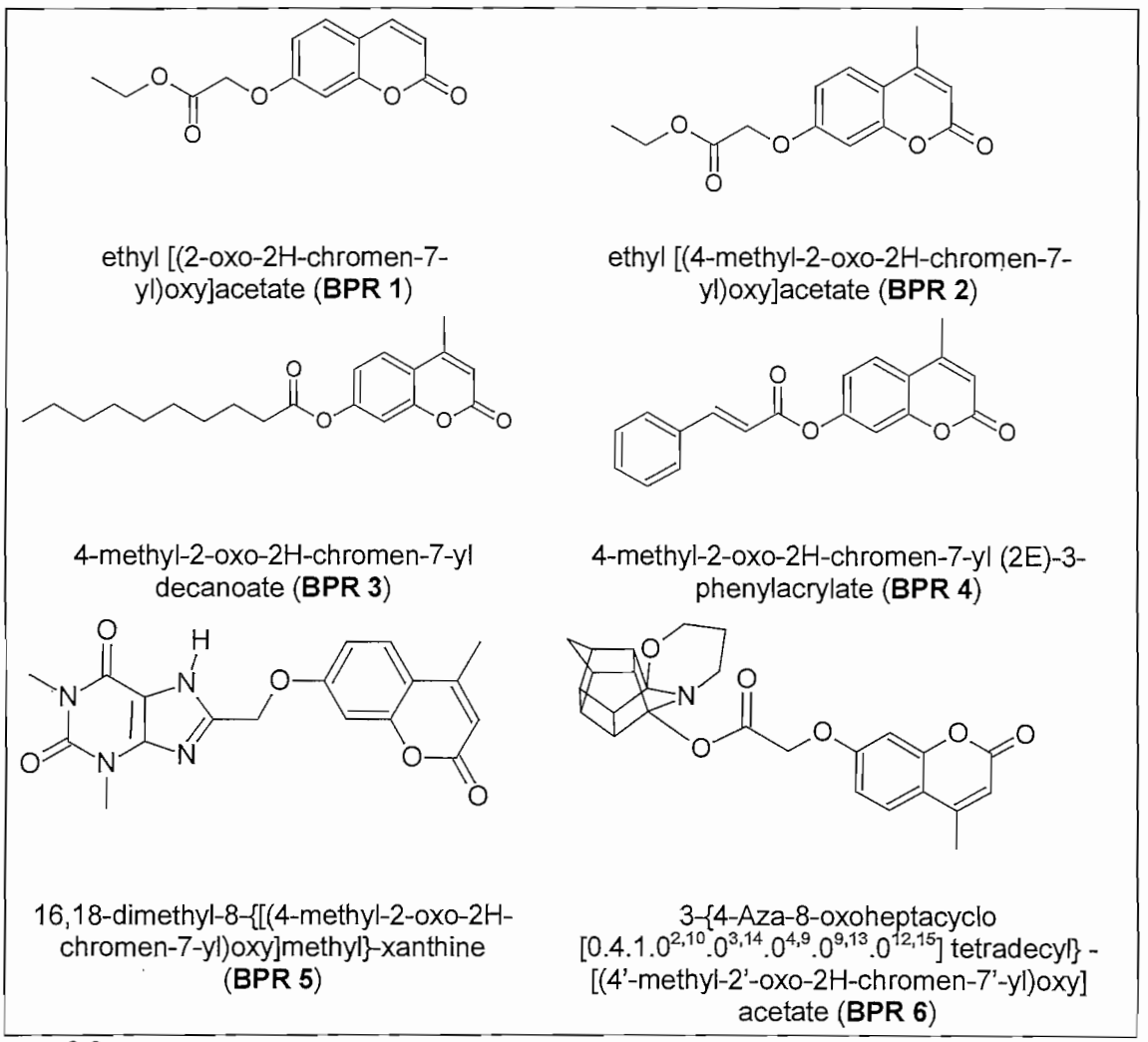

Figure 3.2: The compounds selected for this study.

In this study a series of 7-substituted coumarin derivatives (Fig. 3.2) were synthesised, evaluated for MAO-B inhibition and submitted to molecular modelling studies. Compounds **BPR 1-3** represent the optimisation of the coumarin pharmacophore while compounds **BPR 4-6** represents the conjugation of the neuroprotective entities.

3.1.3 Pharmacokinetics

The blood-brain barrier (BBB) is a membranic structure, composed of tightly packed endothelial cells. This arrangement of high density cells protects the brain from chemicals in the blood, while still allowing essential metabolic functions. This protective role however restricts the delivery of many potentially important therapeutic agents to the brain. Understanding the role of the physicochemical properties in membrane permeability relevant to important processes such as blood-brain barrier crossing, brings rational drug delivery more within reach and some models have been developed to describe this concept mathematically.

The following guidelines for compounds intended to enter the brain are presented.

- For good blood-brain barrier permeation, the compound's polar surface area (PSA) should be below a certain limit. The PSA is a measure of a molecule's hydrogen-bonding capacity and is commonly calculated by summing the contributions to the molecular surface area from oxygen and nitrogen atoms. Kelder *et al.* (1999) proposed a limit of 60-70 $Å^2$ while Van de Waterbeemd *et al.* (1998) suggested a much higher limit of 90 $Å^2$. The molecular weight should be restricted below 450 Da to facilitate brain permeation (Van de Waterbeemd *et al.*, 1998).
- If the sum of the nitrogen and the oxygen (N + O) atoms in the molecule is five or less, the compound should enter the BBB (Norinder & Haeberlein., 2002).
- If C log P_{oct} – (N + O) > 0, then the ratio of the steady-state concentrations of the compound in the brain to those in the blood, denoted as log BB, is likely to be positive. In this rule, C log P_{oct} denotes the logarithm of the n-octanol-water partition coefficient (P_{oct}) of a compound. P_{oct} is the ratio of the concentration of the compound in octanol to the concentration of the compound in water (Norinder & Haeberlein., 2002).
- The log P_{oct} value should be in the region of 2. The logarithm of the n-octanol-water partition coefficient (log P_{oct}) is an expression of lipophilicity which is essential for optimum diffusion into the central nervous system (Levin, 1980).
- A log D_{oct} value in the range 1-3 is recommended (Van de Waterbeemd *et al.*, 1998). Log D is the logarithm of the distribution coefficient (D) of a compound. D is the ratio of the sum of the concentrations of all species of the compound in octanol to the sum of the concentrations of all species of the compound in water. For neutral compounds, log D is equal to log P_{oct}.

Table 3.1: Physicochemical properties of synthesised compounds.

Compound	Log D	PSA (Å^2)	Molecular weight (Da)	Log P
BPR 1	1.11	61.83	248.23	1.11 ± 0.30
BPR 2	2.18	61.83	262.26	2.18 ± 0.40
BPR 3	6.11	52.60	330.42	6.11 ± 0.38
BPR 4	3.84	52.60	306.31	3.84 ± 0.44
BPR 5	1.22	91.42	368.35	1.62 ± 0.57
BPR 6	2.18	74.30	447.49	2.18 ± 0.66

The influence of electronic properties, resonance and steric effects like conformational crowding and molecular folding on lipophilicity, should also be considered (Leo *et al.*, 1971). BBB permeability may be enhanced by simply increasing the side chain length attatched to the coumarin (**BPR 3**) or by conjugation with a *trans* aromatic moiety while keeping the ester unit intact at position 7 (**BPR 4**). Incorporating a limited number of polar entities (**BPR 1** & **BPR 2**) or conjugating the coumarin with certain neuroprotective moieties (**BPR 5** & **BPR 6**) might have additional advantages.

Parameters (Table 3.1) were computed using the LogD and LogP suite of ACD® version 4.0 software for Microsoft Windows®.

3.2 STANDARD EXPERIMENTAL PROCEDURES

3.2.1 Materials

All starting materials were purchased from Sigma-Aldrich (Steinheim, Germany), Merck (Wadeville, South Africa) and SAARCHEM (Wadeville, South Africa), unless specified elsewhere, and were used without further purification.

3.2.2 Instrumentation

3.2.2.1 Nuclear Magnetic Resonance Spectroscopy (NMR)

Proton (^{1}H) and carbon (^{13}C) NMR spectra were recorded on a Varian Gemini 300 spectrometer. Proton (^{1}H) spectra were recorded at a frequency of 300 MHz and carbon (^{13}C)

spectra at 75 MHz. This was done in a 7 Tesla magnetic field and tetramethylsilane (TMS) was used as internal standard. A bandwidth of 1000 MHz at 24 kG was applied for ^{1}H-^{13}C-decoupling. Chemical shifts are reported in parts per million (δ) downfield from the signal of tetramethylsilane TMS (δ = 0) dissolved in either deuterated chloroform ($CDCl_3$-D1) or dimethyl sulphoxide (DMSO-D6). Spin multiplicities are given as s (singlet), d (doublet), t (triplet) or m (multiplet) and the coupling constants (J) are given in hertz (Hz).

3.2.2.2 Mass Spectroscopy (MS)

The MS spectra were recorded on an analytical VG 70-70E mass spectrometer using fast atom bombardment (FAB) or electron ionization (EI at 70 eV) as ionisation techniques.

3.2.2.3 Melting Point (MP) Determination

Melting points were determined using a Stuart SMP-300 melting point apparatus and capillary tubes. The melting points are uncorrected.

3.2.3 Chromatographic Techniques

3.2.3.1 Thin Layer Chromatography (TLC)

Analytical TLC was performed on 0.20 mm aluminium silica gel sheets (Alugram® SIL G/UV254, Kieselgel 60, Macherey-Nagel, Düren, Germany). Mobile phases were prepared on a volume-to-volume basis using the Prism model of Nyiredy *et al.* (1985), and visualisation was achieved using UV light (254 nm and 366 nm), iodine vapours or an ethanol solution of ninhydrin.

3.2.3.2 Column Chromatography

Product mixtures were purified using standard glass columns varying in size. Flash column chromatography was applied to some of the mixtures. The stationary phase used was silica gel (0.063 – 0.200 mm/70 – 230 mesh ASTM, Macherey-Nagel, Düren, Germany) with mobile phases as indicated for each compound.

3.3 SYNTHESIS

3.3.1 Polycyclic compounds

The route of synthesis (Fig. 3.3) included the preparation of the well known Cookson diketone (**D**), which was formed by the photocyclisation of the Diels-Alder adduct (**C**) resulting from the reaction between p-bensoquinone (**A**) and cyclopentadiene (**B**) (Cookson *et al.*, 1964). Further

reaction with the diketone with 3-amino-1-propanol yielded the rearranged 3-hydroxy-4-aza-8-oxaheptacyclotetradecane (**G**) (Prins *et al.*, 2007).

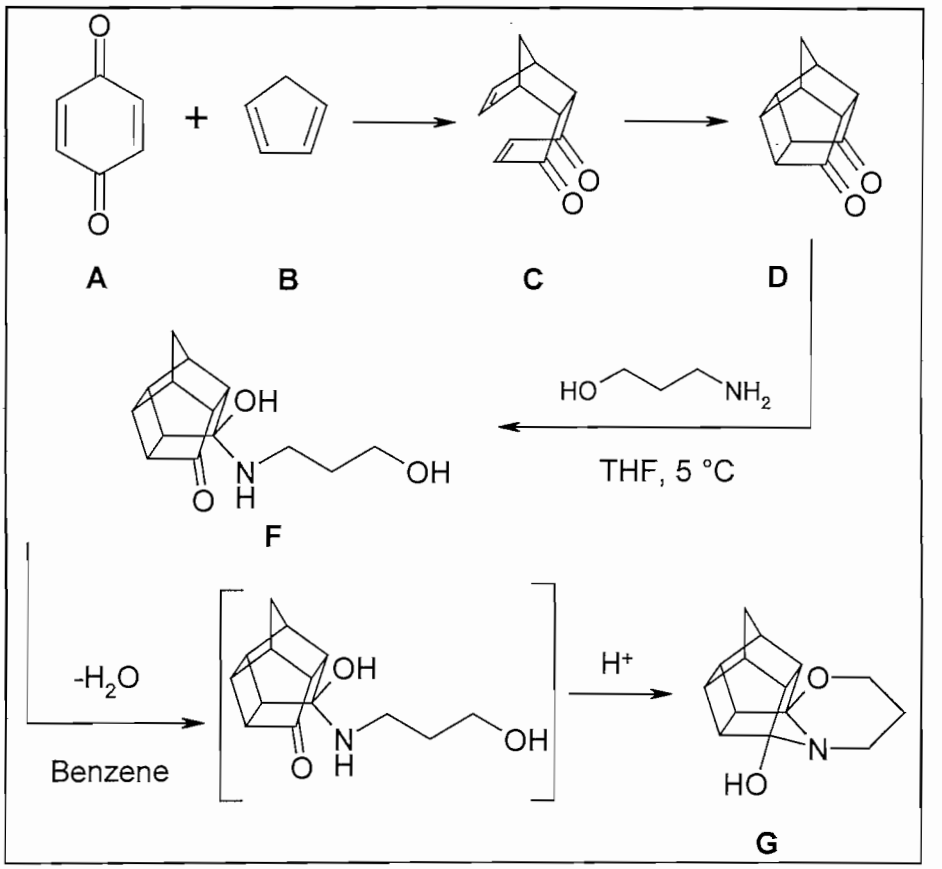

Figure 3.3: The synthesis of the 3-hydroxy-4-aza-8-oxaheptacyclotetradecane (**G**).

3.3.2 5,6-Diaminouracil for caffeine synthesis

The preparation of 5,6-diaminouracil was accomplished using the method described by Blicke & Godt (1954). N,N'-Dimethylurea (**H**) and cyanoacetic acid (**I**) in acetic anhydride were heated, with the exclusion of moisture at 60 °C for 3 hours. The excess anhydride and the acetic acid formed during the reaction were removed under reduced pressure. A 5% sodium hydroxide solution was added slowly to the cooled, stirred residue (**J**) whereupon the 1,3-dimethyl-6-amino-uracil (**K**) precipitated.

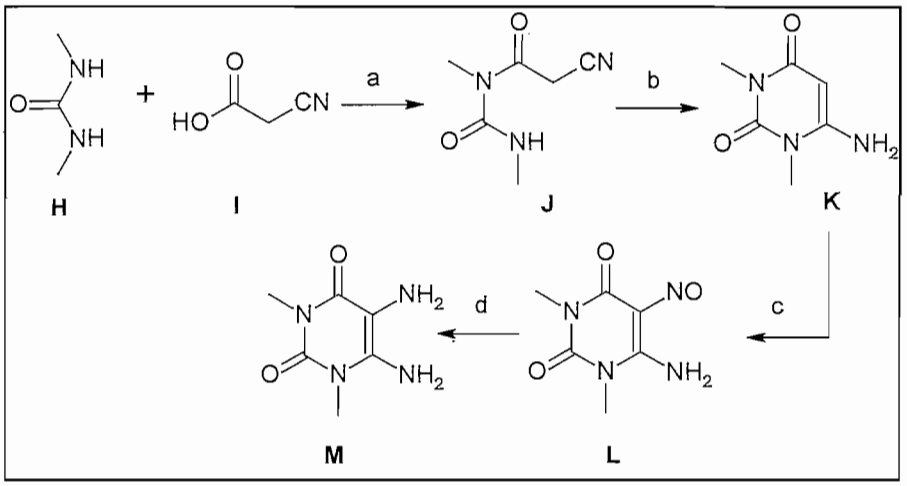

Figure 3.4: Synthetic pathway to substituted 5,6-diaminouracil derivatives (**M**). (**a**) acetic anhydride. (**b**) NaOH (aq). (**c**) $NaNO_2$, CH_3CO_2H. (d) $Na_2O_4S_2$.

An aqueous solution of sodium nitrite was added to the cooled, stirred mixture of **K** and the reaction was acidified by the dropwise addition of acetic acid (37%) over a period of 20 minutes. The stirring was continued for an additional 3 hours at room temperature. The mixture was thoroughly cooled, the violet precipitate (**L**) was filtered and washed with water and diethylether.

To compound **L** was added 35% ammonia solution. The resulting yellow-orange ammonium salt was warmed on a oil bath, stirred and a solution of sodium hydrosulfide in water was added during a 20 minute period. The salt was dissolved and the solution was stirred and heated for 15 minutes. After cooling to 0 °C the white precipitate (**M**) that formed was collected by filtration.

3.3.3 Coumarin and conjugation thereof

Williamson etherfication (Fig. 3.5) of 7-hydroxycoumarin (**O**) and 4-methyl-7-hydroxycoumarin (**P**) with ethylbromoacetate yielded the corresponding coumarin methoxy esters, **BPR 1** and **BPR 2**. The coumarin methoxy ester (**BPR 2**) was hydrolysed using KOH to yield the corresponding coumarin carboxylic acid **S**. This acid was subsequently conjugated to the 3-hydroxy-4-aza-8-oxaheptacyclotetradecane compound (**G**) using activation chemistry with DCC (N,N - dicyclohexylcarbodiimide) and DMAP (4 - dimethylaminopyridine) as a catalyst to give the coumarin polycyclic cage compound ester (**BPR 6**). In addition, the acid (**S**) was conjugated to the caffeine moeity using EDAC [1-ethyl-3-(3 - dimethylaminopropyl) carbodiimide hydrochloride] to yield the coumarin caffeine conjugate (**BPR 5**). To investigate the effect of chain length and a *trans* geometry, compound **P** was subjected to esterfication with *trans* cinnamoyl chloride and decanoyl chloride to yield **BPR 3** and **BPR 4**.

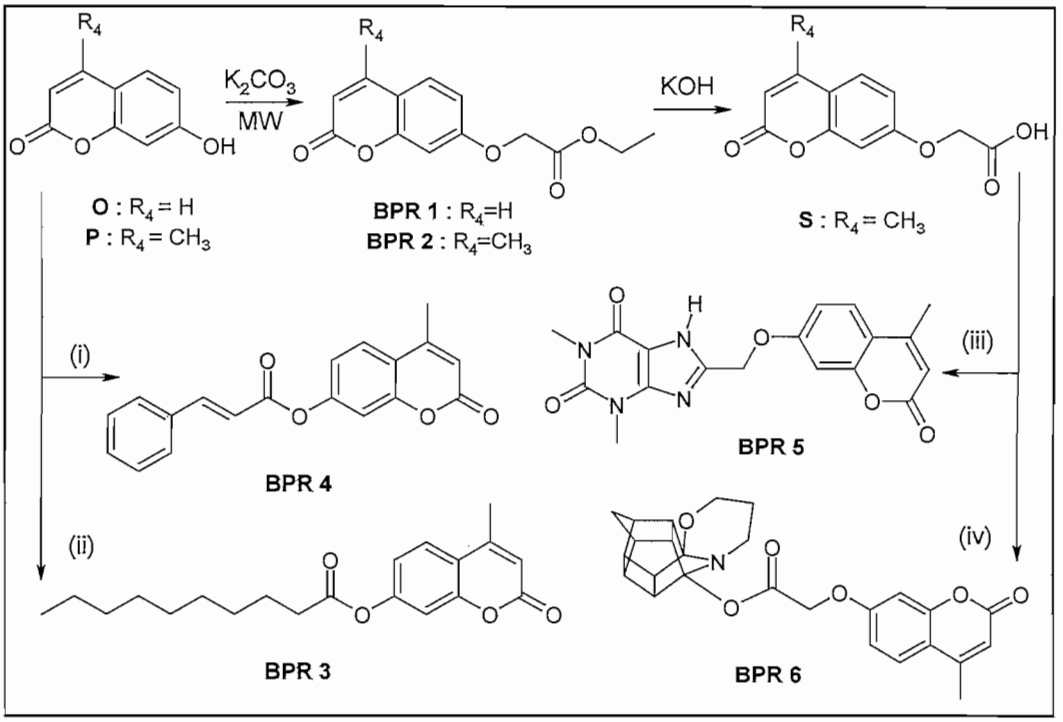

Figure 3.5: General outline of the synthesis of the test compounds. (**i**) THF, NaH, *trans* cinnamoyl chloride. (**ii**) THF, NaH, decanoyl chloride. (**iii**) Dioxane/H_2O, EDAC, 1,3-dimethyl-5,6-diaminouracil (**M**), NaOH. (**iv**) THF, DDC, DMAP, 3-hydroxy-4-aza-8-oxaheptacyclo tetradecane (**G**).

3.4 SYNTHETIC PROCEDURES

3.4.1 Pentacyclo[5.4.0.$0^{2,6}$.^{03,10}.$0^{5,9}$]undecane-8,11-dione (D)

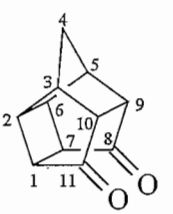

p-Benzoquinone (10 g, 9.251 mmol) was dissolved in dried benzene (400 ml) and oxidised with MnO_2 (50 mg) by refluxing the mixture for 20 minutes. The reaction mixture was protected from light by means of aluminium foil. 5 Spatula (20 mm) measures of activated charcoal were added and the mixture was allowed to reflux for a further 5 minutes. This was done in order for fine impurities to be absorbed from the reaction mixture. The hot mixture was vacuum-filtered through Celite® to produce a clear yellow solution. Recrystallisation of the freshly oxidised p-

benzoquinone was suppressed by flushing the same filtering system with dried methanol (100 ml). This solution was cooled to 5 °C by placing it in an external ice bath. Freshly monomerised cyclopentadiene (12.229 g, 9.251 mmol) was slowly and stoichiometrically added keeping the reaction temperature between 5 and 18 °C. The reaction was monitored by means of TLC and presumed complete as soon as the p-benzoquinone spot was no longer visible on the TLC plate. The photolabile reaction mixture was removed from the external ice bath, protected from light and stirred for 1 hour at room temperature. Thereafter 3 spatula measures of activated charcoal were added and the mixture stirred at room temperature for a further 30 minutes. Removal of the activated charcoal, followed by in vacuo evaporation of benzene resulted in the formation of an intensely coloured amber oil. Excess solvent was allowed to fully evaporate in a dark fume hood to afford the yellow Diels-Alder adduct crystals. The crystals were dissolved in ethyl acetate (4 g per 100 ml) and irradiated with UV light for 6 hours, using a photochemical reactor. Decolouration of the solution indicated that cyclisation of the adduct was complete. Evaporation of the solution afforded a light yellow residue, which was purified by Soxhlett extraction with cyclohexane to produce the cage compound as fine white crystals (Yield: 13 g, 7.471 mmol, 80.759 %). The physical characteristics (melting point = 245 °C) of these crystals correlated with that in Cookson *et al.* (1958, 1964) and therefore no spectral data is presented.

3.4.2 3-Hydroxy-4-aza - 8 - oxoheptacyclo - [9.4. $1.0^{2,10}.0^{3,14}.0^{4,9}.0^{9,13}.0^{12,15}$] tetradecane (G)

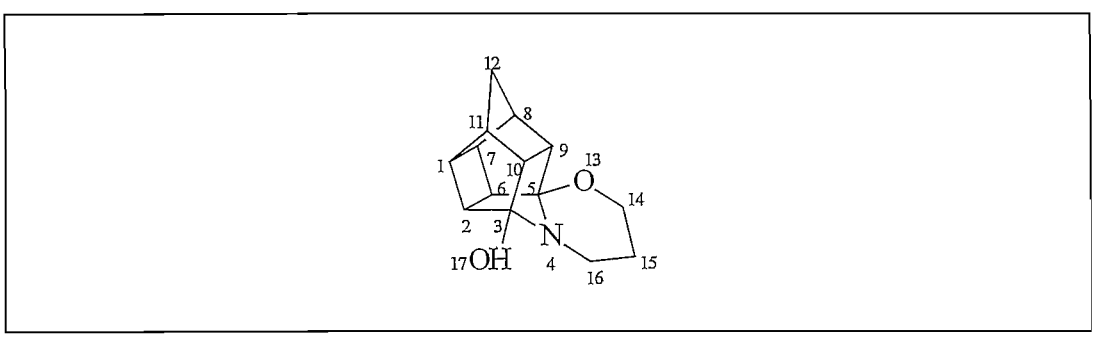

Pentacyclo[5.4.$0^{2,6}$.$0^{3,10}$.$0^{5,9}$]undecane-8,11-dione (**D**, 3 g, 17.24 mmol) was dissolved in 30 ml of tetrahydrofuran (THF) and cooled down to 5 °C while stirring in an ice bath. 3-Amino-1-propanol (**E**) (1,311 ml, 17.22 mmol), dissolved in 6 ml THF, was added slowly with continued stirring of the reaction mixture at 5 °C. The carbinolamine (**F**) started precipitating after approximately 15 min, and the reaction was stirred for a further 30 min. Water was azeotropically removed from the reaction mixture by refluxing it in 60 ml dry benzene using a Dean-Stark apparatus for 1 hour or until water collection was no longer observed. The benzene was removed under reduced pressure and the rearranged cage was obtained as a yellow oil, which was crystallised from THF to render the final product as a colourless crystalline solid (**G**).

(Yield: 3 g, 12.987 mmol, 75.33 %). The physical characteristics (see below) of the precipitate correlated with that cited in Prins (2007), and therefore no spectral data is presented.

Physical data: $C_{14}H_{17}NO_2$; **mp**: 171-173 °C.

3.4.3 Ethyl [(2-oxo-2H-chromen-7-yl)oxy] acetate (BPR 1)

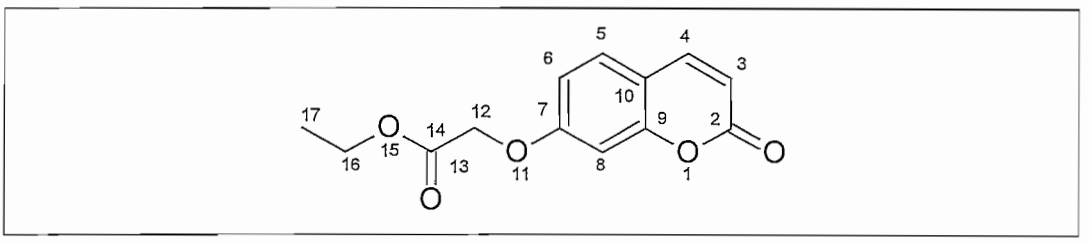

A solution of 7-hydroxycoumarin (1.005 g, 6.17 mmol), ethyl bromoacetate (2.054 g, 12,3 mmol) and anhydrous K_2CO_3 (1.700 g, 12,3 mmol) in dry DMF (15 ml) was irradiated in a household microwave oven (MW) at 200 W (defrost setting) for 4½ minutes. After irradiation, the mixture was filtered. Cold water (20 ml) was added to the solution and it was extracted into ethyl acetate (3 X 15 ml) and CH_2Cl_2 (3 X 15 ml). The organic phase extracts were combined, dried over with anhydrous $MgSO_4$, filtered and concentrated in vacuum. The residue was recrystallised to afford **BPR 1** as a white solid (Yield: 82.7 %, 1.266g, 5.1 mmol).

Physical and spectral data: $C_{13}H_{12}O_5$; **mp**: 108-108 °C; ^{1}**H NMR** (300 MHz, $CDCl_3$) δ_H (Spectrum 1): 7.59 (d, J = 8.96 Hz, 1H, H-4), 7.36 (d, J = 8.57 Hz, 1H, H-5), 6.85 (dd, J = 2.51 Hz. J = 6.11 Hz, 1H, H-6), 6.74 (d, J = 2.50 Hz, 1H, H-8), 6.23 (d, J = 9.48 Hz, 1H, H-3), 4.63 (s, 2H, H-12), 4.25 (q, J = 7.14 Hz, 2H, H-16), 1.27 (t, J = 1.17 Hz, 3H, H-17). ^{13}**C NMR** ($CDCl_3$) δ_C (Spectrum 7): 167.84 (C-14), 160.79 (C-2), 155.62 (C-7), 143.13 (C-9), 128.91 (C-4), 113.71 (C-5/6), 113.29 (C-5/6), 112.78 (C-10), 101.71 (C-3/4), 65.37 (C-12), 61.65 (C-16), 14.08 (C-17); **MS** (EI, 70 eV) *m/z* (Spectrum 13): 248 (M^+), 220, 175, 145, 133, 89, 77, 51, 29.

3.4.4 Ethyl [(4-methyl-2-oxo-2H-chromen-7-yl)oxy] acetate (BPR 2)

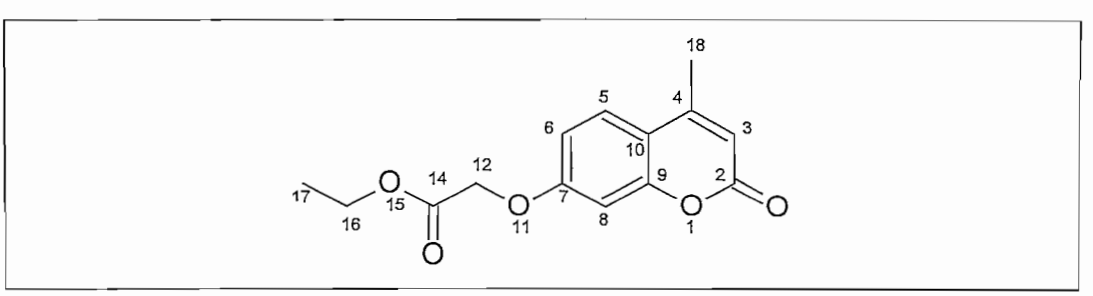

A solution of 4-methyl-7-hydroxycoumarin (1.0869 g, 6.17 mmol), ethyl bromoacetate (2.054 g, 12,3 mmol) and anhydrous K_2CO_3 (1.700 g, 12,3 mmol,) in dry DMF (15 ml) was irradiated in a

household microwave oven (MW) at 200 W (defrost setting) for 5 minutes. After irradiation, the mixture was filtered. Cold water (20 ml) was added to the solution and it was extracted with ethyl acetate (3 X 15 ml) and CH_2Cl_2 (3 X 15 ml). The organic phase extracts were combined, dried over with anhydrous $MgSO_4$, filtered and concentrated in vacuo. The residue was recrystallised to afford **BPR 2** as colourless needles (Yield: 86.4%, 1.398 g, 5.33 mmol).

Physical and spectral data: $C_{14}H_{14}O_5$; **mp**: 101-104°C; **^{1}H NMR** (300 MHz, $CDCl_3$) δ_H (Spectrum 2): 7.47 (d, J = 8.82 Hz, 1H, H-5), 6.85 (dd, J = 2.58 Hz , J = 8.84 Hz, 1H, , H-6), 6.72 (d, J = 2.60 Hz, 1H, , H-8), 6.09 (s, 1H, H-3), 4.63, (s, 2H, H-12), 4.23 (q, J = 7.14 Hz, 2H, , H-16), 2.34 (s, 3H, H-18), 1.26 (t, J = 7.41 Hz, 3H, H-17); **^{13}C NMR** ($CDCl_3$) δ_C (Spectrum 8): 167.88 (C-14), 160.91 (C-2), 154.97 (C-9), 152.31 (C-7), 125.69 (C-5/6), 114.32 (C-5/6), 112.42 (C-10), 112.38 (C-3/4), 101.68 (C-3/4), 65.30 (C-12), 61.59 (C-16), 18.25 (C-18), 14.05 (C-17), **MS** (EI, 70 eV) *m/z* (Spectrum 14): 262 (M^+), 234, 189, 159, 147, 91, 77, 55.

3.4.5 [(4-Methyl-2-oxo-2H-chromen-7-yl)oxy] acetic acid (S)

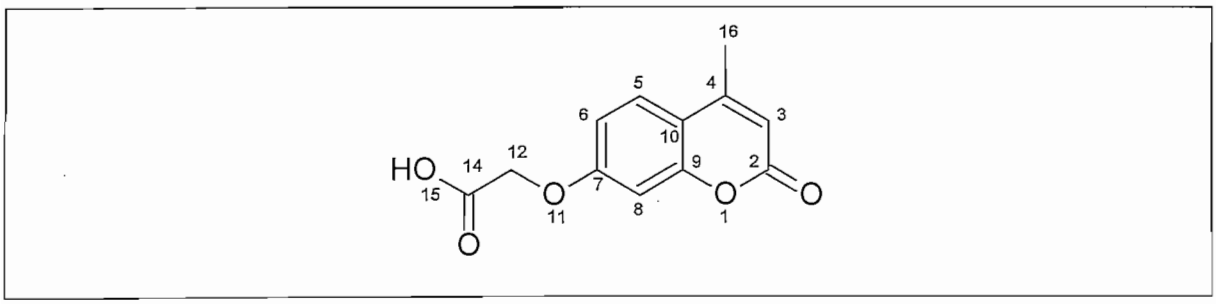

A mixture of **BPR 2** (2.640 mg, 3.2 mmol), KOH (11.754 mg , 63.9 mmol) and 10 ml water was ground in a mortar under heating (below 70 °C) over a period of 30 min. After cooling, the pH of the solution was adjusted to 1 with 12 N HCl. The precipitate was filtered, washed with water and methanol, and dried to afford a white solid (**S**) (Yield: 46.8%, 0.351 g, 1.5 mmol).

Physical and spectral data: $C_{12}H_{10}O_5$; **mp**: 205-208 °C; **^{1}H NMR** (300 MHz, $CDCl_3$) δ_H (Spectrum 3): 7.65 (d, J = 8.61 Hz, 1H, H-5), 6.93 (dd, J = 7.17 Hz, 1H, H-6), 6.92 (d, J = 2.20 Hz, 2H, H-8), 5.47 (s, 1H, H-3), 2.00 (s, 2H, H-12), 1.88 (s, 3H, H-16). **^{13}C NMR** ($CDCl_3$) δ_C (Spectrum 9): 169.57 (C-13), 160.74 (C-2), 160.01 (C-7), 154.50 (C-9), 153.24 (C-4), 126.40 (C-5/6), 113.49 (C-5/6), 112.2 (C-10), 111.35 (C-3), 101.47 (C-8), 64.84 (C-16), 18.05 (C-12), **MS** (EI, 70 eV) *m/z* (Spectrum 15): 234 (M^+)206, 147, 91, 77, 55.

3.4.6 4-Methyl-2-oxo-2H-chromen-7-yl decanoate (BPR 3)

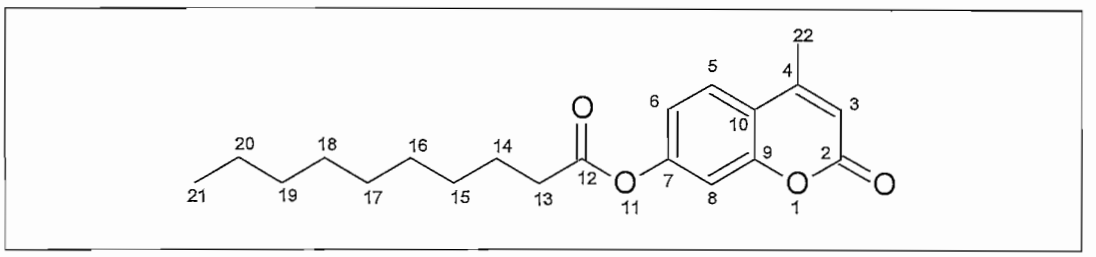

A solution of 4-methyl-umbelliferone (217 mg, 1.23 mmol) in anhydrous THF (3 ml) was treated with NaH (98 mg of a 80% suspension in oil, 2.829 mmol) and stirred for 30 min at 25 °C and was then allowed to cool down to 0 °C. The decanoyl chloride (353 mg, 1.85 mmol) was added as a solution in dry THF and stirred for 3 hours at 25 °C. The reaction mixture was poured into water (50 ml) and extracted with dichloromethane (3 X 15 ml). The organic phase was dried over Na_2SO_4, concentrated and precipitated from dichloromethane/hexane (9:1) to yield a white solid **BPR 3** (Yield: 78%, 0.96 mmol, 317 mg).

Physical and spectral data: $C_{20}H_{26}O_4$; **mp**: 46-49 °C; **^{1}H NMR** (300 MHz, DMSO-D6) δ_H (Spectrum 4): 7.58 (d, J = 6.77 Hz, 1H, H-5), 7.09 (dd, J = 8.50 Hz, 1H, H-6), 6.01 (d, J = 1.40 Hz, 1H, H-8), 6.20 (s, J = 1.15 Hz, 1H, H-3), 2.53 (t, J = 2.81 Hz, 2H, H-21), 2.37 (s, 3H, H-4), 1.74 (m, 2H, , H-18,19,14,20), 1.29 (m, 2H, H-17,16,15,14), 0.82 (t, J = 7.2 Hz, 3H, H-22), **^{13}C NMR** (DMSO-D6) δ_C (Spectrum 10): 171.56 (C-12), 160.45 (C-2), 154.18 (C-7), 153.85 (C-9), 125.27 (C-5/6), 121.52 (C-8), 118.06 (C-5/6), 117.43 (C-10), 114.43 (C-3/4), 110.40 (C-3/4), 34.32 (C-13), 31.81 (C-14), 29.36 (C-15), 29.19 (C-16), 24.77 (C-17), 22.61 (C-18), 18.63 (C-19), 15.10 (C-22), 14.04 (C-20), 12.3 (C21); **MS** (EI, 70 eV) *m/z* (Spectrum 16): 330 (M^+), 176, 148, 91, 43.

3.4.7 4-Methyl-2-oxo-2H-chromen-7-yl-(2E)-3-phenylacrylate (BPR 4)

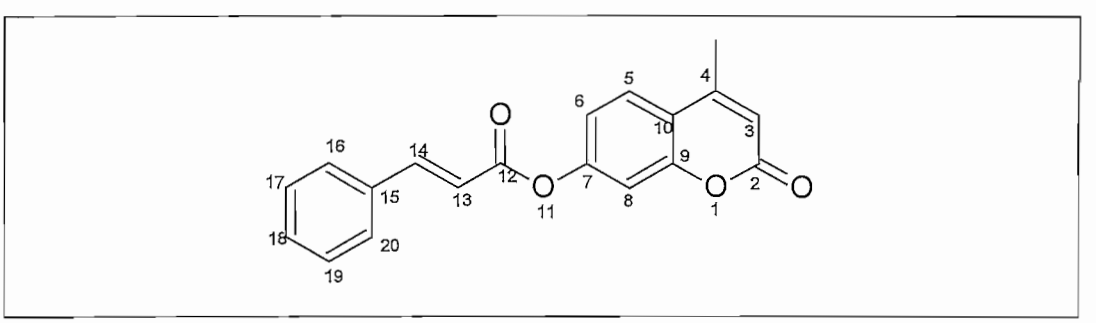

A solution of 4-methyl-umbelliferone (217 mg, 1.23 mmol) in anhydrous THF (3 ml) was treated with NaH (98 mg, 80% suspension in oil) and stirred for 30 min at 25 °C and then cooled down to 0 °C. The *trans* cinnamoyl chloride (308 mg, 1.85 mmol) was added as a solution in dry THF and the mixture was stirred for 3 hours at 25 °C. The reaction mixture was poured into water

(50 ml) and extracted with dichloromethane (3 X 15 ml). The organic phase was dried over Na_2SO_4, concentrated and precipitated from DCM/hexane (8:2) to yield a white solid **BPR 4** (Yield: 73 %, 290 mg, 0.90 mmol). The physical characteristics of these crystals correlated with that cited in Nakayama & Kanaoka, (1973), and therefore no spectral data is presented.

Physical data: $C_{19}H_{14}O_4$; **mp**: 148-151 °C; **MS** (EI, 70 eV) *m/z* (Spectrum 17): 306 (M^+), 131, 91, 77, 51.

3.4.8 16,18-Dimethyl-8-{[(4-methyl-2-oxo-2H-chromen-7-yl)-oxy]methyl}-xanthine (BPR 5)

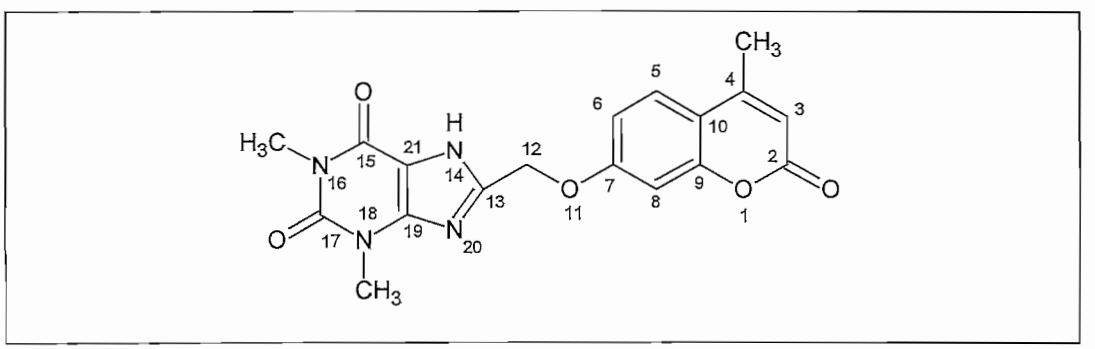

The preparation of **BPR 5** was accomplished using the procedure described by Suzuki *et al.* (1993). To a solution of 1,3-dimethyl-5,6-diaminouracil (**M**), (460 mg, 2.7 mmol) and 1-ethyl-2-[3-(dimethylamino)propyl]-carbodiimide hydrochloride (EDAC; 748 mg, 3.9 mmol) in 20 ml dioxane/H_20 (1:1) was added the coumarin acetic acid (**S**) (680 mg, 2.9 mmol). The pH of the suspension was adjusted to 5 with 2 N aqueous hydrochloric acid and stirring was continued for an additional 2 hours. Following neutralisation with 1 N aqueous sodium hydroxide the reaction was cooled to 0 °C and the precipitate was collected by filtration. The crude product was dissolved in 30 ml aqueous sodium hydroxide (1 N)/dioxane (1:1) and refluxed for 45 minutes. After cooling to 0 °C the solution was acidified to a pH of 4 with 4 N aqueous hydrochloric acid and the resulting precipitate was collected by filtration. Methylation of the heterocyclic amine was attempted, but the product presented with solubility problems and could not be characterised (Yield: 81.4%, 733 mg, 2.2 mmol).

Physical and spectral data: $C_{18}H_{16}N_4O_5$; **mp**: 240-242 °C. **^{1}H NMR** (300 MHz, DMSO-D6) δ_H (Spectrum 5): 7.975 (d, J = 1.086, 1H, H-3), 7.637 (d, J = 2.754, 1H, H-5), 7.038 (d, J = 2.203, J = 4.165, 1H, H-8), 6.294 (d, J = 1.0315, 3H, H-4), 5.242 (s, 2H, H-12), 3.419 (s, 3H, H-16), 3.220 (s, 3H, H-18), **^{13}C NMR** (DMSO-D6) δ_C (Spectrum 11): 160.704 (C-2), 160.105 (C-15), 155.140 (C-17), 154.378 (C-7), 151.109 (C-9), 147.794 (C-15), 147.620 (C-4), 144.132 (C-5) 129.490 (C-6), 112.894 (C-3), 112.871 (C-10), 112.794 (C-8), 107.534 (C-13) 101.622 (C-21),

63.369 (C-12), 29.754 (C-16), 27.691 (C-18); **MS** (EI, 70 eV) *m/z* (Specrum 18): 368 (M^+), 262, 234, 189, 159, 147, 103, 91, 77, 51.

3.4.9 3-{4-Aza-8-oxoheptacyclo[0.4.1.$0^{2,10}$.$0^{3,14}$.$0^{4,9}$.$0^{9,13}$.$0^{12,15}$]-tetradecyl} - [(4'-methyl-2'-oxo-2H-chromen-7'-yl)oxy] acetate (BPR 6)

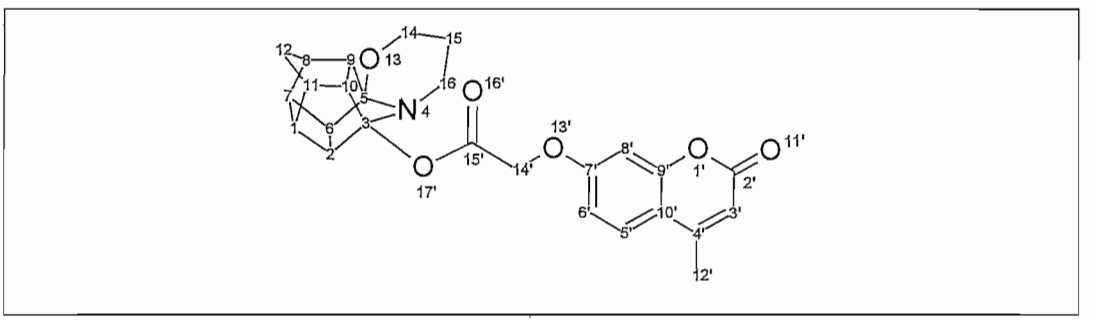

3-Hydroxy-4-aza-8-oxaheptacyclotetradecane (**G,** 0.81 g, 0.011 mol), coumarin acetic acid (**S**, 0.8 g, 0.011 mol) and 3 spatula tips (7 mm) of 4-*N,N*-dimethylaminopyridine (DMAP) were dissolved in 40 ml anhydrous THF. After the dropwise addition at 0 °C of *N,N*-dicyclohexylcarbodiimide (DCC) (1.52 g, 0.023 mol), the solution was stirred for 36 hours. The white suspension was filtered, 70 ml of cold water was added and the mixture was extracted with DCM (3 X 50 ml). The organic solution was dried over $MgSO_4$ and the solvent was removed *in vacuo* to afford the crude product. After recrystallisation from ethyl acetate/cyclohexane (7:3), **BPR 6** was obtained as a brownish coloured precipitate (Yield: 7.53%, 0.36 g, 0.0008 mol).

Physical and spectral data: $C_{25}H_{24}NO_6$; **mp**: 279-281 °C. ^{1}**H NMR** (300 MHz, DMSO-D6) δ_H (Spectrum 6): 7.610 (d, J = 3.815 Hz, 1H, H-5'), 7.347 (dd, J = 13.115 Hz, J = 1.746 Hz, 1H, H-6'), 6.874 (d, J = 2.86 Hz, 1H, H-8'), 6.830 (s, 1H, H-3'), 4.422 (s, 2H, H-14), 3.372 (2 x m, 4H, H-14), 2.768 (3 x m, 8H, H-1, 2, 6, 7, 8, 9, 10, 11), 1.393 (s, 3H, H-12'), 1.172 (2 x m, 4H, H-12, 15), ^{13}**C NMR** (DMSO-D6) δ_C (Spectrum 12): 167.975 (C-15'), 166.738 (C-2'), 160.015 (C-7'), 104.700 (C-3), 102.573 (C-5), 142.975 (C-6'), 104.700 (C-3'), 155.651 (C-9'), 143.140 (C-4'), 129.151 (C-5') 128.942 (C-8'), 114.128 (C-10'), 65.386 (C-9), 63.606 (C-14), 55.987 (C-2), 53.383 (C-6), 45.711 (C-16), 43.933 (C-1), 42.134 (C-12), 41.887 (C-7), 41.771 (C-10/11), 41.186 (C-10/11), 29.631 (C-8), 24.209 (C-15), 15.559 (C-12'), 14.746 (C-14'), **MS** (FAB) *m/z* (Spectrum 19): 446 (M^+), 359, 288, 231, 151, 136, 91, 69.

3.5 CONCLUSION

The synthesis resulted in 6 novel compounds. The yields of the synthetic procedures ranged from 7.53% to 86.4%. The lower yields were attributed to the formation of various possible by-products during the synthetic procedure as well as inadequate purification. Yields could be improved through optimisation of reaction conditions and purification techniques. The structures were characterised using the analytical instrumentation described in section 3.2.2. Characteristic NMR and MS signals obeserved for specific compounds gave confirmation of their structures.

Chapter 4

Monoamine Oxidase B Inhibition

4.1 INTRODUCTION

The active site of the MAO-B enzyme consists of two cavities namely the entrance cavity and the substrate cavity (Hubálek *et al.*, 2005). At the end of the substrate cavity is the FAD coenzyme which is covalently bound by an 8α-thioether linkage to cysteine 397 (Keraney *et al.*, 1961). Analysis of the active site confirms it to be very hydrophobic with sites for favourable amine binding near the flavin involving two nearly parallel tyrosyl (398 and 435) residues that form what has been termed an 'aromatic cage' (Fig. 4.1) and which, as described in section 2.2.1 has catalytic significance (Edmondson *et al.*, 2007).

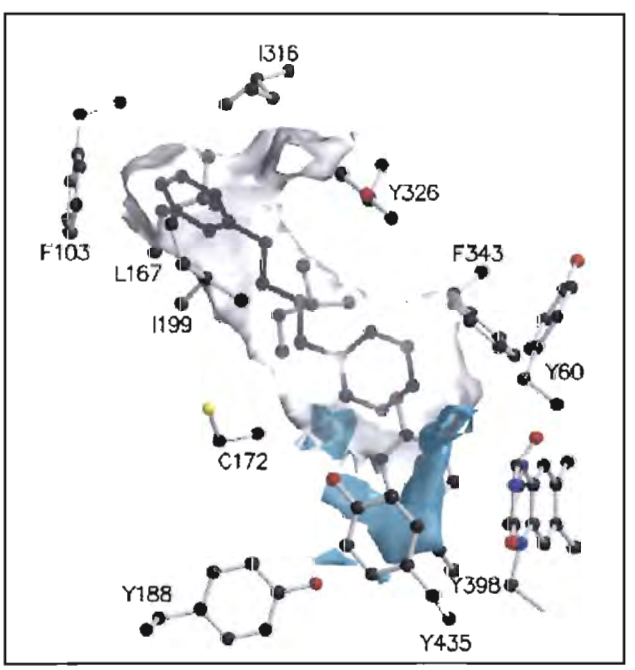

Figure 4.1: Isocontours of GRID molecular interaction fields computed an aromatic sp^2 carbon probe (gray) and a neutral NH_2 probe (cyan) of the coordinates representation by the fused entrance and substrate cavities in the human MAO-B complexed with the inhibitor 1,4-diphenyl-2-butene (Edmondson *et al.*, 2007).

For MAO inhibition, the proposed inhibitor should occupy at least the substrate cavity of the enzyme.

4.1.1 Mechanistic proposals for monoamine catalysed amine oxidation

Monoamine oxidase catalyses the α-carbon oxidation of amines to imines and iminium ions with simultaneous reduction of the covalently bound FAD cofactor. The enzyme is regenerated by reoxidation of the reduced FAD with simultaneous reduction of molecular oxygen to hydrogen peroxide (Fig. 4.2). One mole of hydrogen peroxide is produced for each mole of substrate oxidised.

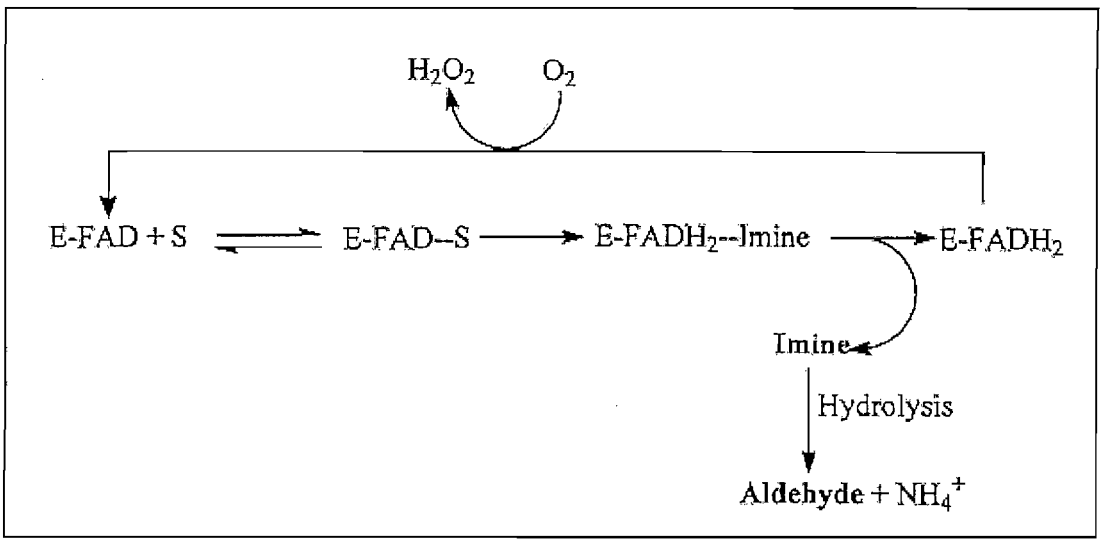

Figure 4.2: The kinetic mechanism of MAO-B. (E-FAD: monoamine oxidase, S: amine, E-FADH$_2$: reduced enzyme).

Two different mechanisms, the single electron transfer and the polar nucleophilic mechanism, have been proposed to describe the catalytic mechanism of MAO-B (Edmondson *et al.*, 2007).

4.1.1.1 Single electron transfer (SET)

The first mechanism is through the single electron transfer (SET) pathway (Silverman, 1995). This mechanism is based on the rationale that one-electron oxidation of the substrate amine nitrogen results in labilisation of the α-CH bond to allow proton abstraction by a basic residue normally associated with proteins. This would also explain the oxidation (Fig. 4.3) observed with cyclopropylamine substrate analogues (Lu *et al.*, 2002).

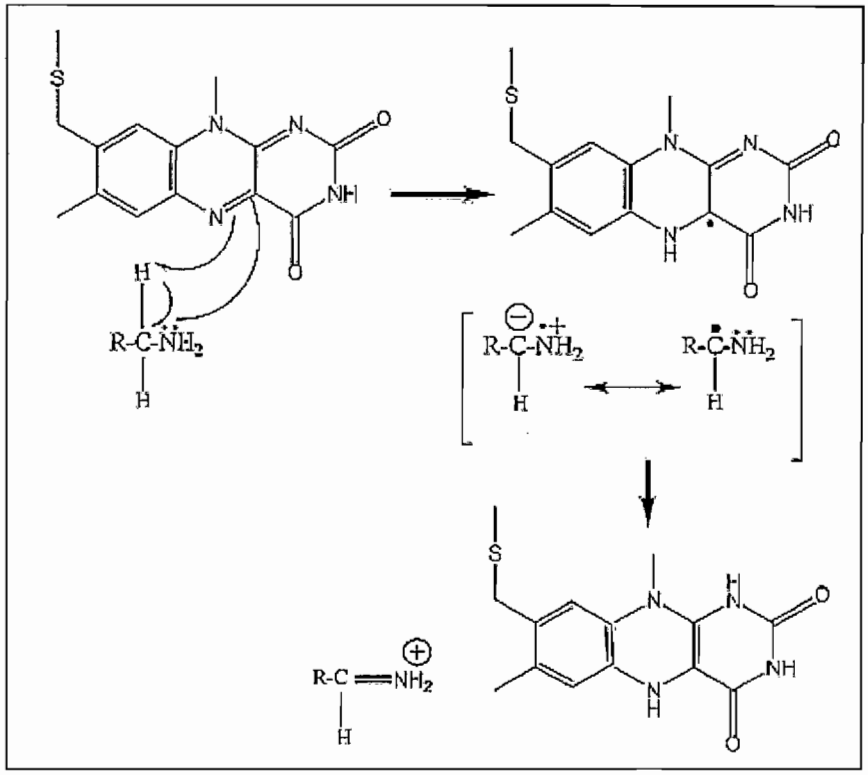

Figure 4.3: The proposed single electron transfer mechanism for the reductive half reaction in MAO catalysis (Lu *et al.*, 2002).

According to this mechanism one electron is transferred form the nitrogen lone pair to the oxidised flavin of MAO to generate an aminyl radical. Following deprotonation of the α-carbon, a second electron is transferred to the flavin to yield an iminium ion. Primary iminium ions are hydrolysed to the matching aldehyde, hence the terminology oxidative deamination.

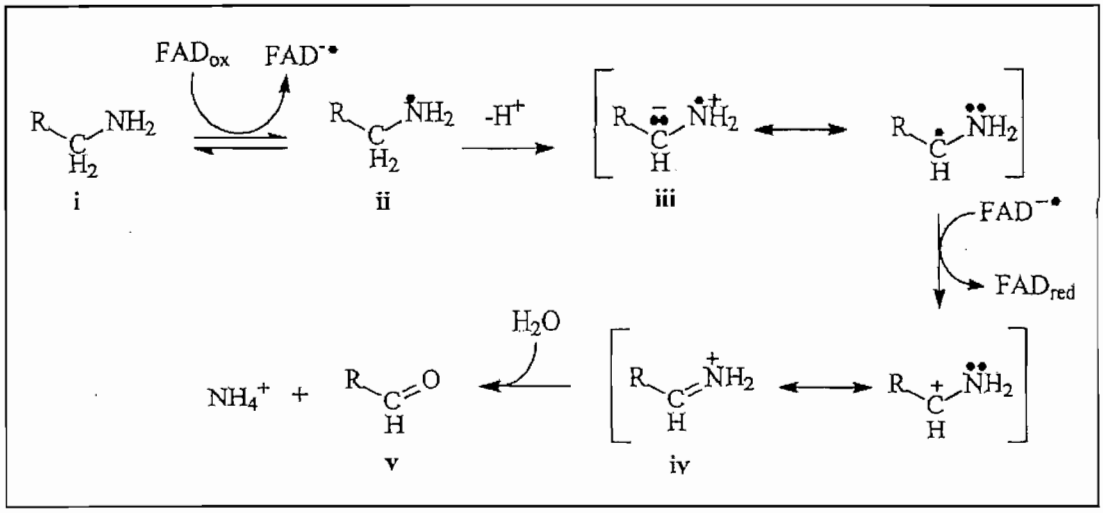

Figure 4.4: The proposed SET pathway-catalysed α-carbon oxidation of amines. (**i**) amine; (**ii**) aminyl radical; (**iii**) product after the loss of a proton; (**iv**) iminium ion; (**v**) matching aldehyde.

4.1.1.2 Polar nucleophillic mechanism

The second mechanism is the polar nucleophilic or group transfer mechanism in which MAO catalysis is proposed to occur via nucleophillic attack at the oxidised flavin 4a position by the amine. It is postulated that an amino acid base in the active site facilitates the proton abstraction from the α-carbon of the amine-flavin adduct. The elimination of the reduced flavin results in the formation of the iminium product (Miller & Edmondson, 1999).

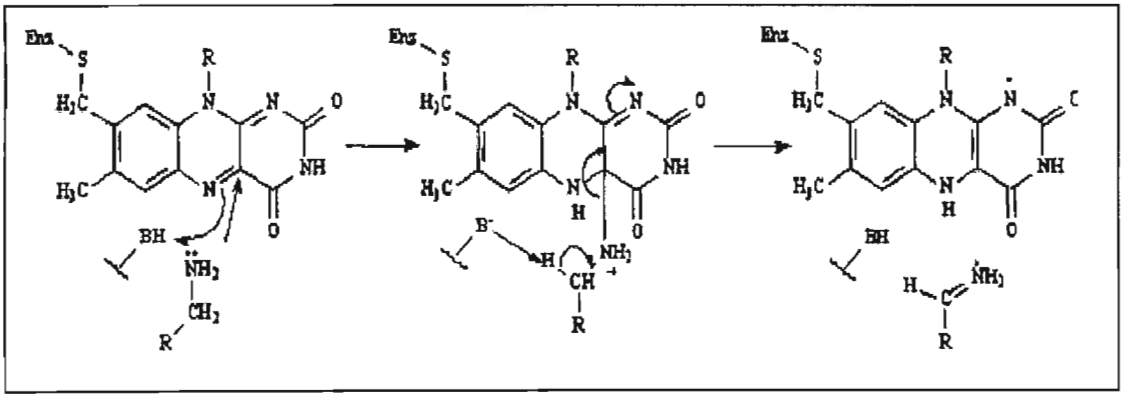

Figure 4.5: The proposed polar nucleophilic pathway for MAO catalysed α-carbon oxidation of amines (cited in Vlok, 2005).

Supporting evidence for the polar nucleophilic mechanism is provided by structural experiments to probe the binding of farnesol, a MAO-B specific inhibitor (Hubalék *et al.*, 2005).

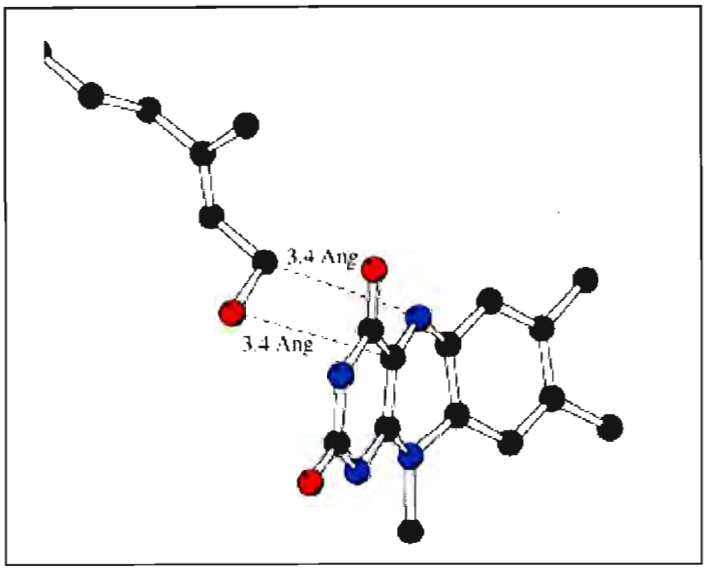

Figure 4.6: Ball and stick representation of the structure of the CH_2-OH moiety of bound trans-trans farnesol and the flavin ring in the structure of human MAO-B. The indicated distances are between the oxygen of farnesol and the C4a of the flavin ring and the α carbon of farnesol and the N5 position of the flavin ring.

This isoprenoid structure binds to MAO-B with the OH group situated directly in front of the C4a position (3.4 Å) of the flavin ring and the α-CH_2 directly in front (also 3.4 Å) of the flavin N5 site. Thus, farnesol binds in a catalytically relevant conformation with turnover not being observed due tot the decreased nucleophilicity of the OH moiety relative to that of an amine group (Edmondson *et al.*, 2007).

4.1.1.3 Funvtional role of the aromatic cage in MAO catalysis

Structural studies show that two tyrosyl residues (398 and 435 in human MAO-B) are situated directly in front of the covalently bound flavin (Binda *et al.*, 2002). To investigate the possible functional roles of the tyrosyl side chains in the active site of MAO-B, a number of site directed mutants of Tyr435 were formed and expressed in human MAO-B and their functional and structural properties compared (Li *et al.*, 2006).

A comparison of the catalytic properties of the MAO-B mutants showed that a correlation existed between k_{cat}/K_m and the interaction energy of the dipole of the substrate amine moiety and the dipole of the side chain amino acid substituent at position 435. One of the functional roles of this 'aromatic cage' is to polarise the amine moiety of the substrate to make it a more effective nucleophile (Fig. 4.7). It also appears to provide a path for guiding the substrate amine towards the reactive positions on the flavin ring (Akyüz *et al.*, 2007).

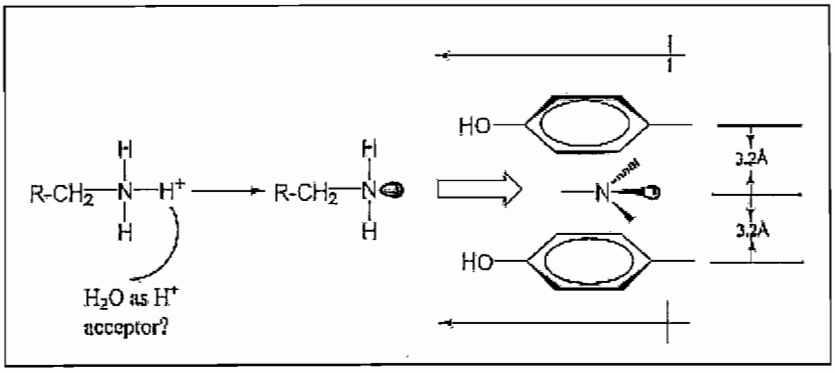

Figure 4.7: Schematic of the proposed effect of the dipole moments of the tyrosyl residues (398 and 435 in MAO-B) on the electron lone pair of the substrate amine moiety before its attack on the flavin ring.

4.2 ASSAYS OF ENZYME REACTIONS AND ENZYME KINETICS

Enzyme kinetics is the field of biochemistry concerned with the quantitative measurement of the rates of enzyme-catalysed reactions and the systematic study of factors that affect these rates.

Kinetic analyses permit scientists to reconstruct the number and order of the individual steps by which enzymes transform substrates into products. The study of enzyme kinetics also represents the principal way to identify potential therapeutic agents that selectively enhance or inhibit the rates of specific enzyme-catalysed processes.

The K_i value for competitive inhibition of MAO-B by test inhibitors can be determined by measuring the extent to which various concentrations of the test compounds slow the rate of oxidation of a substrate to the corresponding product.

Most measurements of the rates of enzyme-catalysed reactions employ relatively short time periods and conditions that approximate initial rate conditions. Under these conditions, only traces of product accumulate, hence the rate of the reverse reaction is negligible. The initial velocity (V_i) of the reaction is thus essentially that of the rate of the forward reaction. Assays of enzyme activity almost always employ a large molar excess of substrate over enzyme. Under these conditions, V_i is proportional to the concentration of enzyme. Measuring the initial velocity therefore permits one to estimate the quantity of enzyme present in a biologic sample.

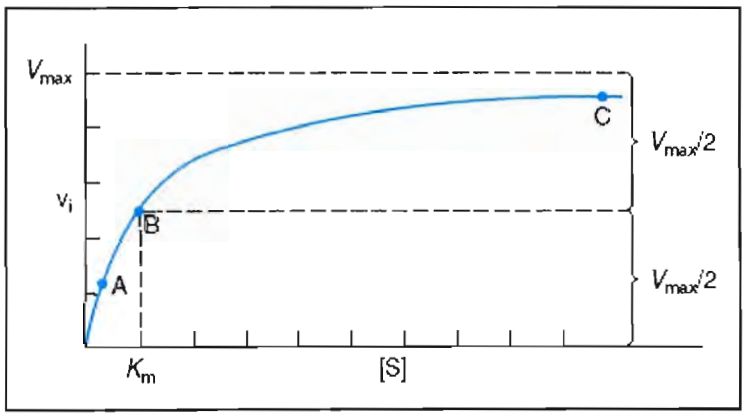

Figure 4.8: Effect of substrate concentration on the initial velocity of an enzyme-catalysed reaction (Murray *et al.*, 2003).

For a typical enzyme, as substrate concentration is increased, V_i increases until it reaches a maximum value V_{max} (Fig. 4.8 and 4.9). When further increases in substrate concentration do not further increase the V_i, the enzyme is said to be "saturated" with substrate and the curve that relates activity to substrate concentration (Fig. 4.8 and 4.9) is hyperbolic. At any given instant, only substrate molecules that are combined with the enzyme as an enzyme-substrate (ES) complex can be transformed into product and the equilibrium constant for the formation of the ES complex is not infinitely large. Therefore, even when the substrate is present in excess, only a fraction of the enzyme may be present as an ES complex.

At points **A** or **B** (Fig. 4.8 and 4.9), increasing or decreasing [S] therefore will thus increase or decrease the number of ES complexes with a corresponding change in V_i. At point **C** (Fig. 4.8 and 4.9), essentially all the enzyme is present as the ES complex.

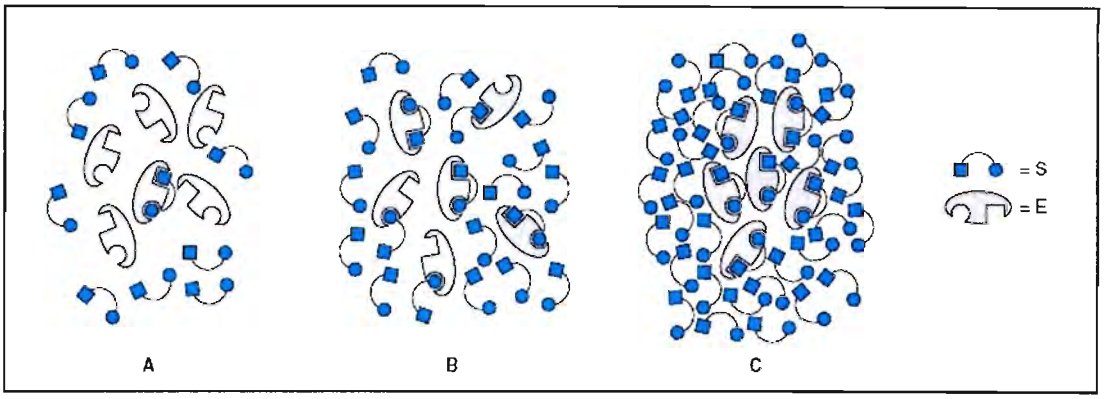

Figure 4.9: Representation of an enzyme at low (**A**), at high (**C**), and at a substrate concentration equal to K_m (**B**). Points **A**, **B**, and **C** correspond to those points in figure 4.8 (Murray *et al.*, 2003).

Since no free enzyme remains available for forming ES, further increases in [S] cannot increase the rate of the reaction. Under these saturating conditions, V_i depends solely on - and is limited by the tempo with which free enzyme is released to combine with more substrate.

4.2.1 The Michaelis-Menten Equation

The Michaelis-Menten equation (**1**) illustrates in mathematical terms the relationship between initial reaction velocity (V_i) and substrate concentration [S], shown graphically in Figure 4.9.

$$v_i = \frac{V_{\max}[S]}{K_m + [S]} \qquad (1)$$

The Michaelis constant K_m is the substrate concentration at which V_i is half the maximal velocity ($V_{max}/2$) attainable at a particular concentration of enzyme. K_m thus has the dimensions of substrate concentration. The dependence of initial reaction velocity on [S] and K_m may be illustrated by evaluating the Michaelis-Menten equation under three conditions:

(1) When [S] is much less than K_m (point **A** in Figures 4.8 and 4.9), the term K_m + [S] is essentially equal to K_m. Replacing K_m + [S] with K_m produces equation **2**

$$v_{1\,i} \approx \frac{V_{\max}[S]}{K_m + [S]} \approx \left(\frac{V_{\max}}{K_m}\right)[S] \qquad (2)$$

where ≈ means "approximately equal to". Since V_{max} and K_m are both constants, their ratio is a constant. In other words, when [S] is considerably below K_m, V_i are directly proportional to k[S]. The initial reaction velocity therefore is directly proportionate to [S].

(2) When [S] is much greater than K_m (point **C** in Figures 4.8 and 4.9), the term K_m + [S] is essentially equal to [S]. Replacing K_m + [S] with [S] reduces equation **1** to:

$$v_i \approx \frac{V_{max}[S]}{[S]} \approx V_{max} \qquad (3)$$

Thus, when [S] greatly exceeds K_m, the reaction velocity is maximal (V_{max}) and unaffected by further increases in substrate concentration.

(3) When [S] = K_m (point **B** in Figures 4.8 and 4.9), the equation is reduced to:

$$v_{1/} = \frac{V_{max}[S]}{K_m + [S]} = \frac{V_{max}[S]}{2[S]} = \frac{V_{max}}{2} \qquad (4)$$

Equation **4** states that when [S] equals K_m, the initial velocity is half-maximal and also reveals that Km may be determined experimentally from the substrate concentration at which the initial velocity is half-maximal.

4.2.2 Lineweaver-Burk plot

The Lineweaver-Burk plot is a linear form of the Michaelis-Menten equation that is used to determine K_m and V_{max}. The direct measurement of the numeric value of V_{max} and therefore the calculation of K_m often requires impractically high concentrations of substrate to achieve saturating conditions. A linear form of the Michaelis-Menten equation circumvents this and permits V_{max} and Km to be extrapolated from initial velocity data obtained at less than saturating concentrations of substrate.

Starting from equation **1**, equation **5** can be derived by inverse, factorisation and simplification.

$$\frac{1}{v_i} = \left(\frac{K_m}{V_{max}}\right)\frac{1}{[S]} + \frac{1}{V_{max}} \qquad (5)$$

Equation **5** is the equation for a straight line, y = ax + b, where y = 1/ V_i and x = 1/[S]. A plot of $1/V_i$ as a function of 1/[S] therefore gives a straight line with y intercept $1/V_{max}$ and slope K_m/V_{max}. This plot is called a double reciprocal or Lineweaver-Burk plot (Fig. 4.10). K_m is thus calculated from the x intercept (equation 6).

$$0 = ax = b$$

therefore,

$$x = \frac{-b}{a} = \frac{-1}{K_m} \tag{6}$$

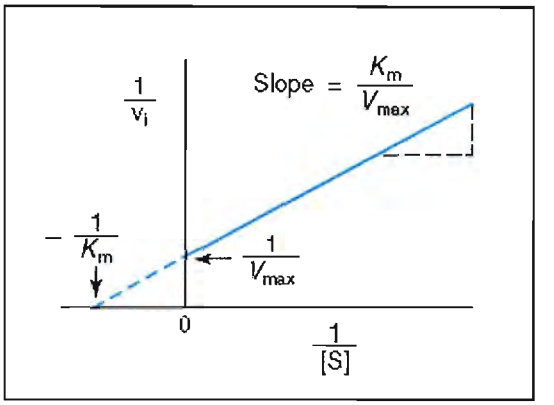

Figure 4.10: Double reciprocal or Lineweaver-Burk plot of $1/V_i$ *versus* 1/[S] used to obtain K_m and V_{max} (Murray *et al.*, 2003).

4.3 INHIBITORS

Inhibitors can be classified based upon their site of action on the enzyme, on whether or not they chemically modify the enzyme, or on the kinetic parameters they influence. Kinetically, we distinguish two classes of inhibitors based upon whether raising the substrate concentration does or does not overcome the inhibition.

4.3.1 Competitive inhibitors

The effects of competitive inhibitors can be overcome by raising the concentration of the substrate. Most frequently, in competitive inhibition, an inhibitor binds to the substrate-binding portion of the active site and blocks access by the substrate. The structures of most classic competitive inhibitors therefore tend to resemble the structures of a substrate and are thus termed substrate analogues.

The formation and dissociation of the EI complex is a dynamic process described by:

$$Enz \underset{k2}{\overset{k1}{\leftrightarrow}} Enz + I \tag{7}$$

For which the equilibrium constant K_i is

$$K_i = \frac{[Enz][I]}{[Enzl]} = \frac{k_1}{k_{-1}}$$

(8)

In effect, a competitive inhibitor acts by decreasing the number of free enzyme molecules available to bind substrate, i.e., to form ES, and thus eventually to form product.

Double reciprocal plots distinguish between competitive and noncompetitive inhibitors and simplify evaluation of inhibition constants, (K_i). Initial reaction velocity is determined at several substrate concentrations both in the presence and in the absence of inhibitor. For classic competitive inhibition, the lines that connect the experimental data points meet at the y axis (*Fig.* 4.11).

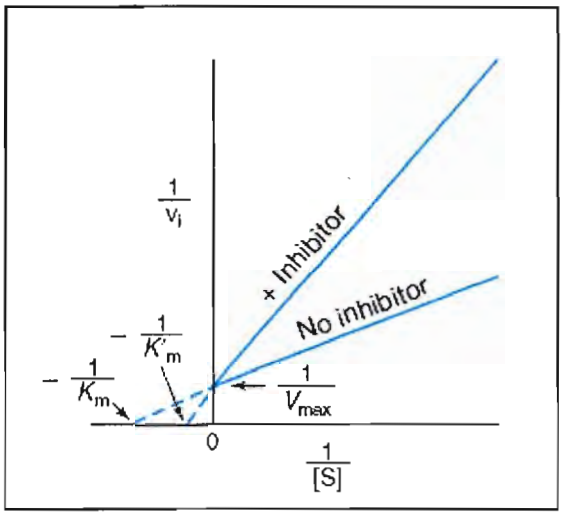

Figure 4.11: Lineweaver-Burk plot of competitive inhibition. Note the complete relief of inhibition at high substrate concentration. (Murray *et al.*, 2003).

Since the y intercept is equal to $1/V_{max}$, this pattern indicates that when 1/[S] approaches 0, V_i is independent of the presence of inhibitor. The intercept on the x axis does vary with inhibitor concentration, and since $-1/K_{m'}$ is smaller than $1/K_m$, $K_{m'}$ (the "apparent K_m") becomes larger in the presence of increasing concentrations of inhibitor. Thus, a competitive inhibitor has no effect on V_{max} but raises K'_m, the apparent K_m for the substrate. For simple competitive inhibition, the intercept on the x axis is:

$$x = \frac{-1}{K_m}\left(1 + \frac{[I]}{K_1}\right)$$

(9)

Once K_m has been determined in the absence of inhibitor, K_i can be calculated from equation **9**. K_i values are used to compare different inhibitors of the same enzyme. The lower the value for K_i, the more effective the inhibitor.

4.3.2 Simple noncompetitive inhibitors

In noncompetitive inhibition, binding of the inhibitor does not affect binding of substrate. Formation of both EI and EIS complexes are therefore possible. However, while the enzyme-inhibitor complex can still bind the substrate, its efficiency at transforming substrate to product, reflected by V_{max}, is decreased. Noncompetitive inhibitors bind enzymes at sites distinct from the substrate-binding site and generally bear little or no structural resemblance to the substrate. For simple noncompetitive inhibition, E and EI possess identical affinity for substrate, and the EIS complex generates product at a negligible rate (Fig. 4.12).

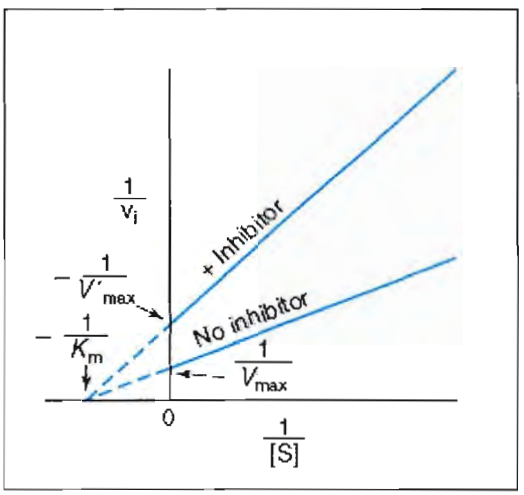

Figure 4.12: Lineweaver-Burk plot for simple noncompetitive inhibition. More complex noncompetitive inhibition occurs when binding of the inhibitor does affect the apparent affinity of the enzyme for substrate (Murray *et al.*, 2003).

4.3.3 Irreversible inhibitors

In the above examples, the inhibitors form a dissociable, dynamic complex with the enzyme. Fully active enzyme can therefore be recovered simply by removing the inhibitor from the surrounding medium. However, a variety of other inhibitors act irreversibly by chemically modifying the enzyme. These modifications generally involve making or breaking covalent bonds with amino acid residues essential for substrate binding, catalysis, or maintenance of the enzyme's functional conformation. Since these covalent changes are relatively stable, an enzyme that has been "poisoned" by an irreversible inhibitor remains inhibited even after removal of the remaining inhibitor from the surrounding medium (Murray *et al.*, 2003).

4.4 INHIBITION STUDIES

Employing a spectrophotometric assay, the activity of the synthesised compounds was evaluated.

4.4.1 Materials and methods

The oxalate salt of MMTP was supplied by Prof. Neal Castagnoli, Jr. UV-Vis spectra were recorded on a Shimadzu UV-visible recording spectrophotometer (UV-2100). Graphpad Prism 5.00® (Graphpad Software, Inc.) was used for all data and statistical analysis.

4.4.1.1 Substrate selection

Inoue *et al.*, (1999) compared the rates of α-carbon oxidation of a variety of tetrahydropyridinyl substrates. Mitochondrial preparations were incubated with substrates at 37 °C in the presence or absence of clorgyline, (R)-deprenyl, or a mixture of these two propargylamines to inhibit MAO-A, MAO-B, or both enzymes. The rates of formation of the corresponding dihydropyridinium metabolites were estimated spectrophotometrically (Inoue *et al.*, 1999).

For this study, MMTP was selected as substrate as it has the following advantages:

- It serves as a good substrate for both forms of the enzyme.
- The dihydropyridinium metabolite is stable, no further oxidation to MMP^+ is observed (Fig. 4.13).
- The relatively large molar extinction coefficient (ε = 25,000 M^{-1}) of $MMDP^+$.
- It has maximal absorbance at 420 nm, which is far removed from the mitochondrial background. The $MMDP^+$ production can thus be measured spectrophotometrically at 420 nm, a wavelength at which neither the substrate nor the test inhibitors absorb light (Inoue *et al.*, 1999).

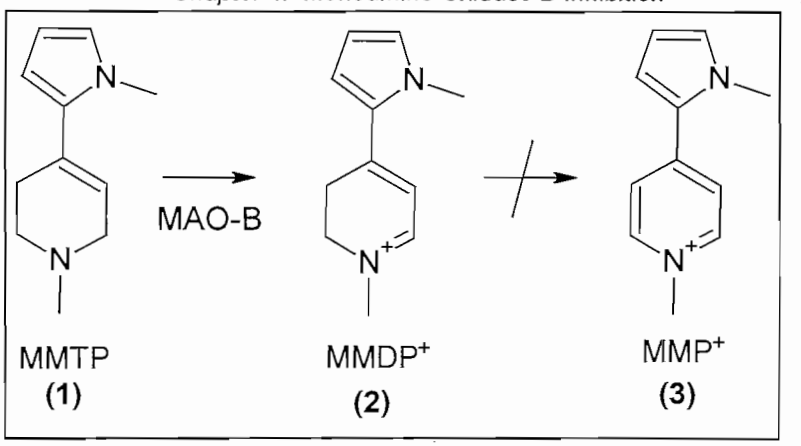

Figure 4.13: The MAO-B catalysed oxidation of MMTP (**1**) to the corresponding dihydropyridinium product (**2**). Futher *in vitro* oxidation to the pyridinium species (**3**) is not observed (Inoue *et al.*, 1999).

A test inhibitor will slow the rate of the MAO-B catalysed oxidation (Fig. 4.13) of 1-methyl-4-(1-methylpyrrol-2-yl)-1,2,3,6-tetrahydropyridine (MMTP) to the corresponding dihydropyridinium ($MMDP^+$) metabolite (Nimkar *et al.*, 1996; Inoue *et al.*, 1999).

4.4.1.2 Enzyme source

In the literature, brain (Naoi *et al.*, 1987), liver (Bembenek *et al.*, 1990), and, especially, blood platelets (Donnelly & Murphy, 1977) have been widely described as sources of human MAO-B for the screening of inhibitors. Above all, blood platelets, containing predominantly the B form of monoamine oxidase, have provided a clinically useful source for selective studies of the properties of this isoform (Wirz-Justice, 1988). However, for ethical and practical reasons, human tissues are difficult to obtain.

Rat brain (Mazouz *et al.*, 1990; Chiba *et al.*, 1984; Snyder & Hendley, 1968; Mazouz *et al.*, 1990) or rat liver, (Yu. 1989, Ali & Robinson, 1991) are easily accessible sources for *in vitro* screening of MAO-B inhibitors, and therefore, rodents have also been employed for *in vitro* studies. Extrapolation from rat to human MAO-B inhibitor potencies may however not always result in a good estimation of human MAO-B inhibitory activity (Novaroli *et al.*, 2006).

As enzyme source, we employed the mitochondrial fraction obtained from baboon liver tissue since it is reported to be devoid of MAO-A activity while exhibiting a high degree of MAO-B catalytic activity. Therefore, even though MMTP is a MAO-A/B mixed substrate, its oxidation by baboon liver mitochondria can be exclusively attributed to the action of the MAO-B isoform (Inoue *et al.*, 1999).

4.4.2 MAO-B activity measurements and inhibition studies

4.4.2.1 IC_{50} determination

Mitochondria were isolated from baboon liver tissue using the method described by Salach and Weyler (1987) and stored at -70 °C in 300 µl aliquots. Following addition of an equal volume of sodium phosphate buffer (100 mM, pH 7.4) containing glycerol (50%, w/v) to the aliquots, the protein concentration were determined by the method of Bradford using bovine serum albumin. Since the mitochondrial fraction obtained from baboon liver tissue is reported to be devoid of MAO-A activity, inactivation of this enzyme was unnecessary. The MAO-A/B mixed substrate MMTP (K_m = 60.9 µM for baboon liver MAO-B) served as substrate (see section 4.4.1.2.) for the inhibition studies. Incubations were carried out in sodium phosphate buffer (100 mM, pH 7.4) and contained MMTP (60 µM), the mitochondrial isolate (0.15 mg protein/ml), and various concentrations of the test inhibitors (0 – 1000 µM). Following incubation at 37 °C for 10 min, the enzyme reactions were terminated by the addition of 10 µl perchloric acid (70%) and the samples centrifuged at 16 000 g for 10 min. The MAO-B catalysed production of $MMDP^+$ is reported to be linear for the first 10 min of incubation under these conditions. The supernatant fractions were removed and the concentrations of the MAO-B generated product, $MMDP^+$, were measured spectrophotometrically at 420 nm (ε = 25,000 M^{-1}). From the total absorbance, the concentration product formed and the Log [ ] was calculated. Product concentration versus Log [ ] were plotted and the IC_{50} calculated.

4.4.2.2 K_i determination

For the K_i determination the same procedure as that described for the IC_{50} determination were followed with the following exceptions. Incubations were carried out in sodium phosphate buffer (100 mM, pH 7.4) and contained MMTP (30-120 µM), the mitochondrial isolate (0.15 mg protein/ml), and various concentrations of the test inhibitors.

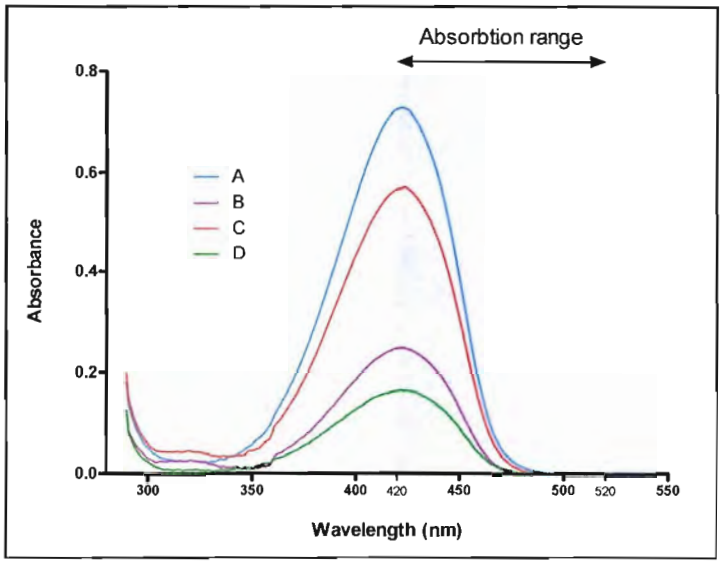

Figure 4.14: Graphical illustration of absorbance vs. wavelength with different concentrations of inhibitor (A=0 µM, B=10 µM, C=5 µM and D=20 µM) is exposed to the substrate.

The maximal absorbance of the $MMDP^+$ at 420 nM (Fig 4.14). The inhibitor suppresses oxidation and a decrease in absorbance is observed. From a replot of the slopes of the Lineweaver-Burk plots *vs* the inhibitor concentration, the K_i values were obtained (Segel, 1993).

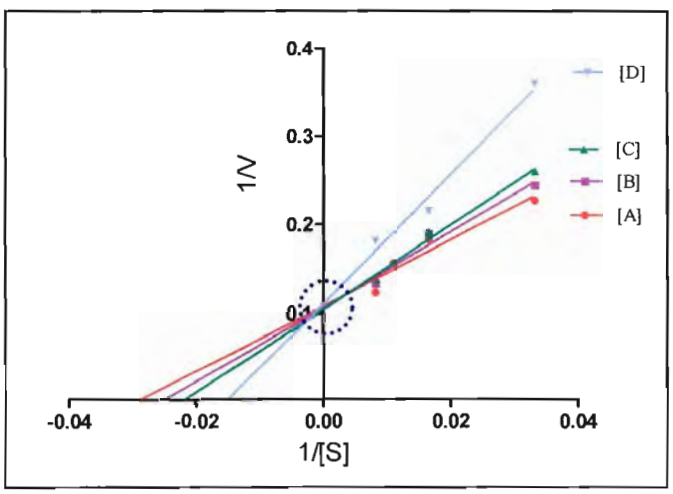

Figure 4.15: Lineweaver-Burk plot for simple competitive inhibition. The lines converged (dotted blue circle) on the y-axis as discussed in section 4.2.5.4.

4.5 RESULTS AND DISCUSSSION

The synthesised compounds with substitution at position 4 and 7 of the coumarin nucleus were subjected to the MAO-B inhibition assays for K_i and IC_{50} determination.

Although IC_{50} is not a direct indicator of affinity, it can be related for at least competitive inhibition by the Cheng-Prusoff equation **10**.

$$K_i = \frac{IC_{50}}{1+(S/K_m)} \quad \textbf{(10)}$$

Where K_i is the binding affinity of the inhibitor, IC_{50} is the functional strength of the inhibitor, S is substrate concentration and K_m is the Michaelis constant for the enzyme. The K_i is the inhibition value for a drug; the concentration of the competing ligand in a competition assay which would occupy 50% of the receptor (Cheng & Prusoff, 1973).

The coumarin analogues bearing a methyl group on the 4 position proved to be effective MAO-B inhibitors with a significant increase in MAO-B inhibition potency (**BPR 1** *vs* **BPR 2**). Substitution at position 7 of the coumarin nucleus with an alkyl methoxy ester was also found to enhance affinity for the MAO-B enzyme. Though an ester as functional group is present, incorporating a long fatty acid chain (**BPR 3**) resulted in a decrease in activity. This probably reflects the limitations of the size of the active site. As with the styrylcaffeine MAO-B inhibitors, MAO-B inhibition was enhanced by substitution with the trans moiety of **BPR 4**. Conjugation of the coumarin and caffeine rings in (**BPR 5**), led to decreased activity. This structure is not planar and confirms the hypothesis that planar structures are more favourable and accepted by the enzyme. Conjugation with the polycyclic cage **BPR 6** impacted negatively on MAO-B activity, suggesting that introducing steric bulk is not favourable for inhibition. In general, the coumarin esters and methoxy ester represents promising compounds that may be subjected to further structure-based optimisation (see chapter 5).

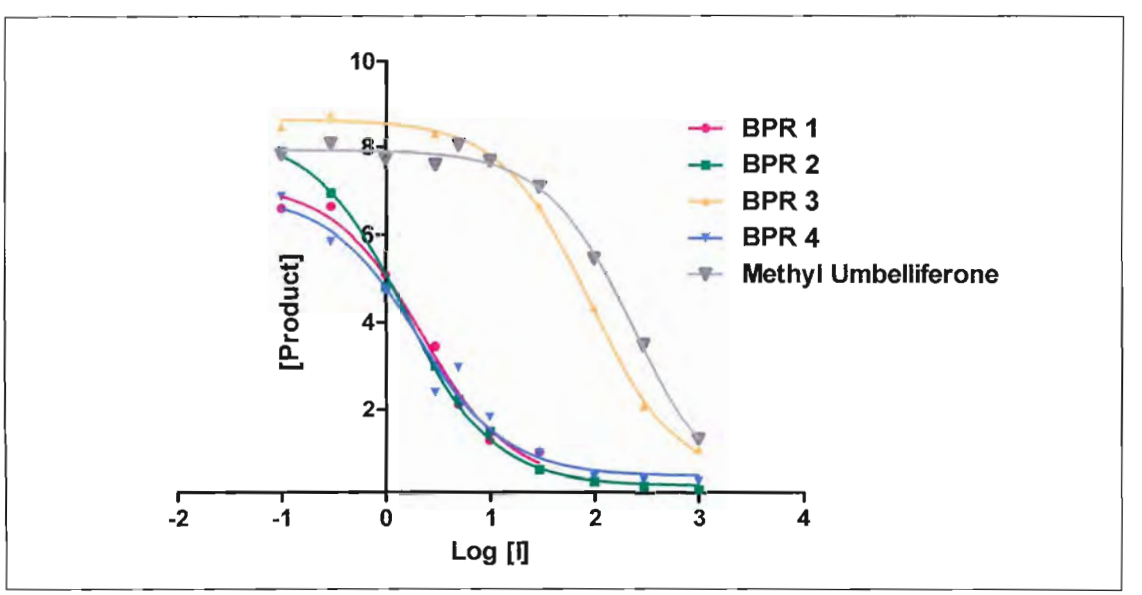

Figure 4.16: Inhibition curves of **BPR 1-4** and methyl umbelliferone.

Table 4.1: Inhibition values (K_i, IC_{50}) obtained with the substituted coumarin analogues.

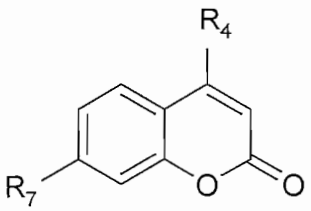

Compound	K_i (μM)	IC_{50} (μM)	Compound	K_i (μM)	IC_{50} (μM)
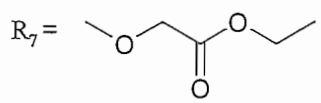 $R_4 = H$ **BPR 1**	1.93	2.30	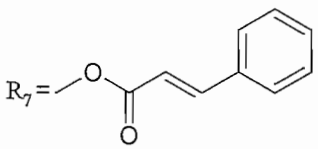 $R_4 = CH_3$ **BPR 4**	0.68	1.63
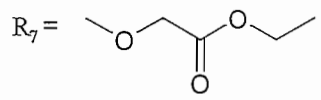 $R_4 = CH_3$ **BPR 2**	0.94	1.55	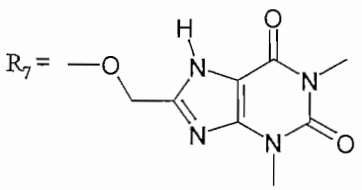 $R_4 = CH_3$ **BPR 5**	72.7	ND*
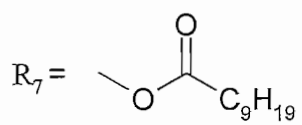 $R_4 = CH_3$ **BPR 3**	98.5	94.4	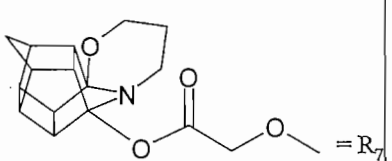 $R_4 = CH_3$ **BPR 6**	263.	ND*

* ND: Not determined

The Lines of the Lineweaver-Burk plots intersected and indicated that the mode of inhibition was competitive. Qualitative inspection of the results (Table 4.1) revealed some important SAR.

4.5.1 Ethyl [(2-oxo-2H-chromen-7-yl)oxy]acetate (BPR 1)

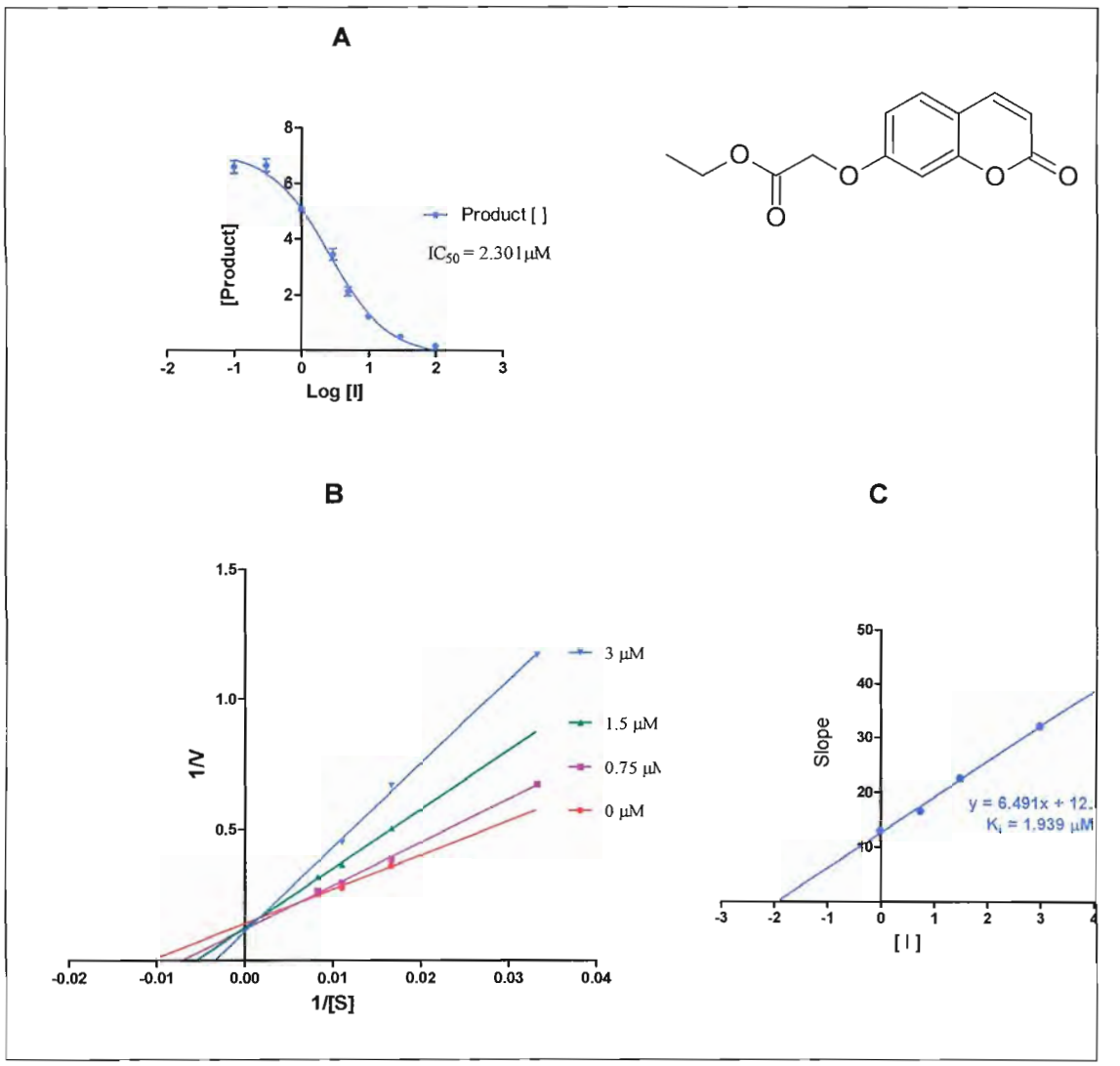

Figure 4.17: Inhibition of MAO-B by **BPR 1** with **A** showing the IC_{50} curve and **B** and **C** illustrating a competitive mode of inhibition via the Lineweaver-Burk plots.

The IC_{50} for **BPR 1** was equal to 2.301 µM and a concentration range of 0 to 3 µM was suitable for the K_i determination. When 1/V *vs* 1/[S] was plotted, the lines converged at the y-axis, thus confirming competitive inhibition. With the slope plotted against the different inhibitor concentrations, a straight line was obtained and the K_i calculated to be 1.939 µM. Substitution in position 7 of the unsubstituted coumarin nucleus with an alkyl methoxy ester resulted in a compound with high affinity for the MAO-B enzyme (Fig. 4.17).

4.5.2 ethyl [(4-methyl-2-oxo-2H-chromen-7-yl)oxy]acetate (BPR 2)

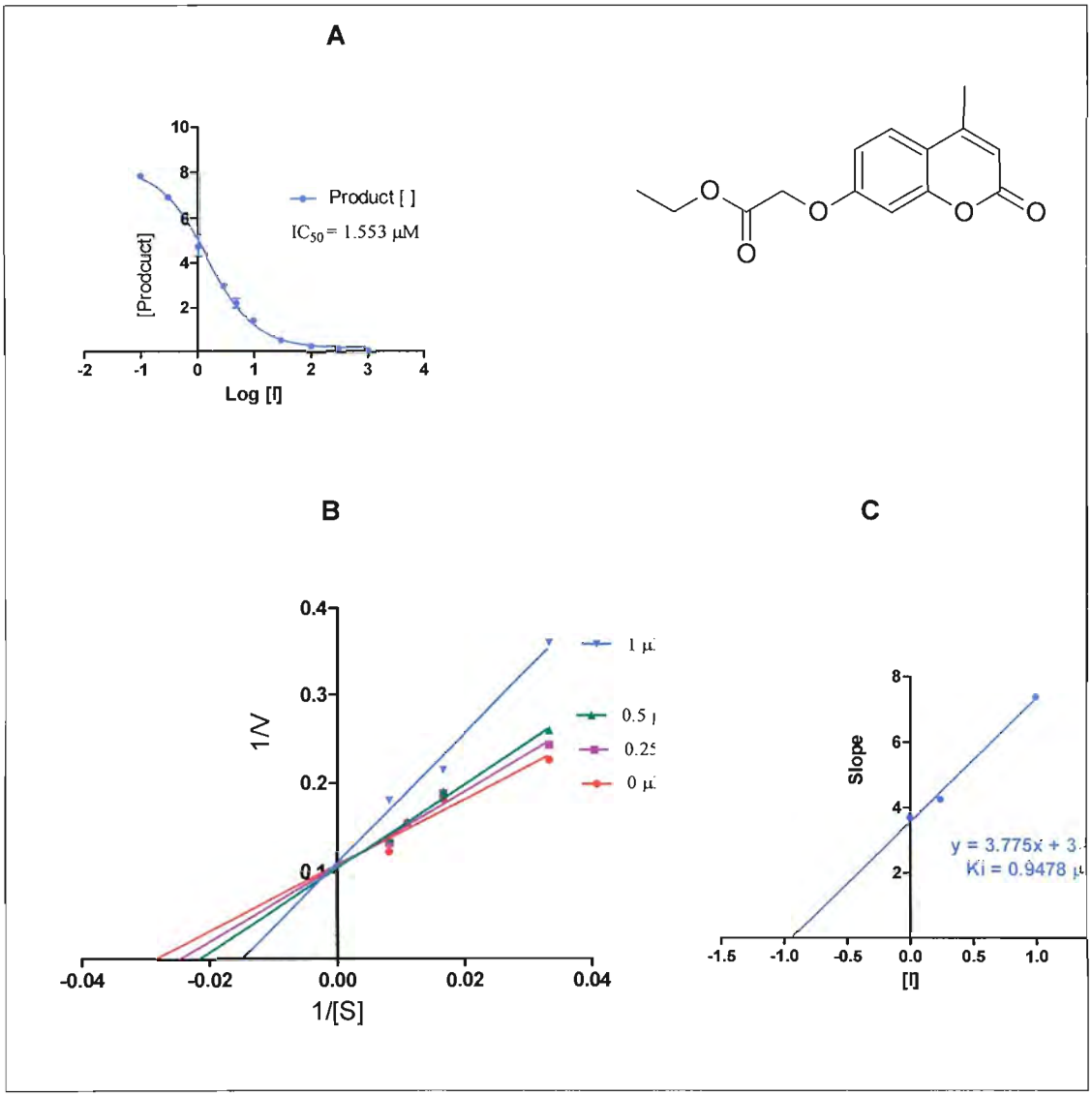

Figure 4.18: Inhibition of MAO-B by **BPR 2** with **A** showing the IC_{50} curve at different inhibitor concentrations and **B** and **C** illustrating a competitive mode of inhibition via the Lineweaver-Burk plots

BPR 2 had an IC_{50} of 1.553 µM and a concentration range of 0 to 1 µM was suitable for the K_i determination. When 1/V *vs* 1/[S] was plotted, the lines converged at the y-axis, thus confirming competitive inhibition. With the slope plotted against the different inhibitor concentrations, a straight line was obtained and the K_i calculated to be 0.9478 µM (Fig. 4.18). Substitution in position 7 with the alkyl methoxy ester on coumarin analogues bearing a methyl group in the 4 position, proved to be more effective inhibitors with a significant increase in MAO-B inhibition potency (**BPR 1** *vs* **BPR 2**).

4.5.3 4-methyl-2-oxo-2H-chromen-7-yl decanoate (BPR 3)

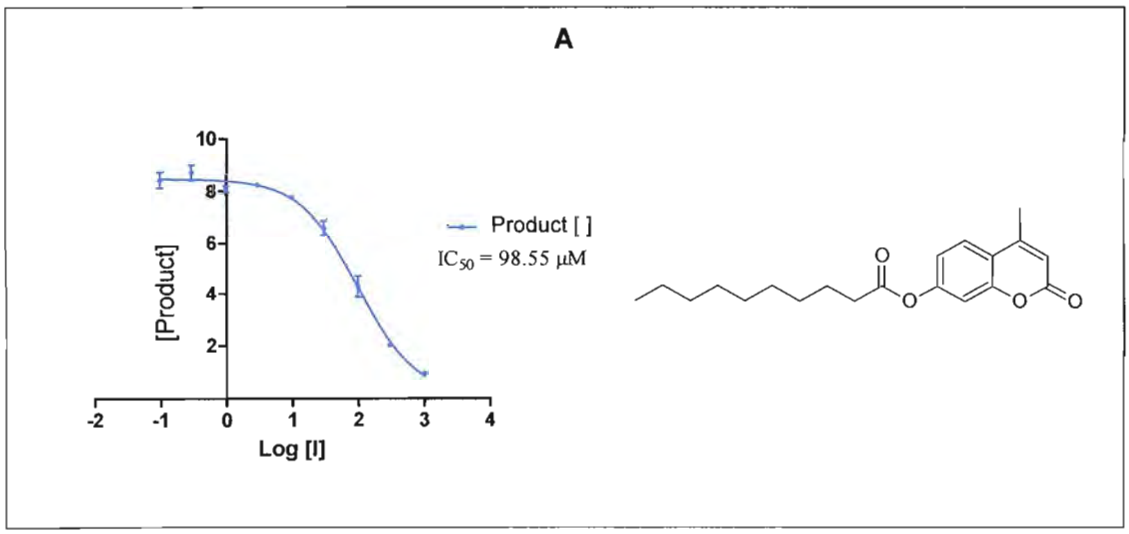

Figure 4.19: Inhibition of MAO-B by **BPR 3** with **A** showing the IC_{50} curve.

An IC_{50} equal to 94.46 µM. Due to the low MAO-B inhibition observed with this compound, a K_i was not determine. Though an ester as functional group is present and nearer to the coumarin, incorporating a long fatty acid chain (**BPR 3**) for increased lipophylicity, resulted in a decrease in activity. This probably suggest limitations in the enzyme cavity size (Fig. 4.19).

4.5.4 4-Methyl-2-oxo-2H-chromen-7-yl (2E)-3-phenylacrylate (BPR 4)

The IC_{50} for **BPR 4** was equal to 1.639 µM and a concentration range of 0 to 1.2 µM was suitable for the K_i determination.

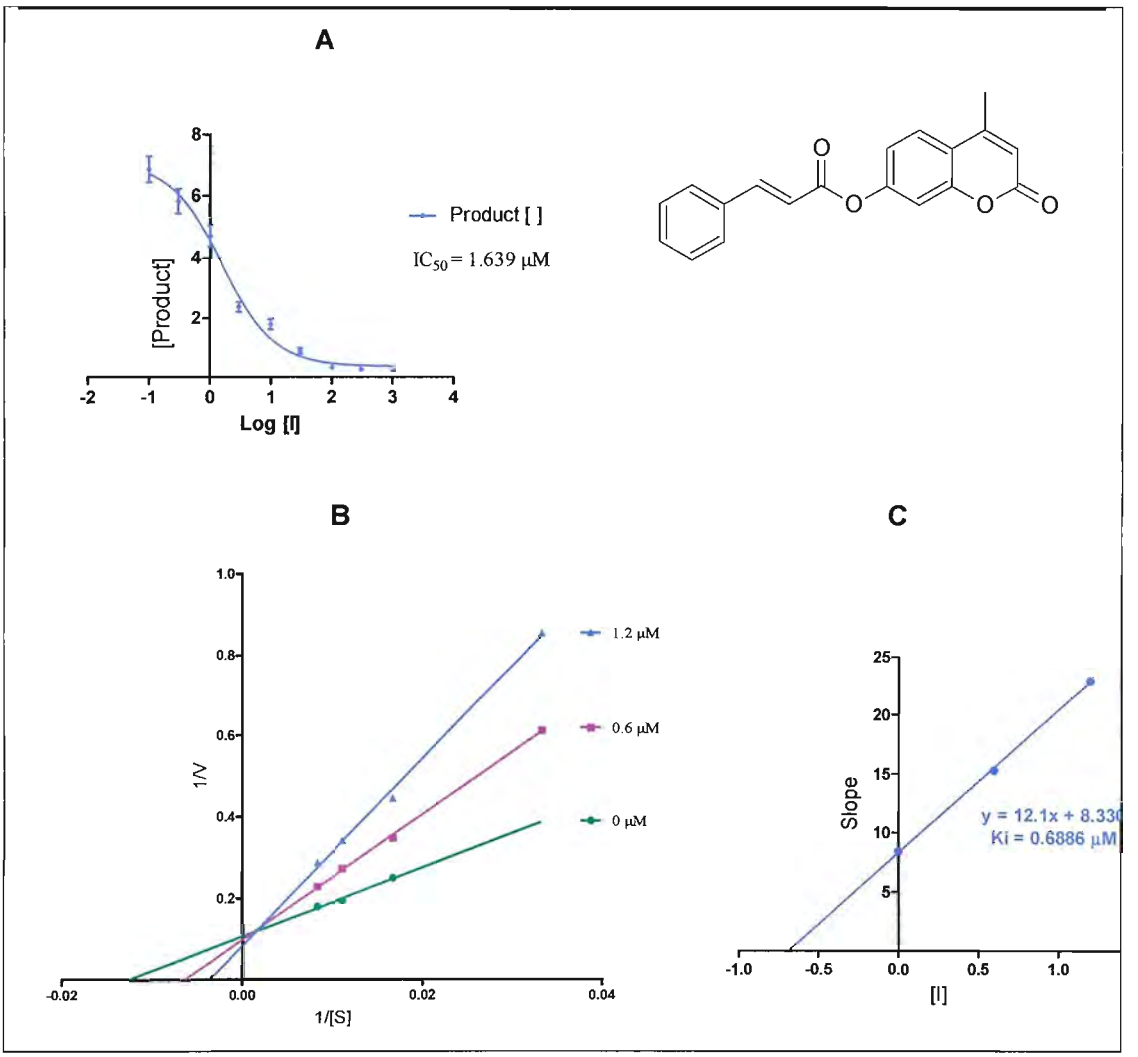

Figure 4.20: Inhibition of MAO-B by **BPR 4** with **A** showing the IC_{50} curve at different inhibitor concentrations and **B** and **C** illustrating a competitive mode of inhibition via the Lineweaver-Burk plots

When 1/*V* *vs* 1/[S] was plotted, the lines converged at the y-axis, thus confirming competitive inhibition. With the slope plotted against the different inhibitor concentrations, a straight line was obtained and the K_i calculated to be 0.6886 µM. This proved to be the most potent compound. Enhancing MAO-B inhibition through the *trans* styryl side chain was very effective (Fig. 4.20).

4.5.5 Methyl umbelliferone

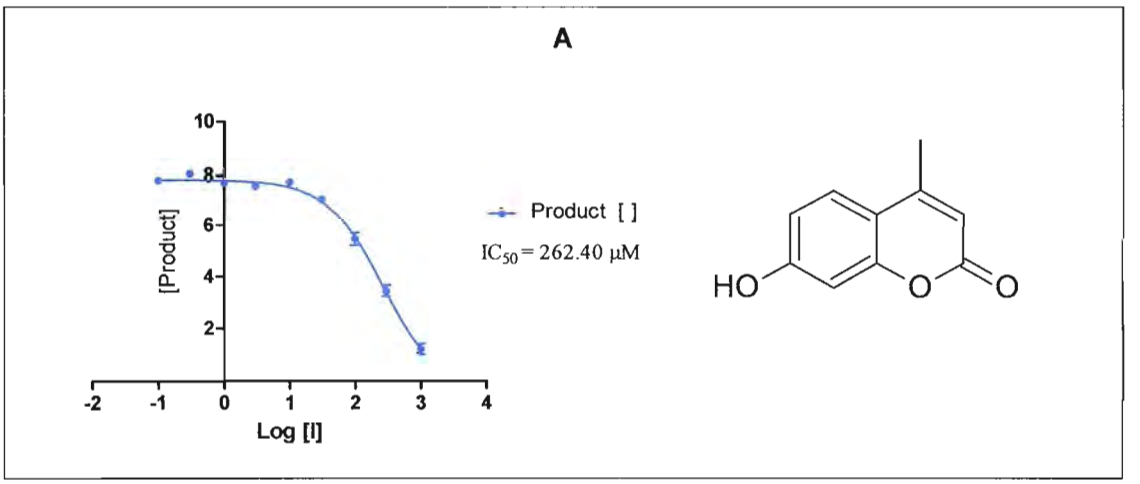

Figure 4.21: Inhibition of MAO-B by methyl umbelliferone with A illustrating the IC_{50} curve.

As a standard the IC_{50} of the unsubstituted methyl umbelliferone was calculated to be 262.40 µM. Compounds in this study thus exhibit a significant increase in MAO-B inhibition potency, up to a 100 fold and more for **BPR 1, 2** and **4** (Fig. 4.21).

4.6 SUMMARY

From the experimental data it was concluded that the mode of inhibition for these compounds was competitive. The ester and methoxy ester analogues revealed promising results that require further investigation. The results indicate that the potencies are dependant upon multiple descriptors such as chain length, bulkiness and planarity. Thus, maintaining functional MAO-B potency whilst altering the pharmacokinetic profile proved difficult.

Chapter 5 Molecular Modelling

5.1 INTRODUCTION

Identifying a small molecule drug candidate for a pharmacological protein target remains a daunting task that could involve synthesising and screening millions of molecules against a particular target. In silico screening is a pre-selective process and can therefore, in principle, help address this predicament and accelerate the development process. It reduces the number of potential ligand molecules that need to be considered for synthesis and examined for their efficacy and mode of action in various biological assays (Krammer *et al.*, 2005).

Molecular modelling is a general term that covers a wide range of molecular graphics and computational chemistry techniques used to build, display, manipulate, simulate and analyse molecular structures. It is used in a number of different research areas and, therefore, the term does not have a rigid definition. To a chemical physicist, molecular modelling might imply performing a high quality quantum mechanical calculation using a supercomputer; to the organic/medical chemist, molecular modelling may mean displaying and modifying a candidate drug molecule on a desktop computer (Vlok, 2005).

Recently there has been exceptional resurgence of interest in MAO-B inhibition and the publication of the human MAO-B crystal structure (Binda *et al.*, 2003) permits modelling and docking of substrates and inhibitors into the active site of this enzyme.

5.1.1 Docking

In silico high-troughput screening can be divided into two major steps, namely *docking and* scoring, which are closely intertwined with each other. The first step is often referred to as finding the right molecular 'key' to a known receptor 'lock' (Fisher, 1894) with the fitting performed purely based on atomic coordinates. As an extension to the simple static 'lock' and 'key' view, the induced fit model (Yakunin *et al.*, 2003), takes into account that the ligand and receptor possess the ability to adapt their 3D structure in such a way as to accommodate the binding to each other.

Docking is thus the procedure of fitting one molecule into another molecule and it involves the combination of two types of molecules or the fitting of a ligand into the active cavity of another molecule or protein. It is a very useful tool to determine the possibility of a theoretical model to bind to a receptor and is extensively utilised to determine the properties necessary *for* high potency.

There are many types of interactions that may occur between a ligand and a macromolecule as well as between atoms or subunits within molecules. These interactions include dispersion interactions, hydrogen bonding, hydrophobic interactions, electrostatic interactions, ionic binding, ion-dipole interactions, dipole-dipole interactions, ion induced dipole interactions, charge transfer and covalent bonding (Vlok, 2005).

Evaluating the fit of a ligand to a protein receptor is commonly referred to as 'scoring' and is closely related to the previous step of docking a ligand into the protein-binding pocket. It calls for devising a function that correctly prioritises the docked ligand poses, and simultaneously correlates with or predicts their binding affinities. The LigScore functions in Discovery Studios® consist of three distinct terms that describe the Van der Waals interaction, the polar attraction between the ligand and protein, and the desolvation penalty attributed to the binding of the polar ligand atoms to the protein and vice versa. LigScore 2 has been reported to have good predictability with regards to experimental pK_i values (Krammer *et al.*, 2005).

Toprakçí *et al*, (2005) docked a series of experimentally tested model compounds to the active site of the MAO-B enzyme (Fig. 5.1). Excellent to good correlations between the calculated and experimental inhibition constants (K_i) were obtained.

Docking Simulation

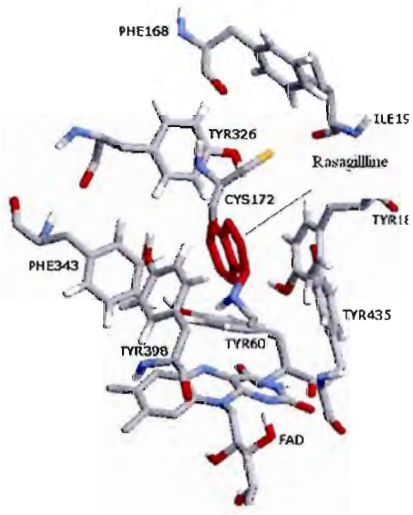

Compound structure

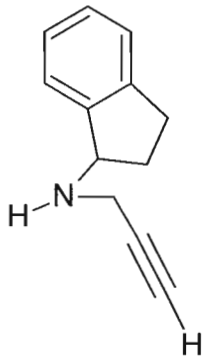

Rasagilline

The indan ring of rasagilline is perpendicular to the the FAD, which itself forms the amine binding site. The aromatic moiety of the rasagiline interacts with the side chains of residues Tyr398, Tyr435 and via a π–π interaction with Tyr188. The propargyl group is aligned with the N5 atom of the FAD. Cys172, Tyr60 and Phe343 also contribute to some of the interactions to stabilise the complex (Toprakçí *et al.*, 2005).

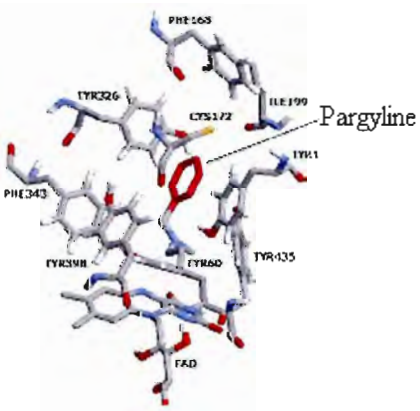

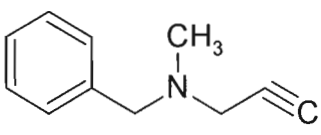

Pargyline

The phenyl ring of pargyline is placed between Tyr398 and Tyr188. The propargyl group extends down from the phenyl ring to the FAD (Toprakçí *et al.*, 2005).

Figure 5.1: Docking complexes between monoamine oxidase-B and selected inhibitors (Toprakçí *et al.*, 2005).

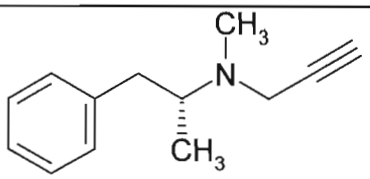

Selegilline

The binding pattern of selegyline/(R)-deprenyl shows binding behaviour similar to that observed of pargyline, except for the phenyl ring, which is bent backwards 90° (Toprakçí *et al.*, 2005).

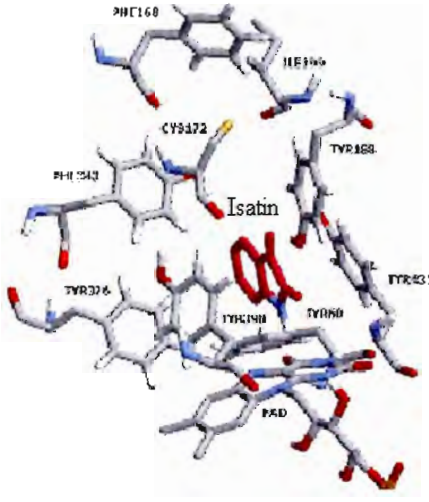

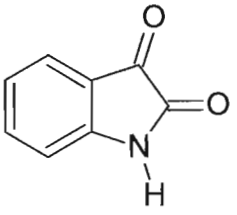

Isatin

The reversible MAO-B inhibitor isatin (indol-2,3-dione) is positioned in the Tyr435 *and* Tyr398 hydrophobic cage in such a manner that the amine group is located near the FAD cofactor. This position satisfies the minimum distance between isatin's nitrogen atom and FAD's N5 atom (Toprakçí *et al.*, 2005).

Figure 5.1: Continued.

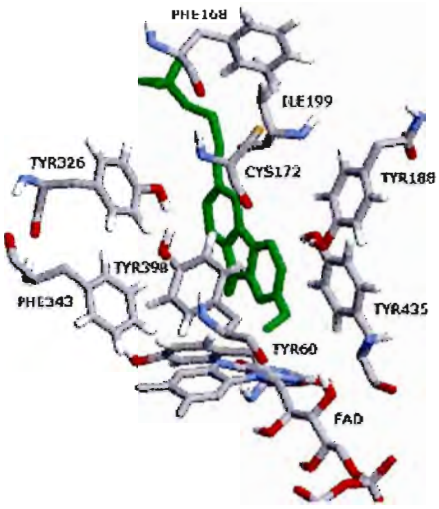

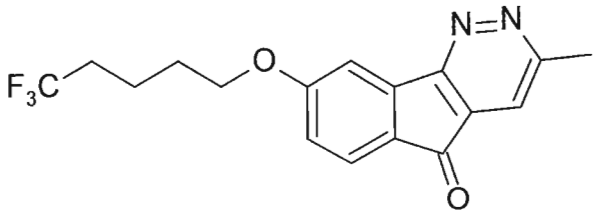

3-Methyl-8-(4,4,4-trifluoro-butoxy)indino [1.2-c]pyridazin-5-one

The indeno[1,2-c]pyridazin-5-one nucleus is sandwiched between Tyr398 and Tyr435. Hydrogen bonds between the carbonyl and pyridazine functional groups of indeno[1,2-c]pyridazin-5-one and Tyr188, Tyr398 and Tyr435 are important, as well as the hydrophobic interaction. The trifluorobutoxy side chain extends itself along the entrance cavity (Toprakçí *et al.*, 2005).

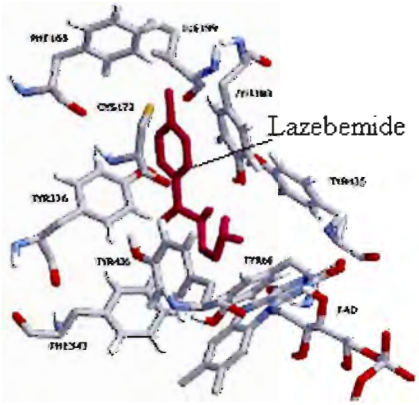

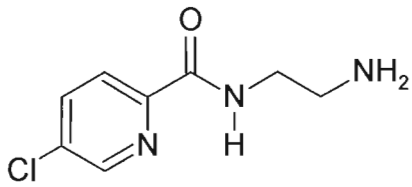

Lazebemide

Lazebemide is localised by interaction with Tyr188. It's aromatic nucleus points away from the FAD cofactor and the side chain with primary amine and amide moieties is positioned in the vicinity of FAD cofactor, approaching the N5 atom of the FAD cofactor as closely as possible (Toprakçí *et al.*, 2005).

Figure 5.1: Continued

5.1.2 Binding mode prediction of coumarin derivatives

The binding site of the human MAO-B crystallographic structure (PDB code 1oj9) after deletion of the co-crystallised ligand and water molecules is frequently used for molecular docking simulations (Fig. 5.2). Three water molecules (Wat1-3) are included in the MAO-B structure and are buried near the flavine adenine dinucleotide cofactor (FAD), the latter being covalently bound to Cys397.

All inhibitors of the coumarin series II (Table 2.3) tranverse both the MAO-B cavities, presenting the coumarin nucleus inside the substrate cavity and the side chain group in the hydrophobic region of the entrance cavity. Ile199 and Tyr326 (Fig. 5.2: carbon atoms in magenta) separates the entrance and substrate cavities (Novaroli *et al.*, 2006).

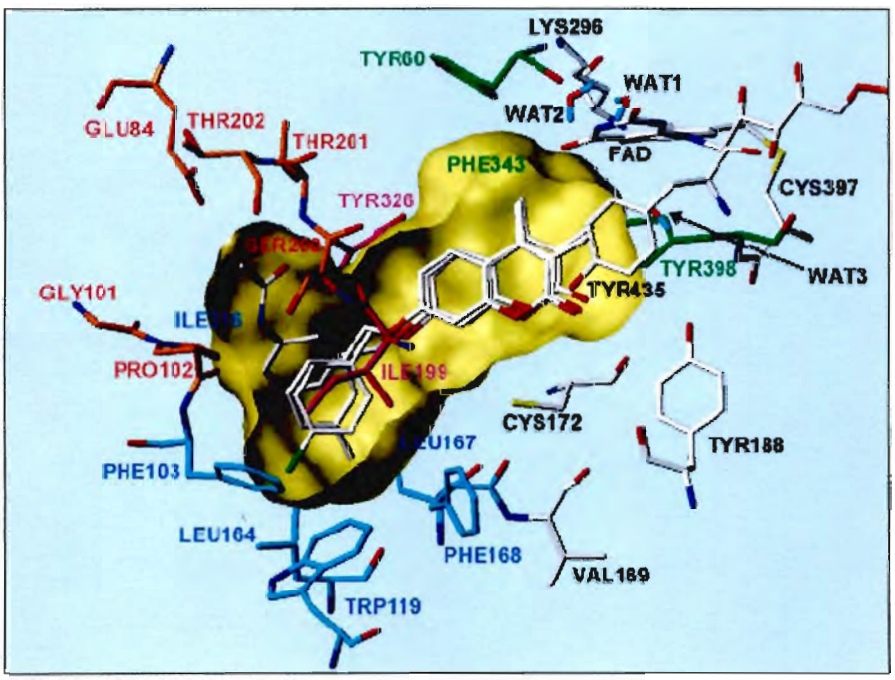

Figure 5.2: MAO-B in complex with 7-X-benzyloxy coumarin derivatives (Novaroli *et al.*, 2006).

The coumarin moiety is stabilised by hydrogen bonds between the lactone oxygens and Cys172, Tyr188, Tyr435 and Wat3. The ether moieties are also potentially involved in a hydrogen bond network, with different residues in the connecting zone between substrate and entrance cavities, notably with Tyr326. The coumarin nucleus in the substrate cavity is placed to minimize unfavourable interactions between the methyl groups and the large polar region and/or to maximize hydrophobic interactions between the 4-methyl group and the small hydrophobic region (Tyr60, Phe343, Tyr398). Various substituents on the 7-benzyloxy ring are able to find favourable interactions to stabilise the complex in the entrance cavity. This is due to the entrance cavity which is composed of a highly hydrophobic pocket and another pocket surrounded by polar residues and with major hydrogen bond capacity amino acids (see section

2.1 and 2.2). Polar substituents such as acetamide (Table 2.3: **6**) are positioned in the polar pocket, while hydrophobic moieties such as methyl (Table 2.3: **3**) or chlorine (Table 2.3: **14**) find a favourable environment in the hydrophobic pocket (Novaroli *et al.*, 2006).

5.2 DOCKING PROCEDURE

The MAO-B crystal structure of 1oj9 (http:www.pdb.org) with a resolution of 2.30 Å in complex with 1,4-diphenyl-2-butene, was obtained from the protein data bank. The rationale for the choice of this structure is that the ligand occupies both the entrance and substrate cavity, and deletion of this inhibitor delivered sufficient 'space' within the enzyme for the docking of larger ligands. The crystal structure was imported into Discovery Studios 1.7® software and the crystallised inhibitor was removed. To remove any unfavourable steric clashes and to optimise hydrogen bonding pattern, the Charm forcefield was applied to the enzyme (chain A) and the binding site was subsequently identified (Site 1 highlighted). Ligands were prepared in a new DS Viewer window using the 'Prepare Ligands' module of Discovery Studios 1.7®. Hydrogens were added according to the expected protonation at experimental pH and the structure was configured in the minimum energy state. All other parameters were kept at default values. Docking was performed in the 'Dock Ligands' module (Ligandfit) with minimisation set as smart minimiser and scoring calculated as Ligandfit 2 and the consensus Dock Score. Hydrogen bond patterns in the vicinity of the ligand binding site were calculated and intermolecular neighbours were included in the docked representation for clarity.

5.3 RESULTS AND DISCUSSION

Common functional groups of the synthesised compounds are ethers, esters and ketones. It is important to note that the functional groups of molecules determine the interactions with the amino acid residues of the MAO-B protein. Figure 5.3 shows the molecular structure of coumarin analogues with the functional groups of the skeletal atoms.

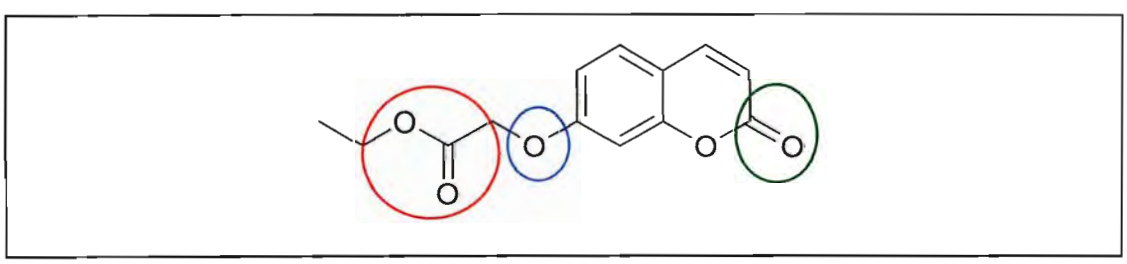

Figure 5.3: Functional groups of coumarin analogues.

Esters (Fig. 5.3: red) participate in hydrogen bonds as hydrogen-bond acceptors, but cannot act as hydrogen-bond donors. The limitations on their hydrogen bonding also make them more hydrophobic. Ethers (Fig. 5.3: blue) are more polar than alkenes but not as polar as alcohols, esters or amides. The presence of the two lone pairs of electrons on the oxygen atom makes hydrogen bonding with water molecules in the vicinity possible. Ketones (Fig. 5.3: green) are relatively polar groups and also act as hydrogen-bond acceptors. The carbonyl groups also interact with water via hydrogen bonding. The electron density maps of the synthesised compounds are included to visualise hydrogen bonding sites and possible molecular interactions.

5.3.1 Ethyl [(2-oxo-2H-chromen-7-yl)oxy]acetate (BPR 1)

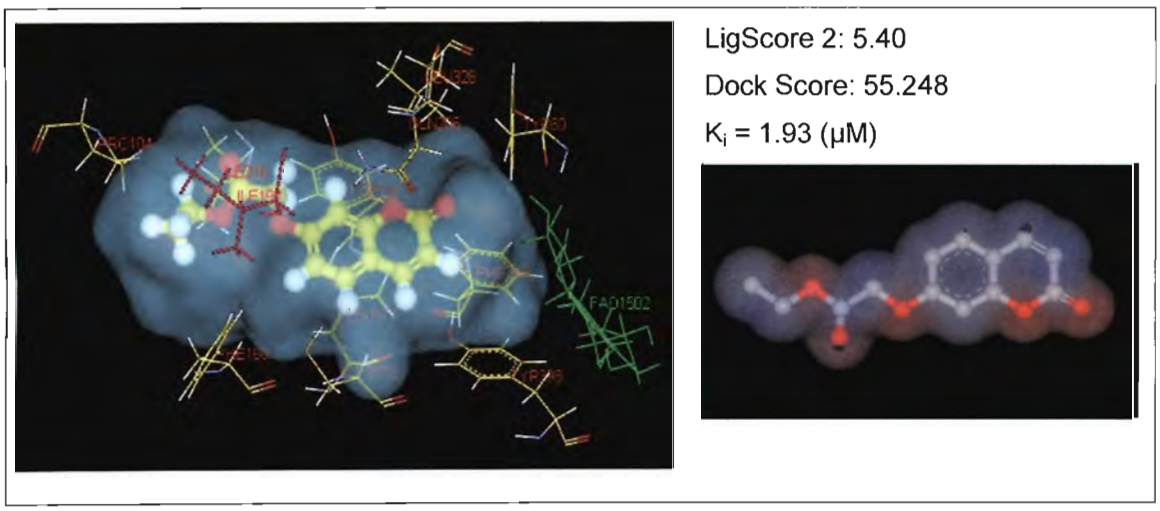

Figure 5.4: **BPR 1** (ball stick representation) in complex with the active site of MAO-B (blue transparent area) illustrating neighbouring amino acids (labelled in red), the FAD (in green) and Ile199 (in violet).

The unsubstituted coumarin nucleus binds in the substrate cavity with the pyran ring oxygen pointing towards Tyr326 at the top of the cavity. The methoxy ester is present near the Ile199 gating area (Fig. 5.4 and table 5.1).

Table 5.1: Molecular neighbours in the vicinity of the functional groups of **BPR 1**.

Ester (side chain)	Ether (side chain)	Coumarin
Ile199	Ile199	Tyr60
Pro104	Pro104	Leu171
Leu171	Ile316	Gln206
Ile316	Tyr326	Leu328
Tyr326		Tyr398
		Met341, Phe343

5.3.2 Ethyl [(4-methyl-2-oxo-2H-chromen-7-yl)oxy]acetate (BPR 2)

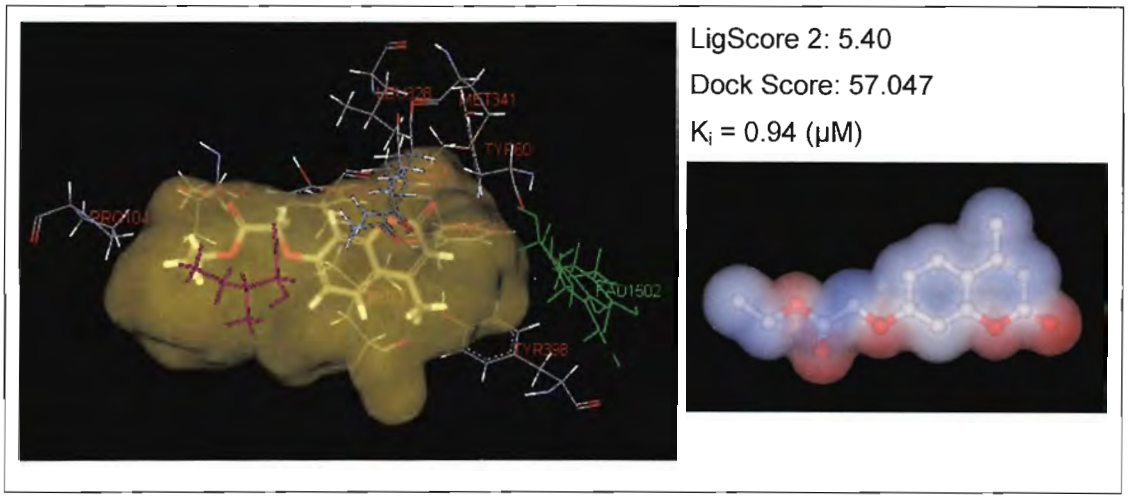

Figure 5.5: **BPR 2** (ball stick representation) in complex with the active site of MAO-B (yellow transparent area) illustrating neighbouring amino acids (labelled in red), the FAD (in green) and Ile199 (in violet).

The 4-substituted coumarin nucleus presents itself in the substrate cavity. The pyran oxygen is pointing towards the top of the cavity and the 4-methyl group downwards, while the methoxy ester side chain is present near the Ile199 gating area (Fig. 5.5 and table 5.2). Molecular modelling correlated with the experimental K_i value, and it was concluded that methoxy ester substitution in position 7 serves as a good pharmacophore model due to it's interactions in the gating area.

Table 5.2: Molecular neighbours in the vicinity of the functional groups of **BPR 2**

Ester (side chain)	Ether (side chain)	Coumarin	4-Methyl
Ile199	Ile199	Tyr60	Leu171
Pro104	Pro104	Leu171	Leu172
Leu171	Ile316	Gln206	Tyr435
Ile316	Tyr326	Leu328	Tyr398
Tyr326		Tyr398	
		Met341	
		Phe343	

5.3.3 4-Methyl-2-oxo-2H-chromen-7-yl decanoate (BPR 3)

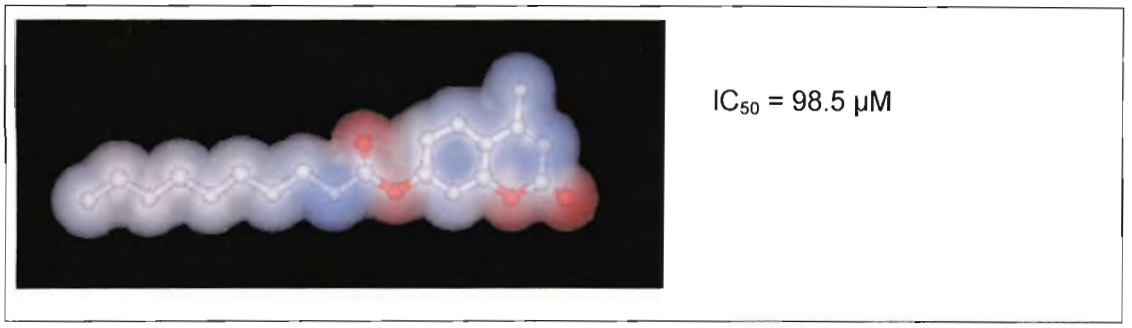

Figure 5.6: The electron density map of **BPR 3**.

No LigScore and Dock score was obtained. Discovery Studios 1.7® software indicated that the Lipinksi filter also did not apply for inhibition simulation. The high IC_{50} value observed (section 4.5.3) corresponds to the fact that the structure could not be docked effectively in the site (Fig. 5.6)

5.3.4 4-Methyl-2-oxo-2H-chromen-7-yl (2E)-3-phenylacrylate (BPR 4)

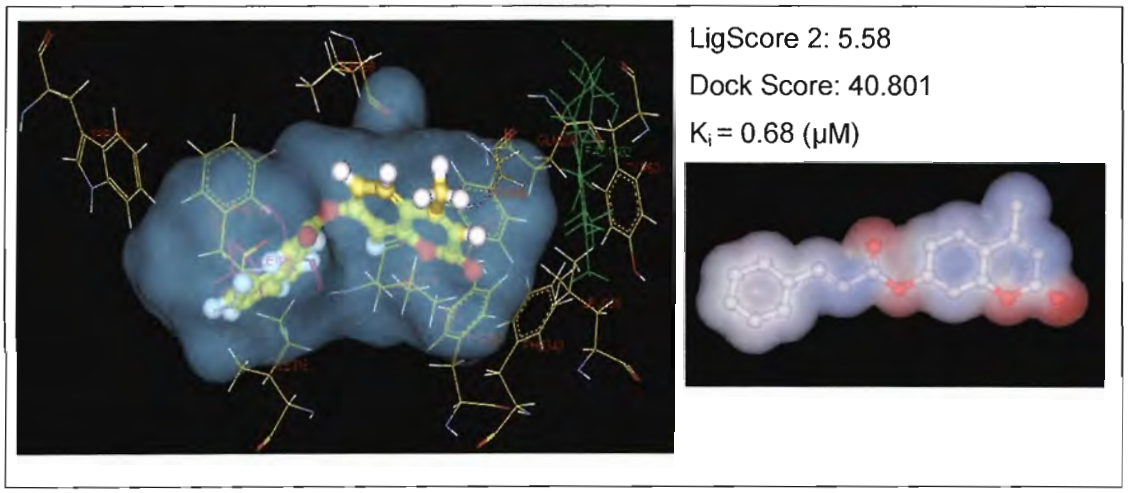

Figure 5.7: **BPR 4** (ball stick representation) in complex with the active site of MAO-B (blue transparent area) illustrating neighbouring amino acids (labelled in red), the FAD (in green) and Ile199 (in violet).

BPR 4 traversed both the entrance and the substrate cavity. The 4-substituted coumarin nucleus presents itself in the substrate cavity with the pyran oxygen at the top of the cavity and the 4-methyl group pointing downwards. The ester moiety is located near the Ile199 gating area, while the trans phenyl ring is localised in the entrance cavity. The styryl ester moiety directly substituted in the 7 position gave good dock scores and experimental K_i values, indicating potent MAO-B inhibition (Fig. 5.7 and table 5.3)

Table 5.3: Molecular neighbours in the vicinity of the functional groups of **BPR 4**

Trans phenyl (side chain)	Ester (side chain)	Coumarin	4-Methyl
Ile199	Phe168	Tyr60	Leu171
Trp119	Leu171	Leu171	Leu172
Leu171	Leu172	Gln206	Tyr435
Ile316	Ile198	Leu328	Tyr398
Tyr326	Ile199	Tyr398	
Phe168		Phe343	
		Tyr326	

5.3.5 1,3-Dimethyl-8-{[(4-methyl-2-oxo-2H-chromen-7-yl)oxy]methyl}-3,4,5,7-tetrahydro-1H-purine-2,6-dione (BPR 5)

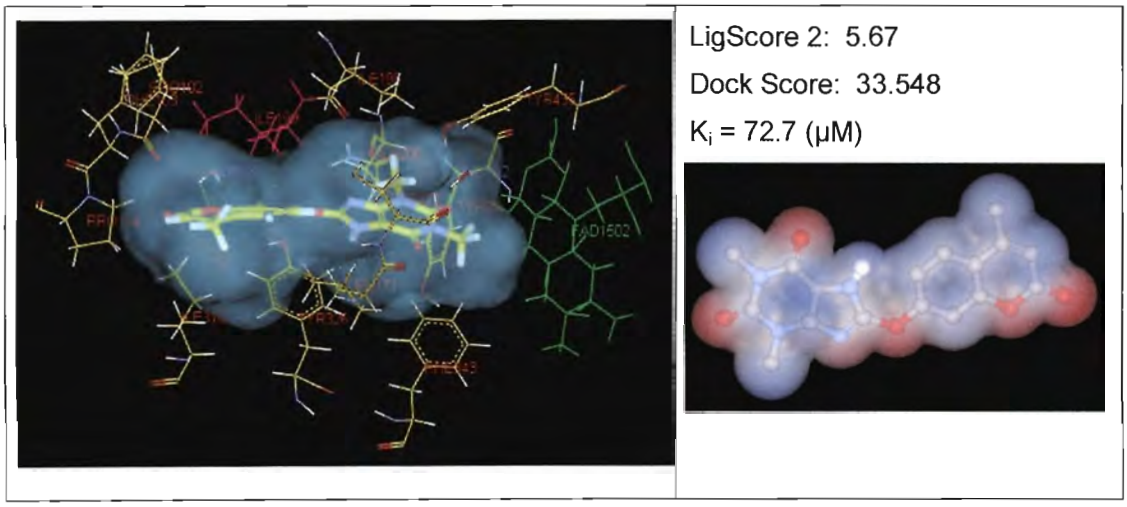

Figure 5.8: **BPR 5** (ball stick representation) in complex with the active site of MAO-B (blue transparent area) illustrating neighbouring amino acids (labelled in red), the FAD (in green) and Ile199 (in violet) are illustrated.

BPR 5 occupies both the cavities. The caffeine is placed in a favourable position within the substrate cavity, with the ether bridge in the Ile199 gating area. In this instance, the coumarin is localised in the entrance cavity. This confirms the theory that the most polar moiety will be situated in the substrate cavity. The higher K_i value could probably be attributed to the larger bulk and close proximity of the two ring structures without the presence of a spacer (Fig 5.8 and table 5.4)

Table 5.4: Molecular neighbours in the vicinity of the functional groups of **BPR 5**.

Caffeine	Ether (side chain)	Coumarin
Leu171	Ile199	Pro102
Cys172	Leu171	Phe103
Ile199	Ile198	Pro104
Gln206	Gln206	Ile199
Tyr326	Tyr326	Ile316
Phe343		Tyr326
Tyr435		
Tyr60		

5.3.6 Polycyclic tetradecane coumarin (BPR 6)

BPR 6 could not be docked within the MAO-B site due to the steric bulk of the cage structure. The active site of the enzyme thus exclude bulky molecules.

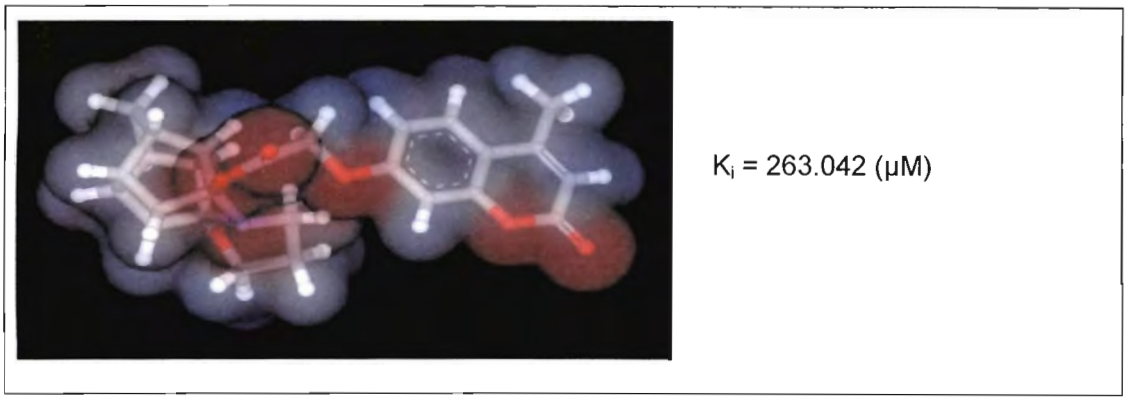

Figure 5.9: The electron density map of **BPR 6**.

5.4 CONCLUSION

Molecular modelling studies supported the experimental IC_{50} and K_i values. The 4-substituted analogues revealed a significant increase in affinity as well as favourable docking within the substrate cavity. The methoxy ester and other ester compounds (**BPR 1**,**2** and **4**) showed enhanced inhibitory activity probably due to multiple interactions with the amino acids in the gating area. Since the active site cavity has a specific and limited volume, certain structures with increased chain length (**BPR 3**) and bulkiness (**BPR 6**) are excluded from the site. Methylation of the caffeinyl inhibitor at C4 of the coumarin ring leads to enhanced MAO-B inhibition potency. Methylation of **BPR 5** could thus increase the affinity of the structure substantially.

In this study molecular modelling was used effectively to predict the inhibitory effect of this series of coumarin structures and identified crucial moieties within the compound for optimal activity.

Chapter 6 Discussion

6.1 INTRODUCTION

Monoamine oxidase B is a neurochemical target and its inhibition could prevent the occurrence of Parkinson's disease and other neurodegenerative disorders. It was hypothesised that combining the known MAO-B inhibition activity of the coumarin with other therapeutic agents, the conjugate could potentialy deliver dual mechanism drugs with enhanced value in the treatment of neurodegenerative diseases.

A series of coumarin analogues was synthesised and subjected to molecular modelling and MAO-B inhibition studies and for the test compounds, both the IC_{50} and K_i value were measured. The lines of the Lineweaver-Burke plots intersected and indicated that the mode of inhibition was competitive. Qualitative inspection of the results revealed some important SAR.

6.2 RESULTS

In this study the coumarin moiety was substituted at the 4 and 7 position and conjugated to the caffeine and tetradecane structure to obtain possible MTLs (multi-target-directed ligands) with neuroproptective properties.

6.2.1 Synthesis

Williamson etherfication (Fig. 6.1) of 7-hydroxycoumarin (**O**) and 4-methyl-7-hydroxycoumarin (**P**) with ethylbromoacetate yielded the corresponding coumarin methoxy esters, **BPR 1** and **BPR 2**. The 4-methylcoumarin methoxy ester was hydrolysed with KOH to yield the corresponding coumarin carboxylic acid **S**. This acid was subsequently conjugated with the 3-hydroxy-4-aza-8-oxaheptacyclotetradecane compound (**G**) using *activation chemistry* with DCC (N,N - dicyclohexylcarbodiimide) and DMAP (4 - dimethylaminopyridine) as a catalyst to give the polycyclic coumarin ester (**BPR 6**). In addition, the acid (**S**) was conjugated to the adenosine antagonist, caffeine, as well as to the styryl phenyl moiety using EDAC [1-ethyl-3-(-dimethylaminpropyl) carbodiimide hydrochloride] as activating agent (**BPR 5** & **BPR 4**). Compound **P** was also esterfied with decanoyl chloride to yield **BPR 3**.

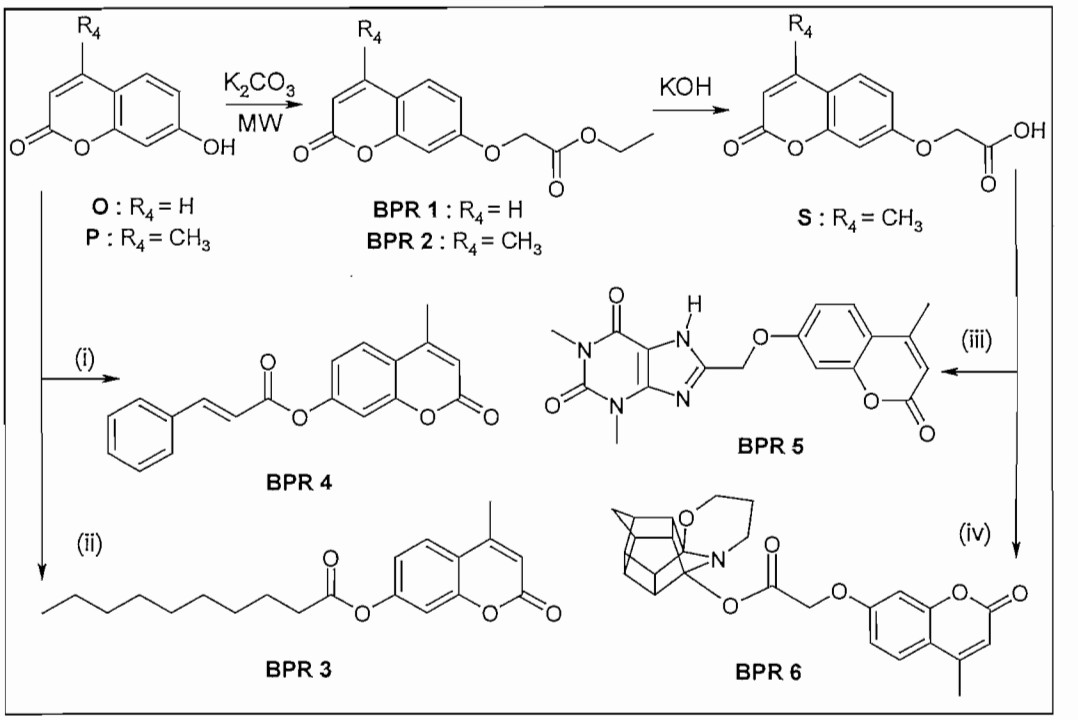

Figure 6.1: General outline of the synthesis of the compounds. (**i**) THF, NaH, decanoyl chloride. (**ii**) THF, NaH, acylchloride. (**iii**) Dioxane/H_2O, EDAC, 1,3-dimethyl-5,6-diaminouracil (**M**), NaOH. (**iv**) THF, DCC, DMAP, 3-hydroxy-4-aza-8-oxaheptacyclotetradecane (**G**).

6.2.2 Biological Evaluation

Employing a spectrophotometric assay, the activity of the synthesised compounds was evaluated. For this study, MMTP was selected as substrate as it has the following advantages: It serves as a good substrate for both forms of the enzyme; the dihydropyridinium metabolite is stable and no further oxidation to MMP^+ is observed [Fig. 6.2 (**A**)]; the relatively large molar extinction coefficient (ε = 25,000 M^{-1}) of $MMDP^+$; it has maximal absorbance at 420 nm, which is far removed from the wavelength of which mitochondrial background absorbance occurs. The $MMDP^+$ production can thus be measured spectrophotometrically at 420 nm, a wavelength at which neither the substrate nor the test inhibitors absorb light (Inoue *et al.*, 1999).

A test inhibitor will slow the rate of the MAO-B catalysed oxidation [Fig 6.2 (**B**)]) of MMTP to the corresponding dihydropyridinium ($MMDP^+$) metabolite (Nimkar *et al.*, 1996; Inoue *et al.*, 1999).

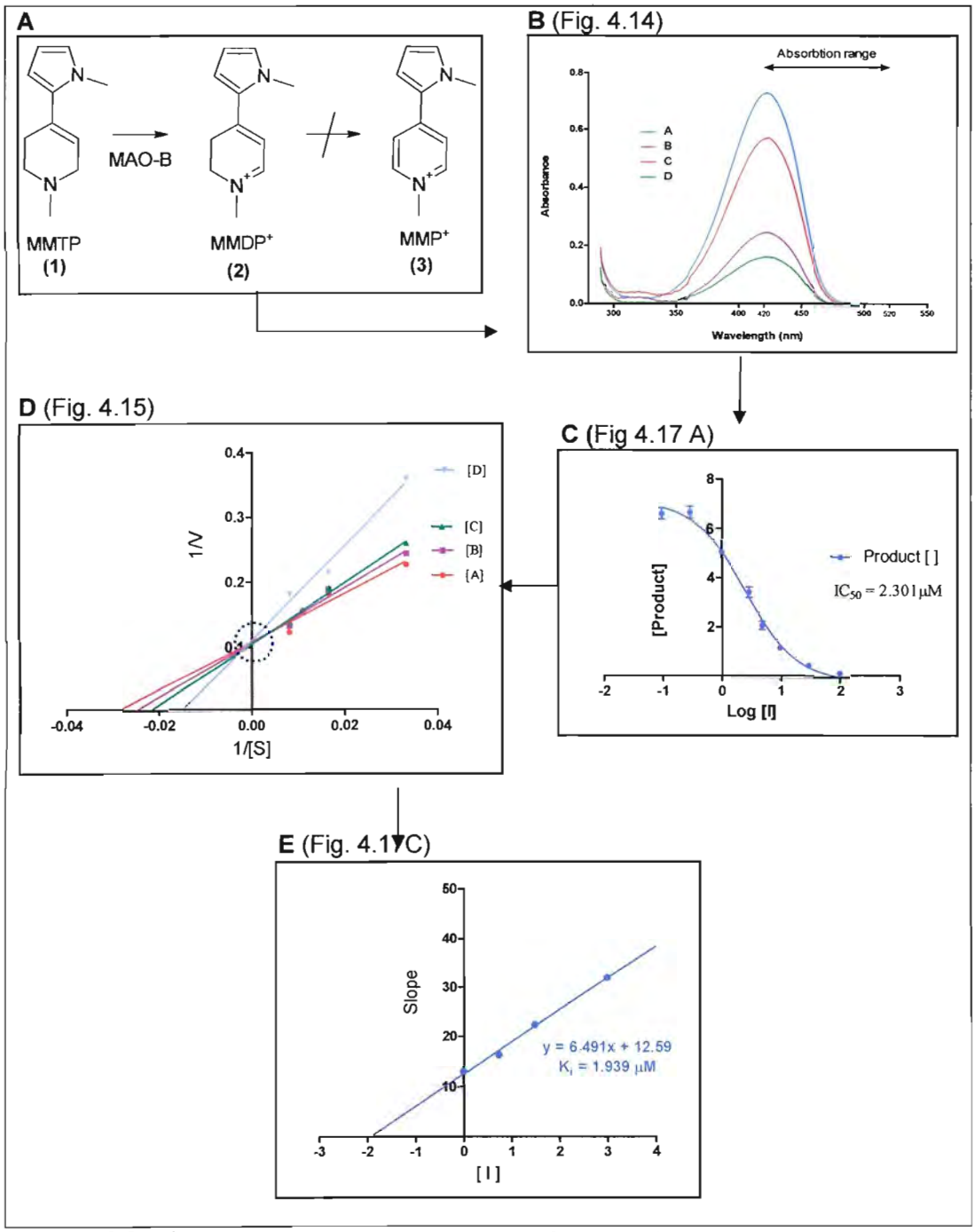

Figure 6.2: (**A**) The MAO-B catalysed oxidation of MMTP (**1**) to the corresponding dihydropyridinium product with different inhibitor concentrations; A=0 µM, B=10 µM, C=5 µM and D=20 µM (**2**). Futher *in vitro* oxidation to the pyridinium species (**3**) is not observed (Inoue *et al.*, 1999). (**B**) Graphical illustration of absorbance *vs.* wavelength with different concentrations inhibitor. (**C**) Product concentration *vs* Log [I] were plotted and the IC_{50} calculated. (**D**) Lineweaver-Burk plot for simple competitive inhibition. The lines converged (dotted blue sircle) on the y-axis. (**E**) The K_i value is obtained from a replot of the slopes of the Lineweaver-Burk plots *vs* the inhibitor concentration.

From a replot of the slopes of the Lineweaver-Burk plots [Fig. 6.2 (**E**)] *vs* the inhibitor concentration, the K_i values were obtained [Fig. 6.2 (**E**)]. The mitochondrial fraction obtained from baboon liver tissue was employed as enzyme source, since it is reported to be devoid of MAO-A activity while exhibiting a high degree of MAO-B catalytic activity. Even though MMTP is a MAO-A/B mixed substrate, its oxidation by baboon liver mitochondria can thus be exclusively attributed to the action of the MAO-B isoform (Inoue *et al.*, 1999).

6.2.2.1 Results

Table 6.1: Inhibition values (K_i, IC_{50}) obtained with the substituted coumarin analogues.

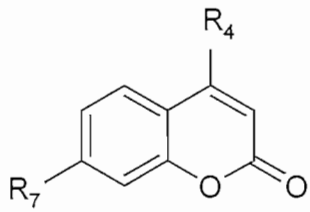

Compound	K_i (μM)	IC_{50} (μM)	Compound	K_i (μM)	IC_{50} (μM)
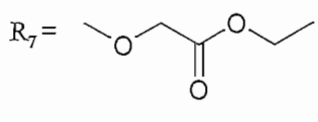 R_4 = H **BPR 1**	1.93	2.30	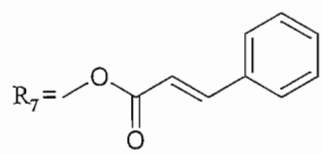 R_4 = CH_3 **BPR 4**	0.68	1.63
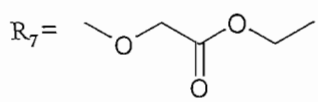 R_4 = CH_3 **BPR 2**	0.94	1.55	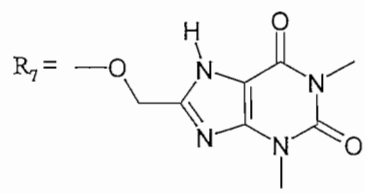 R_4 = CH_3 **BPR 5**	72.7	ND*
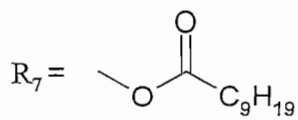 R_4 = CH_3 **BPR 3**	98.5	94.4	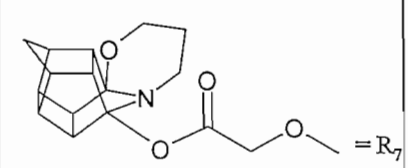 R_4 = CH_3 **BPR 6**	263.	ND*

ND: Not determined

The coumarin analogues containing a methyl group in the 4 position proved to be effective MAO-B inhibitors with a significant increase in MAO-B inhibition potency from the unsibstituted coumarin analogues (**BPR 1** *vs* **BPR 2**). Incorporating an alkyl methoxy ester in the 7 position improved the affinity for the MAO-B enzyme, while a long fatty acid chain (**BPR 3**) resulted in decreased MAO-B inhibitory activity. As with the previously reported caffeine MAO-B inhibitors, MAO-B inhibition was enhanced by substitution with the *trans* styryl side chain of **BPR 4**. Conjugating the coumarin and caffeine rings (**BPR 5**), led to decreased activity. Conjugation with the 3- hydroxy-4-aza-8-oxaheptacyclotetradecane compound (**BPR 6**) also impacted negatively on MAO-B activity.

6.2.3 Molecular Modelling

The MAO-B crystal structure of 1oj9 (http:www.pdb.org) with a resolution of 2.30 Å in complex with 1,4-diphenyl-2-butene, was obtained from the protein data bank. The crystal structure was imported into the Discovery Studios 1.7® software and the crystallised inhibitor was removed to allow docking of the proposed ligands. Docking was performed in the 'Dock Ligands' module (Ligandfit) with minimisation set as smart minimiser and scoring calculated as Ligandfit 2 and the consensus Dock Score. Hydrogen bond patterns in the vicinity of the ligand binding site were calculated and intermolecular neighbours were included in the docked representation for clarity (example: **BPR 1** in Fig. 6.3)

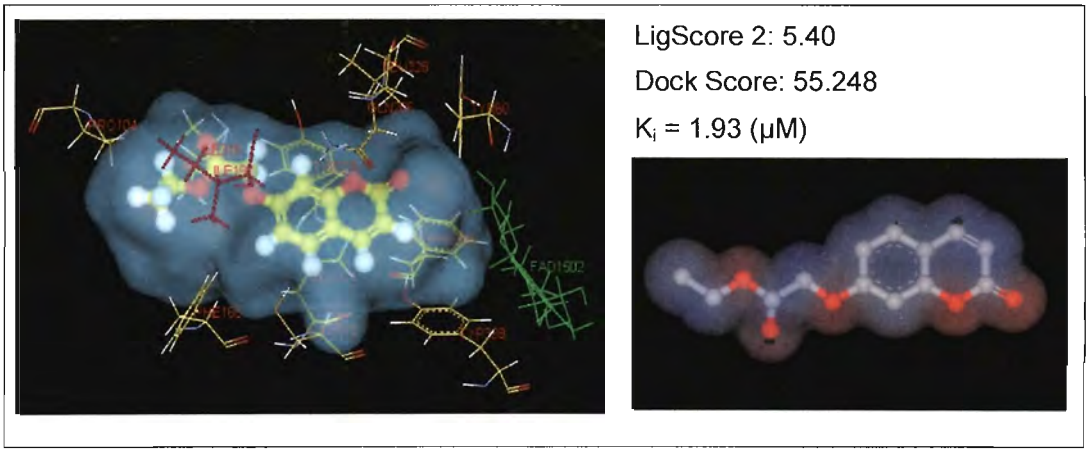

Figure 6.3: **BPR 1** (ball stick representation) in complex with the active site MAO-B (blue transparent area) illustrating neighbouring amino acids (labelled in red), the FAD (in green) and Ile199 (in violet).

The proposed inhibitors occupied both the substrate and the entrance cavities and the docking scores correlated with the experimental K_i and IC_{50} values. The highest Dock Score was obtained for **BPR 2**, while **BPR 3** and **BPR 6** could not be docked. The coumarin was presented inside the substrate cavity (except for **BPR 5**), while the ester and ether moieties

interacted with Leu171, Pro104 and Ile199 in the gating area. The 4 substituted coumarin also interacted with Leu328, Tyr398, Met341 and Phe343 near the FAD cofactor.

6.3 DISCUSSION

6.3.1 Ethyl [(2-oxo-2H-chromen-7-yl)oxy]acetate (BPR 1) and ethyl [(4-methyl-2-oxo-2H-chromen-7-yl)oxy]acetate (BPR 2)

Substitution at position 4 of the coumarin ring resulted in a signifficant increase of MAO-B inhibitory activity. This was evident from the K_i and IC_{50} values of **BPR 1** (1.939 µM and 2.301 µM) compound *versus* that of **BPR 2** (0.947 µM and 1.55 µM). The methyl group's influence on the activity of **BPR 2** may be explained by an increased binding in the substrate cavity and better occupation of this region. For **BPR 2**, Tyr434 and Tyr398 were drawn closer to the coumarin, resulting in tighter binding and a higher MAO-B potency. A dock score of 55.248 for **BPR 1** and 57.047 for **BPR 2** was obtained. The simulation data also indicated favourable binding in the substrate cavity. Small hydrophobic groups may thus be substituted on this position for further investigation.

Both **BPR 1** & **BPR 2** have lower IC_{50} values than umbelliferone and a methoxy ester in position 7 proved to elevate the MAO-B potency of the coumarin ring. This polar ester region of the compounds are situated in the gating area of the enzyme. The influence of the alkyl methoxy ester thus causes tighter binding in the gating area, as more amino acid residues are involved in binding. Another hypothesis is that the gating area with Ile199 'pushes' the coumarin closer to the FAD within the substrate cavity.

6.3.2 4-Methyl-2-oxo-2H-chromen-7-yl decanoate (BPR 3)

We examined the effect that the chain length of the C-7 side chain has on the inhibition activity of the coumarin. The weak IC_{50} of 98.55 µM obtained, corresponded to the fact that **BPR 3** could not be docked. This structure may simply be too 'stretched' for the enzyme and suggest limitations on the size of the active site. Another consideration is that the high Log D value for this compound did not fit the pharmacokinetic profile. No docking was obtained even when the Lipinksi filter setting was ignored. Lipinski's Rule (Lipinski *et al.*, 2001) can be used as a rule of thumb to indicate whether a molecule is likely to be orally bioavailable (bioactive).

In general, an orally active drug has:

- Not more than 5 hydrogen bond donors (OH and NH groups).
- Not more than 10 hydrogen bond acceptors (sum of N and O).
- A molecular weight under 500 g/mol.
- A partition coefficient log P less than 5.

The rules have spawned many extensions, for example:

- Partition coefficient log P of 0.4 to +5.6 range.
- Molar refractivity from 40 to 130.
- Molecular weight from 160 to 480.
- Number of heavy atoms from 20 to 70 (Ghose *et al.*, 1999).

6.3.3 4-Methyl-2-oxo-2H-chromen-7-yl (2E)-3-phenylacrylate (BPR 4)

Incorporation of a *trans* styryl ester moiety at the C-7 of the coumarin ring, resulted in potent MAO-B activity. With a K_i of 0.68 µM and an IC_{50} of 1.68 µM, **BPR 4** proved to be the most potent inhibitor of this series. The coumarin is presented in the substrate cavity, the ester functional group in the gating area while the phenyl is situated in the entrance cavity to give a dock score of 40.801. It's hypothesised that filling the entrance cavity with a limited bulkier structure, pushes the compound into the substrate cavity. Saturation of bonds as well as conjugation with an aromatic moiety thus resulted in high MAO-B inhibition.

6.3.4 16,18-Dimethyl-8-{[(4-methyl-2-oxo-2H-chromen-7-yl)oxy]methyl}-xanthine (BPR 5)

BPR 5 exhibited very weak activity and a high K_i value of 72.7 µM was obtained. Because an inhibitor must transverse the entrance cavity to gain access to the FAD, it became clear that a planar structure is absolutely essential for MAO-B ihibition and too many free rotations are not well tolerated. Although previous authors have demostrated that an ether in position 7 is favourable, **BPR 5** is not planar enough. With molecular modelling, both the cavities are occupied, presenting a low dock score of 33.548. The high K_i value observed corresponds to the lower dock score. The partial solubility and large PSA of 91.42 $Å^2$ of the compound may also be contributing factors. In the docking study, the coumarin is observed in the entrance cavity while the the more polar caffeine is found in the substrate cavity.

6.3.5 3-{4-Aza-8-oxoheptacyclo[0.4.1.$0^{2,10}$.$0^{3,14}$.$0^{4,9}$.$0^{9,13}$.$0^{12,15}$] tetradecyl} - [(4'-methyl-2'-oxo-2H-chromen-7'-yl)oxy] acetate (BPR 6)

Conjugation with the 3-hydroxy-4-aza-8-oxaheptacyclotetradecane (**BPR 6**) yielded a coumarin strucutre with a K_i value of 263.04 µM. The weak affinity for the enzyme may be due to the steric bulk of the structure. Because the active site of the enzyme has a limited size, **BPR 6** could not be accommodated. Docking of this ligand could not be performed, even with an enlarged active site.

6.4 Conclusion.

The most potent inhibitor among the analogues was the 4-methyl-2-oxo-2H-chromen-7-yl (2E)-3-phenylacrylate (**BPR 4**) while the least potent inhibitor was found to be the tetradecane conjugate (**BPR 6**). The results obtained established that the potency of MAO-B inhibition by the coumarin derivatives examined is depended on chain length, lipophilicity, planarity and steric bulk of the substituents in position 7 of the coumarin.

The potency of MAO-B inhibition by the coumarin derivatives examined can be summarised as follows:

- Methyl substitution in position 4 improved affinity and K_i (**BPR 1** *vs.* **BPR 2**)
- An ester or alkyl methoxy ester in position 7 (**BPR 4**) leads to favourable MAO-B inhibition.
- Extended chain length (**BPR 3**), nonplanarity (**BPR 5**) and steric bulk (**BPR 6**) impacted negatively on MAO-B inhibition.

In conclusion, the ester and methoxy ester coumarin derivatives proved to be highly potent, competitive MAO-B inhibitors and further studies to establish a comprehensive SAR and possible dual mechanism of action (eg. A_{2A} and NMDA antagonism) for these compounds are warranted.

References

ABELES, R.H. & MAYCOCK, A.L. 1976. Suicide enzyme inactivators. *Accounts of chemical research*, **9**(1), pp. 313-319.

ADOLFSSON, R., GOTTFRIES, C., ORELAND, L., WIBERG, Å and WINBLAD, B., 1980. Increased activity of brain and platelet monoamine oxidase in dementia of Alzheimer type. *Life Sciences,* **27**(12), pp. 1029-1034.

AGID, Y., AHLSKOG, E., ALBANESE, A., CALNE, D., CHASE, T., DE YEBENES, J., FACTOR, S., FAHN, S., GERSHANIK, O., GOETZ, C., KOLLER, W., KURTH, M., LANG, A., LEES, A., LEWITT, P., MARSDEN, D., MELAMED, E., MICHEL, P.P., MIZUNO, Y., OBESO, J., OERTEL, W., OLANOW, W., POEWE, W., POLLAK, P. and TOLOSA, E., 1999. Levodopa in the treatment of Parkinson's disease: a consensus meeting. *Movement Disorders: Official Journal Of The Movement Disorder Society,* **14**(6), pp. 911-913.

ALI, A. and ROBINSON, J.B., 1991. Synthesis, biological evaluation and quantitative structure activity relationship analysis of nuclear-substituted pargylines as competitive inhibitors of MAO-A and MAO-B. *The Journal of pharmacy and pharmacology,* **43**(11), pp. 750-757.

AKYÜZ, M.A., ERDEM, S.S. and EDMONDSON, D.E., 2007. The aromatic cage in the active site of monoamine oxidase B: effect on the structural and electronic properties of bound benzylamine and p-nitrobenzylamine. *Journal of neural transmission,* **114**(6), pp. 693-698.

ALVAREZ, A., BRONFMAN, F., PEREZ, C.A., VICENTE, M., GARRIDO, J. & INESTROSA, N.C. 1995. Acetylcholinesterase, a senile plaque component, affects the fibrillogenesis of amyloid-beta-peptides. *Neuroscience Letters*, **201**(1), pp. 49–52.

ARTAL-SANZ, M. and TAVERNARAKIS, N., 2005. Proteolytic mechanisms in necrotic cell death and neurodegeneration. *Federation of European Biochemical Societies letters,* **579**(15), pp. 3287-3296.

BACH, A.W., LAN, N.C., JOHNSON, D.L., ABELL, C.W., BEMBENEK, M.E., KWAN, S.W., SEEBURG, P.H. and SHIH, J.C., 1988. cDNA cloning of human liver monoamine oxidase A and B: molecular basis of differences in enzymatic properties. *Proceedings of the National Academy of Sciences of the United States of America,* **85**(13), pp. 4934-4938.

BARA-JIMENEZ, W., SHERZAI, A., DIMITROVA, T., FAVIT, A., BIBBIANI, F., GILLESPIE, M., MORRIS, M.J., MOURADIAN, M.M. and CHASE, T.N., 2003. Adenosine A_{2A} receptor antagonist treatment of Parkinson's disease. *Neurology,* **61**(3), pp. 293-296.

BEAL, M.F., 2003. Mitochondria, oxidative damage, and inflammation in Parkinson's disease. *Annals of the New York Academy of Sciences,* **991**(1), pp. 120-131.

BEMBENEK, M.E., ABELL, C.W., CHRISEY, L.A., ROZWADOWSKA, M.D., GESSNER, W. and BROSSI, A., 1990. Inhibition of monoamine oxidases A and B by simple isoquinoline alkaloids: racemic and optically active 1,2,3,4-tetrahydro-, 3,4-dihydro-, and fully aromatic isoquinolines. *Journal of medicinal chemistry,* **33**(1), pp. 147-152.

BINDA, C., HUBÁLEK, F., LI, M., EDMONDSON, D.E. and MATTEVI, A., 2004. Crystal structure of human monoamine oxidase B, a drug target enzyme monotopically inserted into the mitochondrial outer membrane. *FEBS letters,* **564**(3), pp. 225.

BINDA, C., HUBÁLEK, F., LI, M., HERZIG, Y., STERLING, J., EDMONDSON, D.E. and MATTEVI, A., 2004. Crystal structures of monoamine oxidase B in complex with four inhibitors of the N-propargylaminoindan class. *Journal of medicinal chemistry,* **47**(7), pp. 1767-1774.

BINDA, C., MATTEVI, A. and EDMONDSON, D.E., 2002. Structure-function relationships in flavoenzyme-dependent amine oxidations. A comparison of polyamine oxidase and monoamine oxidase. *The Journal of Biological Chemistry,* **277**(27), pp. 23973-23976.

BINDA, C., MIN LI, HUBÁLEK, F., RESTELLI, N., EDMONDSON, D.E. and MATTEVI, A., 2003. Insights into the mode of inhibition of human mitochondrial monoamine oxidase B from high-resolution crystal structures. *Proceedings of the National Academy of Sciences of the United States of America,* **100**(17), pp. 9750-9755.

BINDA, C., NEWTON-VINSON, P., HUBÁLEK, F., EDMONDSON, D.E. and MATTEVI, A., 2002. Structure of human monoamine oxidase B, a drug target for the treatment of neurological disorders. *Nature structural biology,* **9**(1), pp. 22.

BISHOP, T. and SHAM, P., 2000. *Analysis of Multifactorial Diseases.* Academic Press: New York, pp. 1-320.

BLICKE, F.F. & GODT, H.C., Jr. 1954. Reactions of 1,3-dimethyl-5,6-diaminouracil. *Journal of the American chemical society*, **76**(1): pp. 2798-2800.

BLISS, T.V.P. and COLLINGRIDGE, G.L., 1993. A synaptic model of memory: Long-term potentiation in the hippocampus. *Nature,* **361**(6407), pp. 31.

BONDI, A. 1964. van der Waals volumes and radii. *The Journal of Physical chemistry*, **68**(3), pp. 441-451.

BRAAK, E., GRIFFING, K., ARAI, K., BOHL, J., BRATZKE, H. and BRAAK, H., 1999. Neuropathology of Alzheimer's disease: what is new since A. Alzheimer? *European Archives of Psychiatry & Clinical Neuroscience,* **249**, pp. S14.

BRAAK, H. and BRAAK, E., 1991. Neuropathological stageing of Alzheimer-related changes. *Acta Neuropathologica,* **82**(4), pp. 239-259.

BRüHLMANN, C., OOMS, F., CARRUPT, P.A., TESTA, B., CATTO, M., LEONETTI, F., ALTOMARE, C. and CAROTTI, A., 2001. Coumarins derivatives as dual inhibitors of acetylcholinesterase and monoamine oxidase. *Journal of medicinal chemistry,* **44**(19), pp. 3195-3198.

CASTAGNOLI, K., PALMER, S., ANDERSON, A., BUETERS, T. and CASTAGNOLI, N., 1997. The neuronal nitric oxide synthase inhibitor 7-nitroindazole also inhibits the monoamine oxidase-B-catalyzed oxidation of 1-methyl-4-phenyl-1,2,3,6-tetrahydropyridine. *Chemical research in toxicology,* **10**(4), pp. 364-368.

CAUGHEY, B. and LANSBURY, P.T.,JR, 2003. Protofibrils, Pores, Fibrils, and Neurodegeneration: Separating the Responsible Protein Aggregates from The Innocent Bystanders. *Annual Review of Neuroscience,* **26**, pp. 267-298.

CAVALLI, G., 2007. Chromosome kissing. *Current Opinion in Genetics & Development,* **17**(5), pp. 443-450.

CHAKRAVORTY, S.G. and HALBREICH, U., 1997. The influence of estrogen on monoamine oxidase activity. *Psychopharmacology bulletin,* **33**(2), pp. 229-233.

CHEN, J., STEYN, S., STAAL, R., PETZER, J.P., XU, K., VAN DER SCHYF,CORNELIS J., CASTAGNOLI, K., SONSALLA, P.K., CASTAGNOLI, N., and SCHWARZSCHILD, M.A., 2002. 8-(3-Chlorostyryl)caffeine may attenuate MPTP neurotoxicity through dual actions of monoamine oxidase inhibition and A2A receptor antagonism. *The Journal Of Biological Chemistry,* **277**(39), pp. 36040-36044.

CHENG, Y. and PRUSOFF, W.H., 1973. Relationship between the inhibition constant (K1) and the concentration of inhibitor which causes 50 per cent inhibition (I50) of an enzymatic reaction. *Biochemical pharmacology,* **22**(23), pp. 3099-3108.

CHIBA, K., TREVOR, A. and CASTAGNOLI, N., 1984. Metabolism of the neurotoxic tertiary amine, MPTP, by brain monoamine oxidase. *Biochemical and biophysical research communications,* **120**(2), pp. 574-578.

COOKSON, R.C., GRUNDWELL, E., HILL, R.R. & HUDEC, J. 1964. Photochemical cyclisation of Diels-Alder adducts. Journal of the Chemical Society, 1, pp. 3062-3075.

COPPEDÈ, F., MANCUSO, M., SICILIANO, G., MIGLIORE, L. and MURRI, L., 2006. Genes and the environment in neurodegeneration. *Bioscience reports,* **26**(5), pp. 341-367.

CRUTS, M. & VAN BROECKHOVEN, C. 1998. Molecular genetics of Alzheimer's disease. *European Journal of Neurology*, **11**(8), pp. 521.

CUTLER, D., 2001. Mice cured of Alzheimer's disease. *Trends in Pharmacological Sciences,* **22**(10), pp. 501-501.

DEANA, A.A., STOKKER, G.E., SCHULTZ, E.M., SMITH, R.L., GRAGOE, E.J., Jr, RUSSO, H.F. & WATSON, L.S. 1983. 2-(Aminomethyl)phenols, a new class of saluretic agents. *Journal of Medicinal chemistry*. **26**(4), pp. 580–585.

DE COLIBUS, L., MIN LI, BINDA, C., LUSTIG, A., EDMONDSON, D.E. and MATTEVI, A., 2005. Three-dimensional structure of human monoamine oxidase A (MAO A): Relation to the structures of rat MAO A and human MAO B. *Proceedings of the National Academy of Sciences of the United States of America,* **102**(36), pp. 12684-12689.

DiMONTE, D.A. 2006. The environment and Parkinson's disease: is the nigrostriatal system preferentially targeted by neurotoxins ? *The Neuroscientist*, **12**(6), pp. 469-476.

DONNELLY, C.H. and MURPHY, D.L., 1977. Substrate- and inhibitor-related characteristics of human platelet monoamine oxidase. *Biochemical pharmacology,* **26**(9), pp. 853-858.

DOODY, R.S., 1999. Therapeutic standards in Alzheimer disease. *Alzheimer Disease and Associated Disorders,* **13 Suppl 2**, pp. S20-6.

DORAISWAMY, P.M. 2002. Non-cholinergic strategies for treating and preventing Alzheimer's disease. *CNS Drugs*, **16**(12), pp. 811–824.

DRUKARCH, B. and VAN MUISWINKEL, F.L., 2000. Drug treatment of Parkinson's disease. Time for phase II. *Biochemical pharmacology,* **59**(9), pp. 1023-1031.

EDMONDSON, D.E., BHATTACHARRYA, A.K. and XU, J., 2000. Evidence for alternative binding modes in the interaction of benzylamine analogues with bovine liver monoamine oxidase B. *Biochimica et biophysica acta,* **1479**(1-2), pp. 52-58.

EDMONDSON, D.E., MATTEVI, A., BINDA, C., LI, M. and HUBÁLEKA, F., 2004. Structure and Mechanism of Monoamine Oxidase. *Current medicinal chemistry,* **11**(15), pp. 1983-1993.

EDMONDSON, D.E., BINDA, C. and MATTEVI, A., 2007. Structural insights into the mechanism of amine oxidation by monoamine oxidases A and B. *Archives of Biochemistry & Biophysics,* **464**(2), pp. 269-276.

EKBLOM, J., JOSSAN, S.S., BERGSTRÖM, M., ORELAND, L., WALUM, E. and AQUILONIUS, S.M., 1993. Monoamine oxidase-B in astrocytes. *Glia,* **8**(2), pp. 122-132.

EKSHYYAN, O. and AW, T.Y., 2004. Apoptosis: A Key in Neurodegenerative Disorders. *Current Neurovascular Research,* **1**(4), pp. 355-371.

ERTL, P., ROHDE, B. & SELZER, P. 2000. Fast Calculation of Molecular Polar Surface Area as a Sum of Fragment-Based Contributions and Its Application to the Prediction of Drug Transport Properties. *Journal of Medicinal Chemistry*, **43**(1): pp. 3714-3717.

FAHN, S., 2000. The spectrum of levodopa-induced dyskinesias. *Annals of Neurology,* **47**(4 Suppl 1), pp. S2-9; discussion S9-11.

FISHER, E. 1894. Einfluss der configuration auf die Wirkung der enzyme. *Berlin Deutsche Chemie Gesellschaft*, **27**(1). pp.85–93.

FEUER, G., 1974. 3 The Metabolism and Biological Actions of Coumarins. In: G.P. ELLIS, and G.B. WEST, ed, *Progress in Medicinal Chemistry,* Elsevier, pp. 85-158.

FOWLER, C.J. and ORELAND, L., 1980. The nature of the substrate-selective interaction between rat liver mitochondrial monoamine oxidase and oxygen. *Biochemical Pharmacology,* **29**(16), pp. 2225-2233.

FRANTZ, S., 2005. Drug discovery: Playing dirty. *Nature,* **437**(7061), pp. 942-943.

FUJITA, T., IWASA, J. & HANSCH, C. A. 1964. New substituent constant, π, derived from partition coefficients. *Journal of the American Chemical Society*, **86**(1), pp. 5175.

GALVA, M.D., BONDIOLOTTI, G.P., OLASMAA, M. and PICOTTI, G.B., 1995. Effect of aging on lazabemide binding, monoamine oxidase activity and monoamine metabolites in human frontal cortex. *Journal Of Neural Transmission.General Section,* **101**(1-3), pp. 83-94.

GEHA, R.M., REBRIN, I. and CHEN, K., 2001. Substrate and inhibitor specificities for human monoamine oxidase A and B are influenced by a single amino acid. *The Journal of Biological Chemistry,* **276**(13), pp. 9877-9882.

GELDENHUYS, W.J., MALAN, S.F., BLOOMQUIST, J.R., MARCHAND, A.P. and VAN DER SCHYF,CORNELIS J., 2005. Pharmacology and structure-activity relationships of bioactive polycyclic cage compounds: a focus on pentacycloundecane derivatives. *Medicinal research reviews,* **25**(1), pp. 21-48.

GERBER, M., BREYTENBACH, J.C. and DU PLESSIS, J., 2008. Transdermal penetration of zalcitabine, lamivudine and synthesised N-acyl lamivudine esters. *International journal of pharmaceutics,* **351**(1), pp. 186-193.

GHOSE, A.K., VISWANADHAN, V.N. and WENDOLOSKI, J.J., 1999. A knowledge-based approach in designing combinatorial or medicinal chemistry libraries for drug discovery. 1. A qualitative and quantitative characterization of known drug databases. *Journal of combinatorial chemistry,* **1**(1), pp. 55-68.

GNERRE, C., CATTO, M., LEONETTI, F., WEBER, P., CARRUPT, P.A., ALTOMARE, C., CAROTTI, A. and TESTA, B., 2000. Inhibition of monoamine oxidases by functionalized coumarin derivatives: biological activities, QSARs, and 3D-QSARs. *Journal of medicinal chemistry,* **43**(25), pp. 4747-4758.

GRAHAM, D.G., TIFFANY, S.M., BELL, W.R., and GUTKNECHT, W.F., 1978. Autoxidation versus covalent binding of quinones as the mechanism of toxicity of dopamine, 6-hydroxydopamine, and related compounds toward C1300 neuroblastoma cells in vitro. *Molecular pharmacology,* **14**(4), pp. 644-653.

GRIMSBY, J., LAN, N.C., NEVE, R., CHEN, K. and SHIH, J.C., 1990. Tissue distribution of human monoamine oxidase A and B mRNA. *Journal of neurochemistry,* **55**(4), pp. 1166-1169.

HALLIWELL, B., 1992. Reactive oxygen species and the central nervous system. *Journal of neurochemistry,* **59**(5), pp. 1609-1623.

HANSCH, C., HOEKMAN, D., LEO, A., ZHANG, L. and LI, P., 1995. The expanding role of quantitative structure-activity relationships (QSAR) in toxicology. *Toxicology letters,* **79**(1-3), pp. 45-53.

HANSCH, C. & LEO, A. 1995. Exploring QSAR. Fundamentals and Applications in Chemistry and Biology. *Journal of the American Chemical Society*, pp. 1–24.

HORNYKIEWICZ, O. and KISH, S.J., 1987. Biochemical pathophysiology of Parkinson's disease. *Advances in Neurology,* **45**, pp. 19-34.

HOULT, J.R. and PAYÁ, M., 1996. Pharmacological and biochemical actions of simple coumarins: natural products with therapeutic potential. *General pharmacology,* **27**(4), pp. 713-722.

HUBÁLEK, F., POHL, J. and EDMONDSON, D.E., 2003. Structural Comparison of Human Monoamine Oxidases A and B. *Journal of Biological Chemistry,* **278**(31), pp. 28612.

HUBÁLEK, F., BINDA, C., KHALIL, A., LI, M., MATTEVI, A., CASTAGNOLI, N. & EDMONDSON. D.E. 2005. Demonstration of isoleucine 199 as a structural determinant for the selective inhibition of human monoamine oxidase B by specific reversible inhibitors. *Journal of Biological Chemistry,* **280**(16), pp. 15761-15766.

HUNOT, S. and BRUGG, B., 1997. Nuclear translocation of NF-kB is increased in dopaminergic neurons of patients with Parkinson's disease. *Proceedings of the National Academy of Sciences of the United States of America,* **94**(14), pp. 7531.

HUNOT, S., DUGAS, N. and FAUCHEUX, B., 1999. FceRII/CD23 is expressed in Parkinson's disease and induces, in vitro, production of nitric oxide and tumor necrosis factor-a in glial cells. *Journal of Neuroscience,* **19**(9), pp. 3440-3447.

HURLEY, S.D., O'BANION, M.K., SONG, D.D., ARANA, F.S., OLSCHOWKA, J.A. and HABER, S.N., 2003. Microglial response is poorly correlated with neurodegeneration following chronic, low-dose MPTP administration in monkeys. *Experimental neurology,* **184**(2), pp. 659.

HYNSON, R.M.G., WOUTERS, J. & RAMSAY, J.R. 2003. Monoamine oxidase A inhibitory potency and flavin perturbation are influenced by different aspects of pirlindole inhibitor structure. *Biochemical Pharmacology*, **65**(11), pp. 1867–1874.

INOUE, H., CASTAGNOLI, K., VAN DER SCHYFF, C.J., MABIC, S., IGARASHI, K. & CASTAGNOLI, N., 1999. Species-dependent differences in monoamine oxidase A and B-catalyzed oxidation of various C4 substituted 1-methyl-4-phenyl-1,2,3,6-tetrahydropyridinyl derivatives. *The journal of pharmacology and experimental therapeutics*, **291**(2), pp. 856-264.

IKEDA, K., KUROKAWA, M., AOYAMA, S. and KUWANA, Y., 2002. Neuroprotection by adenosine A_{2A} receptor blockade in experimental models of Parkinson's disease. *Journal of neurochemistry,* **80**(2), pp. 262-270.

ISCHIROPOULOS, H. and BECKMAN, J.S., 2003. Oxidative stress and nutrition in neurodegeneration: Cause, effect, or association? *Journal of Clinical Investigation,* **111**(2), pp. 163.

JACOBSON, K.A., NIKODIJEVIC, O., PADGETT, W.L., GALLO-RODRIGUEZ, C., MAILLARD, M. and DALY, J.W., 1993. 8-(3-Chlorostyryl)caffeine (CSC) is a selective A2-adenosine antagonist in vitro and in vivo. *FEBS letters,* **323**(1-2), pp. 141-144.

JANCA, A. 2004. WHO global campaigns: a way forward in addressing public health importance of common neurological disorders. *Annals of General Hospital Psychiatry*, **3**(1), pp. 9.

JELLINGER, K.A., 2003. General aspects of neurodegeneration. *Journal of neural transmission.Supplementum,* **(65)**(65), pp. 101-144.

JOSSAN, S.S., GILLBERG, P.G., GOTTFRIES, C.G., KARLSSON, I. and ORELAND, L., 1991. Monoamine oxidase B in brains from patients with Alzheimer's disease: a biochemical and autoradiographical study. *Neuroscience,* **45**(1), pp. 1-12.

KAGAN, B.L., HIRAKURA, Y., AZIMOV, R., AZIMOVA, R. and LIN, M., 2002. The channel hypothesis of Alzheimer's disease: current status. *Peptides,* **23**(7), pp. 1311.

KANDA, T., JACKSON, M.J., SMITH, L.A., PEARCE, R.K., NAKAMURA, J., KASE, H., KUWANA, Y. and JENNER, P., 2000. Combined use of the adenosine A(2A) antagonist KW-6002 with L-DOPA or with selective D1 or D2 dopamine agonists increases antiparkinsonian activity but not dyskinesia in MPTP-treated monkeys. *Experimental neurology,* **162**(2), pp. 321-327.

KEARNEY, E.B., SALACH, J.I., WALKER, W.H., SENG, R.L., KENNEY, W., ZESZOTEK, E. and SINGER, T.P., 1971. The covalently-bound flavin of hepatic monoamine oxidase. 1. Isolation and sequence of a flavin peptide and evidence for binding at the 8alpha position. *European Journal Of Biochemistry,* **24**(2), pp. 321-327.

KELDER, J., GROOTENHUIS, P.D., BAYADA, D.M., DELBRESSINE, L.P. and PLOEMEN, J.P., 1999. Polar molecular surface as a dominating determinant for oral absorption and brain penetration of drugs. *Pharmaceutical research,* **16**(10), pp. 1514-1519.

KIAEI, M., KIPIANI, K., CALINGASAN, N.Y., WILLE, E., CHEN, J., HEISSIG, B., RAFII, S., LORENZL, S. and BEAL, M.F., 2007. Matrix metalloproteinase-9 regulates TNF-α and FasL expression in neuronal, glial cells and its absence extends life in a transgenic mouse model of amyotrophic lateral sclerosis. *Experimental neurology,* **205**(1), pp. 74-81.

KLEBANOFF, S.J., 2005. Myeloperoxidase: friend and foe. *Journal of leukocyte biology,* **77**(5), pp. 598-625.

KLINMAN, J.P. and MU, D., 1994. Quinoenzymes in biology. *Annual Review of Biochemistry,* **63**, pp. 299-344.

KNOLL, J. and MAGYAR, K., 1972. Some puzzling pharmacological effects of monoamine oxidase inhibitors. *Advances in Biochemical Psychopharmacology,* **5**, pp. 393-408.

KORNHUBER, J., KONRADI, C., MACK-BURKHARDT, F., RIEDERER, P., HEINSEN, H. and BECKMANN, H., 1989. Ontogenesis of monoamine oxidase-A and -B in the human brain frontal cortex. *Brain research,* **499**(1), pp. 81-86.

KRAMMER, A., KIRCHHOFF, P.D., JIANG, X., VENKATACHALAM, C.M. and WALDMAN, M., 2005. LigScore: a novel scoring function for predicting binding affinities. *Journal of molecular graphics & modelling,* **23**(5), pp. 395-407.

KRUEGER, M.J., MAZOUZ, F., RAMSAY, R.R., MILCENT, R. and SINGER, T.P., 1995. Dramatic species differences in the susceptibility of monoamine oxidase B to a group of powerful inhibitors. *Biochemical and biophysical research communications,* **206**(2), pp. 556-562.

KURKOWSKA-JASTRZEBSKA, I., WROŃSKA, A., KOHUTNICKA, M., CZŁONKOWSKI, A. and CZŁONKOWSKA, A., 1999. The inflammatory reaction following 1-methyl-4-phenyl-1,2,3, 6-tetrahydropyridine intoxication in mouse. *Experimental neurology,* **156**(1), pp. 50-61.

LANCASTER, J.R., 1996. Diffusion of free nitric oxide. *Methods in enzymology,* **268**, pp. 31-50.

LANGSTON, J.W., BALLARD, P., TETRUD, J.W. and IRWIN, I., 1983. Chronic Parkinsonism in humans due to a product of meperidine-analog synthesis. *Science (New York, N.Y.),* **219**(4587), pp. 979-980.

LANGSTON, J.W., FORNO, L.S., TETRUD, J., REEVES, A.G., KAPLAN, J.A. and KARLUK, D., 1999. Evidence of active nerve cell degeneration in the substantia nigra of humans years after 1-methyl-4-phenyl-1,2,3,6-tetrahydropyridine exposure. *Annals of Neurology,* **46**(4), pp. 598-605.

LEO, A., HANCH, C. and ELKINS, D., 1971. Partition coefficients and their uses. Chemical reviews, **71**(6), pp. 525-616.

LEVIN, V.A., 1980. Relationship of octanol/water partition coefficient and molecular weight to rat brain capillary permeability. *Journal of medicinal chemistry,* **23**(6), pp. 682-684.

LI, M., BINDA, A., MATTEVI, A., EDMONDSON, D.E., 2006. Functional role of the "aromatic cage" in human monoamine oxidase B: structures and catalytic properties of Tyr435 mutant proteins. *Biochemistry*, **45**(15), pp. 4775–4784.

LIN, M.T. and BEAL, M.F. 2006. Mitochondrial dysfunction and oxidative stress in neurodegenerative diseases. *Nature*, **443**(1), pp. 787-795.

LIPINSKI, C.A., LOMBARDO, F., DOMINY, B.W. and FEENEY, P.J., 2001. Experimental and computational approaches to estimate solubility and permeability in drug discovery and development settings. *Advanced Drug Delivery Reviews,* **46**(1-3), pp. 3-26.

LORENZL, S., CALINGASAN, N., YANG, L., ALBERS, D.S., SHUGAMA, S. & GREGORIO, J. 2004. Matrix metalloproteinase-9 is elevated in 1-methyl-4-phenyl-1,2,3,6-tetrahydropyridine-induced parkinsonism in mice. *Neuromolecular Medicine*, **5**(1), pp. 119–32.

LU, R., LEE, J., KO, H., LIN, W., CHEN, K. and SHIH, J.C., 2002. No association of the MAOA gene with alcoholism among Han Chinese males in Taiwan. *Progress in Neuro-Psychopharmacology and Biological Psychiatry,* **26**(3), pp. 457-461.

LYLES, G.A. and CHALMERS, J., 1995. Aminoacetone metabolism by semicarbazide-sensitive amine oxidase in rat aorta. *Biochemical Pharmacology,* **49**(3), pp. 416-419.

MA, J., YOSHIMURA, M., YAMASHITA, E., NAKAGAWA, A., ITO, A. and TSUKIHARA, T., 2004. Structure of Rat Monoamine Oxidase A and Its Specific Recognitions for Substrates and Inhibitors. *Journal of Molecular Biology,* **338**(1), pp. 103.

MANFREDINI, S., VERTUANI, S., PAVAN, B., VITALI, F., SCAGLIANTI, M., BORTOLOTTI, F., BIONDI, C., SCATTURIN, A., PRASAD, P. and DALPIAZ, A., 2004. Design, synthesis and in vitro evaluation on HRPE cells of ascorbic and 6-bromoascorbic acid conjugates with neuroactive molecules. *Bioorganic & Medicinal Chemistry,* **12**(20), pp. 5453-5463.

MARX, J., 1996. Searching for drugs that combat Alzheimer's. *Science,* **273**(5271), pp. 50.

MASON, R.P., OLMSTEAD, E.G., & JACOB, R.F. 2000. Antioxidant activity of the monoamine oxidase B inhibitor lazabemide. *Biochemical Pharmacology*, **60**(5), pp. 709-716.

MATTHEWS, R.T., YANG, L. and BEAL, M.F., 1997. S-Methylthiocitrulline, a neuronal nitric oxide synthase inhibitor, protects against malonate and MPTP neurotoxicity. *Experimental neurology,* **143**(2), pp. 282-286.

MATTSON, M.P., 1994. Calcium and neuronal injury in Alzheimer's disease. Contributions of beta-amyloid precursor protein mismetabolism, free radicals, and metabolic compromise. *Annals of the New York Academy of Sciences,* **747**, pp. 50-76.

MAZOUZ, F., GUEDDARI, S., BURSTEIN, C., MANSUY, D. and MILCENT, R., 1993. 5-[4-(benzyloxy)phenyl]-1,3,4-oxadiazol-2(3H)-one derivatives and related analogues: new reversible, highly potent, and selective monamine oxidase type B inhibitors. *Journal of medicinal chemistry,* **36**(9), pp. 1157-1167.

MAZOUZ, F., LEBRETON, L., MILCENT, R. & BURSTEIN, C. 1990. 5-Aryl-1,3,4- oxadiazol-2(3H)-one derivatives and sulfur analogues as new selective and competitive monoamine oxidase type B inhibitors. *European Journal of Medicinal Chemistry*, **25**(1), pp. 659-671.

MCNAUGHT, K.S., THULL, U., CARRUPT, P.A., ALTOMARE, C., CELLAMARE, S., CAROTTI, A., TESTA, B., JENNER, P. and MARSDEN, C.D., 1996. Effects of isoquinoline derivatives structurally related to 1-methyl-4-phenyl-1,2,3,6-tetrahydropyridine (MPTP) on mitochondrial respiration. *Biochemical pharmacology,* **51**(11), pp. 1503-1511.

MEDVEDEV, A.E., IVANOV, A.S., KAMYSHANSKAYA, N.S., KIRKEL, A.Z., MOSKVITINA, T.A., GORKIN, V.Z., LI, N.Y. and MARSHAKOV VYU, 1995. Interaction of indole derivatives with monoamine oxidase A and B. Studies on the structure-inhibitory activity relationship. *Biochemistry and molecular biology international,* **36**(1), pp. 113-122.

MEDVEDEV, A.E., VESELOVSKY, A.V., SHVEDOV, V.I., TIKHONOVA, O.V., MOSKVITINA, T.A., FEDOTOVA, O.A., AXENOVA, L.N., KAMYSHANSKAYA, N.S., KIRKEL, A.Z. and IVANOV, A.S., 1998. Inhibition of monoamine oxidase by pirlindole analogues: 3D-QSAR and CoMFA analysis. *Journal of chemical information and computer sciences,* **38**(6), pp. 1137-1144.

MELCHIORRE, C., ANTONELLO, A., BANZI, R., BOLOGNESI, M.L., MINARINI, A., ROSINI, M. and TUMIATTI, V., 2003. Polymethylene tetraamine backbone as template for the development of biologically active polyamines. *Medicinal research reviews,* **23**(2), pp. 200-233.

MELCHIORRE, C., ANDRISANO, V., BOLOGNESI, M.L., BUDRIESI, R., CAVALLI, A., CAVRINI, V., ROSINI, M., TUMIATTI, V. and RECANATINI, M., 1998. Acetylcholinesterase noncovalent inhibitors based on a polyamine backbone for potential use against Alzheimer's disease. *Journal of medicinal chemistry,* **41**(22), pp. 4186-4189.

MENCHER, S.K. and WANG, L.G., 2005. Promiscuous drugs compared to selective drugs (promiscuity can be a virtue). *BMC Clinical Pharmacology,* **5**(1), pp. 3-

MICHAEL NUSSBAUM, E. and BENDIXEN, L.D., 2003. Approaching and avoiding arguments: The role of epistemological beliefs, need for cognition, and extraverted personality traits. *Contemporary Educational Psychology,* **28**(4), pp. 573-595.

MILLER, J.R. and EDMONDSON, D.E., 1999. Structure–activity relationships in the oxidation of para-substituted benzylamine analogues by. *Biochemistry,* **38**(41), pp. 13670.

MILLER, G.W. and GAINETDINOV, R.R., 1999. Dopamine transporters and neuronal injury. *Trends in pharmacological sciences,* **20**(10), pp. 424.

MIN LI, BINDA, C., MATTEVI, A. and EDMONDSON, D.E., 2006. Functional Role of the "Aromatic Cage" in Human Monoamine Oxidase B: Structures and Catalytic Properties of Tyr435 Mutant Proteins. *Biochemistry,* **45**(15), pp. 4775-4784.

MIZUNO, Y., MATUDA, S., YOSHINO, H., MORI, H., HATTORI, N. and IKEBE, S., 1994. An immunohistochemical study on alpha-ketoglutarate dehydrogenase complex in Parkinson's disease. *Annals of Neurology,* **35**(2), pp. 204-210.

MORPHY, R., KAY, C. and RANKOVIC, Z., 2004. From magic bullets to designed multiple ligands. *Drug discovery today,* **9**(15), pp. 641-651.

MORPHY, R. and RANKOVIC, Z., 2007. Fragments, network biology and designing multiple ligands. *Drug discovery today,* **12**(3), pp. 156-160.

MORPHY, R. and RANKOVIC, Z., 2005. Designed multiple ligands. An emerging drug discovery paradigm. *Journal of medicinal chemistry,* **48**(21), pp. 6523-6543.

MUKASA, H., NAKAMURA, J., YAMADA, S., INOUE, M. and NAKAZAWA, Y., 1990. Platelet monoamine oxidase activity and personality traits in alcoholics and methamphetamine dependents. *Drug and Alcohol Dependence,* **26**(3), pp. 251-254.

MÜLLER, T., BÜTTNER, T., GHOLIPOUR, A. and KUHN, W., 2003. Coenzyme Q_{10} supplementation provides mild symptomatic benefit in patients with Parkinson's disease. *Neuroscience letters,* **341**(3), pp. 201.

MURRAY, R.D.H., JORGE, Z.D. and LAWRIE, K.W.M., 1982. Synthesis of the coumarin, hortiolone. *Tetrahedron Letters,* **23**(46), pp. 4847-4848.

MURRAY, R.K.; GRANNER, D.K.; MAYES, P.A., RODWELL, VICTOR, W. 2003. Enzymes: Kinetics. (*In* Harper's Illustrated Biochemistry 26th eds). McGraw-Hill. pp. 60-71.

NAKAMURA, S., 1990. Molecular biology of Alzheimer's disease. *Nippon rinsho.Japanese journal of clinical medicine,* **48**(11), pp. 2710-2721.

NAKAYAMA, H. and KANAOKA, Y., 1973. A photoaffinity labeling of the active site of alpha-chymotrypsin with TPDK. *FEBS letters,* **37**(2), pp. 200-202.

NANDIGAMA, R.K. and EDMONDSON, D.E., 2000. Structure-Activity Relations in the Oxidation of Phenethylamine Analogues by Recombinant.. *Biochemistry,* **39**(49), pp. 15258.

NAOI, M., TAKAHASHI, T. and NAGATSU, T., 1987. Metabolism of N-methyl-4-phenyl-1,2,3,6-tetrahydropyridine in a rat pheochromocytoma cell line, PC12h. *Life Sciences,* **41**(24), pp. 2655-2661.

NASER-HIJAZI, B., STOLZE, B. & ZANKER, K.S. 1994. Proceedings of the International Society of the Coumarin Investigators; Springer: Berlin.

NIMKAR, S.K., ANDERSON, A.H., RIMOLDI, J.M., STANTON, M., CASTAGNOLI, K.P., MABIC, S., WANG, Y.X. and CASTAGNOLI, N., 1996. Synthesis and monoamine oxidase B catalyzed oxidation of C-4 heteroaromatic substituted 1,2,3,6-tetrahydropyridine derivatives. *Chemical research in toxicology,* **9**(6), pp. 1013-1022.

NOMOTO, M., 2003. Clinical pharmacology and neuroprotection in Parkinson's disease. *Parkinsonism & related disorders,* **9 Suppl 2**, pp. S55-8.

NORINDER, U. and HAEBERLEIN, M., 2002. Computational approaches to the prediction of the blood–brain distribution. *Advanced Drug Delivery Reviews,* **54**(3), pp. 291-313.

NORMAN, T.R., CHAMBERLAIN, K.G. and FRENCH, M.A., 1987. Platelet monoamine oxidase: Low activity in cigarette smokers. *Psychiatry Research,* **20**(3), pp. 199-205.

NOVAROLI, L., DAINA, A., FAVRE, E., BRAVO, J., CAROTTI, A., LEONETTI, F., CATTO, M., CARRUPT, P.A. and REIST, M., 2006. Impact of species-dependent differences on screening, design, and development of MAO B inhibitors. *Journal of medicinal chemistry,* **49**(21), pp. 6264-6272.

NUSSBAUM, R.L. and ELLIS, C.E., 2003. Alzheimer's disease and Parkinson's disease. *The New England journal of medicine,* **348**(14), pp. 1356-1364.

OOMS, F., FRÉDÉRICK, R., DURANT, F., PETZER, J.P., CASTAGNOLI JR., N., VAN DER SCHYF,CORNELIS J. and WOUTERS, J., 2003. Rational approaches towards reversible inhibition of type B monoamine oxidase. Design and evaluation of a novel 5H-Indeno[1,2-c]pyridazin-5-one derivative. *Bioorganic & medicinal chemistry letters,* **13**(1), pp. 69.

OTTOBONI, S., CALDERA, P. and TREVOR, A., 1989. Deuterium isotope effect measurements on the interactions of the neurotoxin 1-methyl-4-phenyl-1,2,3,6-tetrahydropyridine with monoamine oxidase B. *The Journal of Biological Chemistry,* **264**, pp. 13684-13688.

PAN, L., TAN, J., HOU, J., HUANG, S., GU, L. and HUANG, Z., 2008. Design, synthesis and evaluation of isaindigotone derivatives as acetylcholinesterase and butyrylcholinesterase inhibitors. *Bioorganic & medicinal chemistry letters,* **18**(13), pp. 3790-3793.

PARDO, L.M. and VAN DUIJN, C.M., 2005. In search of genes involved in neurodegenerative disorders. *Mutation Research: Fundamental & Molecular Mechanisms of Mutagenesis,* **592**(1), pp. 89-101.

PETZER, J.P., STEYN, S., CASTAGNOLI, K.P., CHEN, J.F., SCHWARZSCHILD, M.A., VAN DER SCHYF,CORNELIS J. and CASTAGNOLI, N., 2003. Inhibition of monoamine oxidase B by selective adenosine A_{2A} receptor antagonists. *Bioorganic & medicinal chemistry,* **11**(7), pp. 1299-1310.

PIAZZI, L., RAMPA, A., BISI, A., GOBBI, S., BELLUTI, F., CAVALLI, A., BARTOLINI, M., ANDRISANO, V., VALENTI, P. and RECANATINI, M., 2003. 3-(4-[[Benzyl(methyl)amino]methyl]phenyl)-6,7-dimethoxy-2H-2-chromenone (AP2238) inhibits both acetylcholinesterase and acetylcholinesterase-induced beta-amyloid aggregation: a dual function lead for Alzheimer's disease therapy. *Journal of medicinal chemistry,* **46**(12), pp. 2279-2282.

PRINS, L.H.A. 2007. Polycyclic cage compounds as carrier molecules for neuroprotective non-steroidal anti-inflammatory drugs. North West University, pp. 39-40.

PRZEDBORSKI, S., JACKSON-LEWIS, V., DJALDETTI, R., LIBERATORE, G., VILA, M., VUKOSAVIC, S. and ALMER, G., 2000. The parkinsonian toxin MPTP: action and mechanism. *Restorative Neurology & Neuroscience,* **16**(2), pp. 135.

PRZEDBORSKI, S. and VILA, M., 2003. The 1-methyl-4-phenyl-1,2,3,6-tetrahydropyridine mouse model: a tool to explore the pathogenesis of Parkinson's disease. *Annals of the New York Academy of Sciences,* **991**, pp. 189-198.

RABEY, J.M., SAGI, I., HUBERMAN, M., MELAMED, E., KORCZYN, A., GILADI, N., INZELBERG, R., DJALDETTI, R., KLEIN, C. and BERECZ, G., 2000. Rasagiline mesylate, a new MAO-B inhibitor for the treatment of Parkinson's disease: a double-blind study as adjunctive therapy to levodopa. *Clinical neuropharmacology,* **23**(6), pp. 324-330.

RANDALL, R.D. and THAYER, S.A., 1992. Glutamate-induced calcium transient triggers delayed calcium overload and neurotoxicity in rat hippocampal neurons. *The Journal Of Neuroscience: The Official Journal Of The Society For Neuroscience,* **12**(5), pp. 1882-1895.

RAVI, K., EDMONDSON, N. & EDMONDSON, E. 2000. Structure-activity relations in the oxidation of phenethylamine analogues by recombinant human liver monoamine oxidase A. *Biochemistry*, **39**(49), pp. 15258-15265.

RIEDERER, P., DANIELCZYK, W. and GRÜNBLATT, E., 2004. Monoamine Oxidase-B Inhibition in Alzheimer's Disease. *Neurotoxicology,* **25**(1), pp. 271.

RIEDERER, P., LACHENMAYER, L. and LAUX, G., 2004. Clinical Applications of MAO-Inhibitors. *Current medicinal chemistry,* **11**(15), pp. 2033-2043.

RIEDERER, P., SOFIC, E., RAUSCH, W.D., SCHMIDT, B., REYNOLDS, G.P., JELLINGER, K. and YOUDIM, M.B., 1989. Transition metals, ferritin, glutathione, and ascorbic acid in parkinsonian brains. *Journal of neurochemistry,* **52**(2), pp. 515-520.

RIEDERER, P., YOUDIM, M.B., RAUSCH, W.D., BIRKMAYER, W., JELLINGER, K. and SEEMANN, D., 1978. On the mode of action of L-deprenyl in the human central nervous system. *Journal of neural transmission,* **43**(3-4), pp. 217-226.

ROBINSON, D.S., DAVIS, J.M., NIES, A., RAVARIS, C.L. and SYLWESTER, D., 1971. Relation of sex and aging to monoamine oxidase activity of human brain, plasma, and platelets. *Archives of General Psychiatry,* **24**(6), pp. 536-539.

ROCCA, W.A., HOFMAN, A., BRAYNE, C., BRETELER, M.M., CLARKE, M., COPELAND, J.R., DARTIGUES, J.F., ENGEDAL, K., HAGNELL, O. and HEEREN, T.J., 1991. Frequency and distribution of Alzheimer's disease in Europe: a collaborative study of 1980-1990 prevalence findings. The EURODEM-Prevalence Research Group. *Annals of Neurology,* **30**(3), pp. 381-390.

SALACH, J.I. and WEYLER, W., 1987. Preparation of the flavin-containing aromatic amine oxidases of human placenta and beef liver. *Methods in enzymology,* **142**, pp. 627-637.

SALMI, M., YEGUTKIN, G.G., LEHVONEN, R., KOSKINEN, K., SALMINEN, T. and JALKANEN, S., 2001. A Cell Surface Amine Oxidase Directly Controls Lymphocyte Migration. *Immunity,* **14**(3), pp. 265-276.

SANTANA, L., URIARTE, E., GONZÁLEZ-DÍAZ, H., ZAGOTTO, G., SOTO-OTERO, R. and MÉNDEZ-ALVAREZ, E., 2006. A QSAR model for in silico screening of MAO-A inhibitors. Prediction, synthesis, and biological assay of novel coumarins. *Journal of medicinal chemistry,* **49**(3), pp. 1149-1156.

SANZ, A., CARO, P., IBANEZ, J., GOMEZ, J., GREDILLA, R. and BARJA, G., 2005. Dietary restriction at old age lowers mitochondrial oxygen radical production and leak at complex I and oxidative DNA damage in rat brain. *Journal of Bioenergetics and Biomembranes,* **37**(2), pp. 83-90.

SASTRA, M. & GARCIA-SEVILLA, J.A. 1993. Opposite age-dependent changes of $\alpha 2_A$-adrenoceptors and non adrenoceptor. *Journal of Neurochemistry*, **61**(1), pp. 881–889.

SAUNDERS, A.M., 2000. Apolipoprotein E and Alzheimer disease: an update on genetic and functional analyses. *Journal of neuropathology and experimental neurology,* **59**(9), pp. 751-758.

SAURA, J., BLEUEL, Z., ULRICH, J., MENDELOWITSCH, A., CHEN, K., SHIH, J.C., MALHERBE, P., DA PRADA, M. and RICHARDS, J.G., 1996. Molecular neuroanatomy of human monoamine oxidases A and B revealed by quantitative enzyme radioautography and in situ hybridization histochemistry. *Neuroscience,* **70**(3), pp. 755-774.

SAURA, J., LUQUE, J.M., CESURA, A.M., DA PRADA, M., CHAN-PALAY, V., HUBER, G., LÖFFLER, J. and RICHARDS, J.G., 1994. Increased monoamine oxidase B activity in plaque-associated astrocytes of Alzheimer brains revealed by quantitative enzyme radioautography. *Neuroscience,* **62**(1), pp. 15-30.

SCHAPIRA, A.H., 1993. Mitochondrial complex I deficiency in Parkinson's disease. *Advances in Neurology,* **60**, pp. 288-291.

SCHAPIRA, A.H., COOPER, J.M., DEXTER, D., JENNER, P., CLARK, J.B. and MARSDEN, C.D., 1989. Mitochondrial complex I deficiency in Parkinson's disease. *Lancet,* **1**(8649), pp. 1269.

SEGEL, I. H. 1993. Enzyme kinetics, Wiley, New York, pp 100-125.

SHEN, Y.Q., HENERT, G., LIN, L.Y., LUO, Y.L., MOZE, E., LI, K.S., *et al.* 2005. Interleukine-1beta and interleukine-6 levels in striatum and other brain structures after MPTP treatment: influence of behavioural lateralization. *Journal Neuroimmunology*, **158**(1-2), pp. 14–25.

SHIH, J.C., CHEN, K. and RIDD, M.J., 1999. Monoamine oxidase: from genes to behavior. *Annual Review of Neuroscience,* **22**, pp. 197-217.

SHIMADA, J., KOIKE, N., NONAKA, H., SHIOZAKI, S., YANAGAWA, K., KANADA, T., KOBAYASHI, H. and FUMIO, S., 1997. Adenosine A_{2A} antagonists with potent anti-cataleptic activity. *Bioorganic & medicinal chemistry letters*, **7**(1), pp. 2349-2352.

SILVERMAN, R.B., 1995. Radical thoughts about the life of MAO. *Progress in brain research,* **106**, pp. 23-31.

SMEYNE, R.J. and JACKSON-LEWIS, V., 2005. The MPTP model of Parkinson's disease. *Molecular Brain Research,* **134**(1), pp. 57-66.

SNYDER, S.H. and HENDLEY, E.D., 1968. A simple and sensitive fluorescence assay for monoamine oxidase and diamine oxidase. *The Journal of pharmacology and experimental therapeutics,* **163**(2), pp. 386-392.

SONSALLA, P.K. and GOLBE, L.I., 1988. Deprenyl as prophylaxis against Parkinson's disease? *Clinical neuropharmacology,* **11**(6), pp. 500-511.

SONSALLA, P.K. and HEIKKILA, R.E., 1988. Neurotoxic effects of 1-methyl-4-phenyl-1,2,3,6-tetrahydropyridine (MPTP) and methamphetamine in several strains of mice. *Progress in Neuro-Psychopharmacology and Biological Psychiatry,* **12**(2-3), pp. 345-354.

SPECIALE, S.G., 2002. MPTP: Insights into parkinsonian neurodegeneration. *Neurotoxicology and Teratology,* **24**(5), pp. 607-620.

STEELE, C.D. 2000. The genetics of Alzheimer disease. *The Nursing Clinics of North America*, 35:687–694.

STOKES; A.H., HASTINGS, T.G. and VRANA, K.E., 1999. Cytotoxic and genotoxic potential of dopamine. *Journal of neuroscience research,* **55**(6), pp. 659-665.

STROLIN BENEDETTI, M. and DOSTERT, P., 1989. Monoamine oxidase, brain ageing and degenerative diseases. *Biochemical pharmacology,* **38**(4), pp. 555-561.

SULZER, D. and ZECCA, L., 2000. Intraneuronal dopamine-quinone synthesis: a review. *Neurotoxicity Research,* **1**(3), pp. 181-195.

SUZUKI, F., SHIMADA, J., SHIOZAKI, S., ICHIKAWA, S., ISHII, A., NAKAMURA, J., NONAKA, H., KOBAYASHI, H. & FUSE, E. 1993. Adenosine A_1 antagonists. Structure-activity relationships on amelioration against scopolamine- or N6-[(R)phenylisopropyl]adenosine-induced cognitive disturbance. *Journal of Medicinal chemistry*, **36**(17), pp. 2508-2518.

TATTON, W.G. and GREENWOOD, C.E., 1991. Rescue of dying neurons: a new action for deprenyl in MPTP parkinsonism. *Journal of neuroscience research,* **30**(4), pp. 666-672.

TEISMANN, P., TIEU, K., COHEN, O., CHOI, D., WU, D.C., MARKS, D., VILA, M., JACKSON-LEWIS, V. and PRZEDBORSKI, S., 2003(b). Pathogenic role of glial cells in Parkinson's disease. *Movement Disorders: Official Journal Of The Movement Disorder Society,* **18**(2), pp. 121-129.

TEISMANN, P., TIEU, K., DONG-KUG CHOI, DU-CHU WU, NAINI, A., HUNOT, S., VILA, M., JACKSON-LEWIS, V. and PRZEDBORSKI, S., 2003(a). Cyclooxygenase-2 is instrumental in Parkinson's disease neurodegeneration. *Proceedings of the National Academy of Sciences of the United States of America,* **100**(9), pp. 5473.

TOPRAKçI, M. & YELEKçI, K. 2005. Docking studies on monoamine oxidase-B inhibitors: Estimation of inhibition constants (K_i) of a series of experimentally tested compounds. *Bioorganic and Medicinal Chemistry Letters*, **20**(15), pp. 4438-4446.

TSE, D.C., MCCREERY, R.L. and ADAMS, R.N., 1976. Potential oxidative pathways of brain catecholamines. *Journal of medicinal chemistry,* **19**(1), pp. 37-40.

VAN DE WATERBEEMD, H., CARTER, R.E., GRASSY, G., KUBINYI, H., MARTIN, Y.C., TUTE, M.S. and WILLETT, P., 1998. Chapter 37. Glossary of Terms Used in Computational Drug Design (IUPAC Recommendations 1997). In: JAMES A. BRISTOL, ed, *Annual Reports in Medicinal Chemistry,* Academic Press, pp. 397-409.

VAN DEN BERG, D., ZOELLNER, K.R., OGUNROMBI, M.O., MALAN, S.F., TERRE'BLANCHE, G., CASTAGNOLI, J., NEAL, BERGH, J.J. and PETZER, J.P., 2007. Inhibition of monoamine oxidase B by selected benzimidazole and caffeine analogues. *Bioorganic & Medicinal Chemistry,* **15**(11), pp. 3692-3702.

VERTUANI, S., ANGUSTI, A. and MANFREDINI, S., 2004. The antioxidants and pro-antioxidants network: an overview. *Current pharmaceutical design,* **10**(14), pp. 1677-1694.

VESELOVSKY, A.V., IVANOV, A.S. and MEDVEDEV, A.E., 2004. Computer Modelling and Visualization of Active Site of Monoamine Oxidases. *Neurotoxicology,* **25**(1), pp. 37.

VESELOVSKY, A.V., MEDVEDEV, A.E., TIKHONOVA, O.V., SKVORTSOV, V.S. and IVANOV, A.S., 2000. Modeling of substrate-binding region of the active site of monoamine oxidase A. *Biochemistry.BiokhimiiA,* **65**(8), pp. 910-916.

VESELOVSKIĬ, A.V., TIKHONOVA, O.V., IVANOV, A.S. and MEDVEDEV, A.E., 2001. [Modeling of monoamine oxidase B active site by computer moulding]. *Voprosy MeditSinskoĭ Khimii,* **47**(6), pp. 642-651.

VLOK, N., MALAN, S.F., CASTAGNOLI, N., BERGH, J.J. and PETZER, J.P., 2006. Inhibition of monoamine oxidase B by analogues of the adenosine A_{2A} receptor antagonist (E)-8-(3-chlorostyryl)caffeine (CSC). *Bioorganic & medicinal chemistry,* **14**(10), pp. 3512-3521.

VLOK, N. 2005. Rational approaches towards the design of (E)-8-(3-Chlrostyryl)-Caffeine derivatives as novel reversible inhibitors of Monoamine Oxidase-B. North West University, Potchefstroom Campus.

WALLACE, D.C., 1999. Mitochondrial Diseases in Man and Mouse. (Cover story). *Science,* **283**(5407), pp. 1482.

WANG, X. and SILVERMAN, R.B., 2000. Monoamine oxidase-catalyzed oxidation of endo,endo-2-amino-6-[(Z)-2'-phenyl]ethenylbicyclo[2.2.1]heptane, a potential probe for a radical cation intermediate. *Bioorganic & medicinal chemistry,* **8**(7), pp. 1645-1651.

WENKERT, E.. & BUCKWALTER, B.L.J. 1972. Cabon-13 nuclear magnetic resonance spectroscopy of naturally occurring substances. X. Pimaradienes. *Journal of the American chemical society*, 94:4367–4369.

WESTLUND, K.N., DENNEY, R.M., ROSE, R.M. and ABELL, C.W., 1988. Localization of distinct monoamine oxidase A and monoamine oxidase B cell populations in human brainstem. *Neuroscience,* **25**(2), pp. 439-456.

WEYLER, W., HSU, Y.P. and BREAKAFIELD, X.O., 1990. Biochemistry and genetics of monoamine oxidase. *Pharmacology & Therapeutics,* **47**(3), pp. 391-417.

WIRZ-JUSTICE, A., 1988. Platelet research in psychiatry. *Experientia,* **44**(2), pp. 145-152.

WOUTERS, J., MOUREAU, F., EVRARD, G., JEGHAM, S., GEORGE, P. and DURANT, F., 1997. Molecular interaction between reversible MAO inhibitors and the two isoforms of MAO. *Biological Psychiatry,* **42**(1, Supplement 1), pp. 126S-126S.

WOUTERS, J., OOMS, F., JEGHAM, S., KOENIG, J., GEORGE, P. and DURANT, F., 1997. Reversible inhibition of type B monoamine oxidase. Theoretical study of model diazo heterocylic compound. *European Journal of Medicinal Chemistry,* **32**(9), pp. 721-730.

WU, H.F., CHEN, K. and SHIH, J.C., 1993. Site-directed mutagenesis of monoamine oxidase A and B: role of cysteines. *Molecular pharmacology,* **43**(6), pp. 888-893.

YAKUNIN, A.F., YEE, A.A., SAVCHENKO, A., EDWARDS, A.M. and ARROWSMITH, C.H., 2004. Structural proteomics: a tool for genome annotation. *Current opinion in chemical biology,* **8**(1), pp. 42-48.

YELEKÇI, K., KARAHAN, Ö and TOPRAKÇI, M., 2007. Docking of novel reversible monoamine oxidase-B inhibitors: efficient prediction of ligand binding sites and estimation of inhibitors thermodynamic properties. *Journal of neural transmission,* **114**(6), pp. 725-732.

YOUDIM, M.B., GRUNBLATT, E., LEVITES., MAOR, G. & MANDEL, S. 2002. Early and late molecular events in neurodegeneration and neuroprotection in Parkinson's disease MPTP model as assessed by cDNA microarray; the role of iron. *Neurotoxicity Research*, **4**(7-8), pp. 679–689.

YOKEL, R.A., 2000. The toxicology of aluminum in the brain: a review. *Neurotoxicology,* **21**(5), pp. 813-828.

YU, P.H., 1989. Deamination of aliphatic amines of different chain lengths by rat liver monoamine oxidase A and B. *The Journal of pharmacy and pharmacology,* **41**(3), pp. 205-208.

XU, K., BASTIA, E. and SCHWARZSCHILD, M., 2005. Therapeutic potential of adenosine A(2A) receptor antagonists in Parkinson's disease. *Pharmacology & therapeutics,* **105**(3), pp. 267-310.

Annexure

Spectral Data

^{1}H NMR, ^{13}C NMR, MS

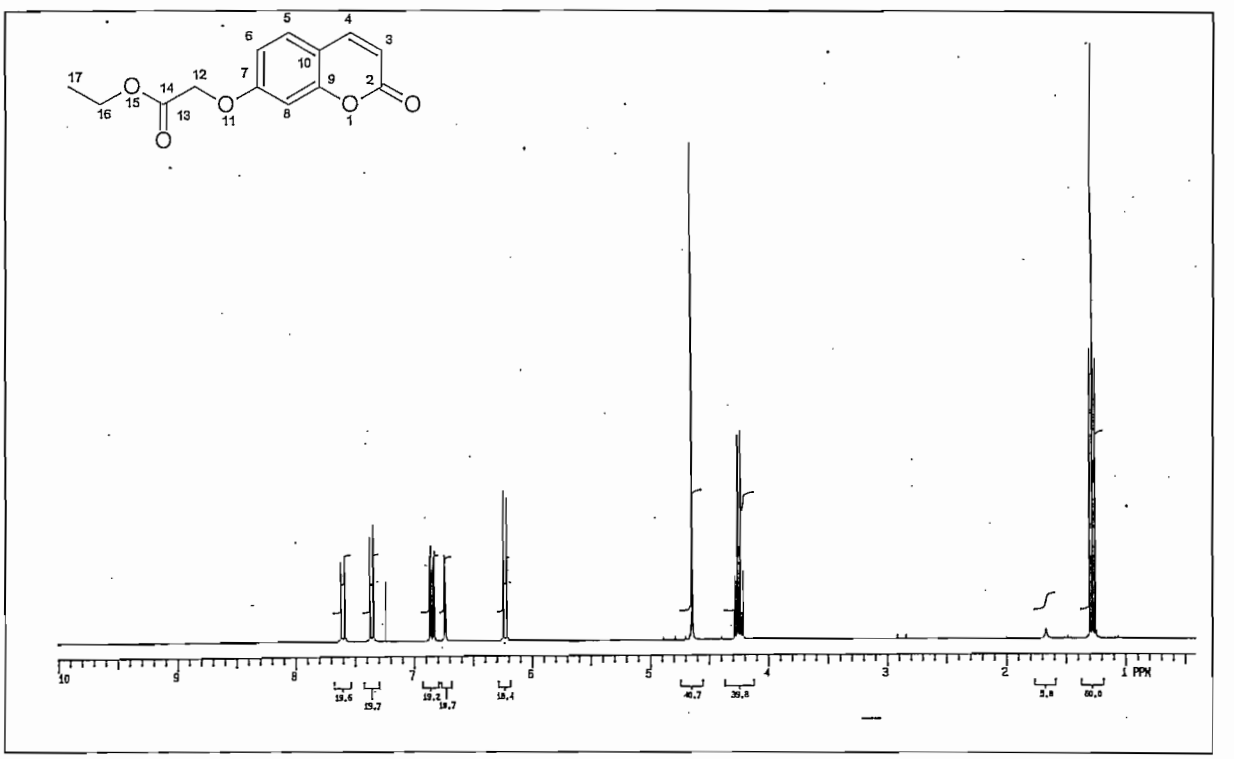

Spectrum 1

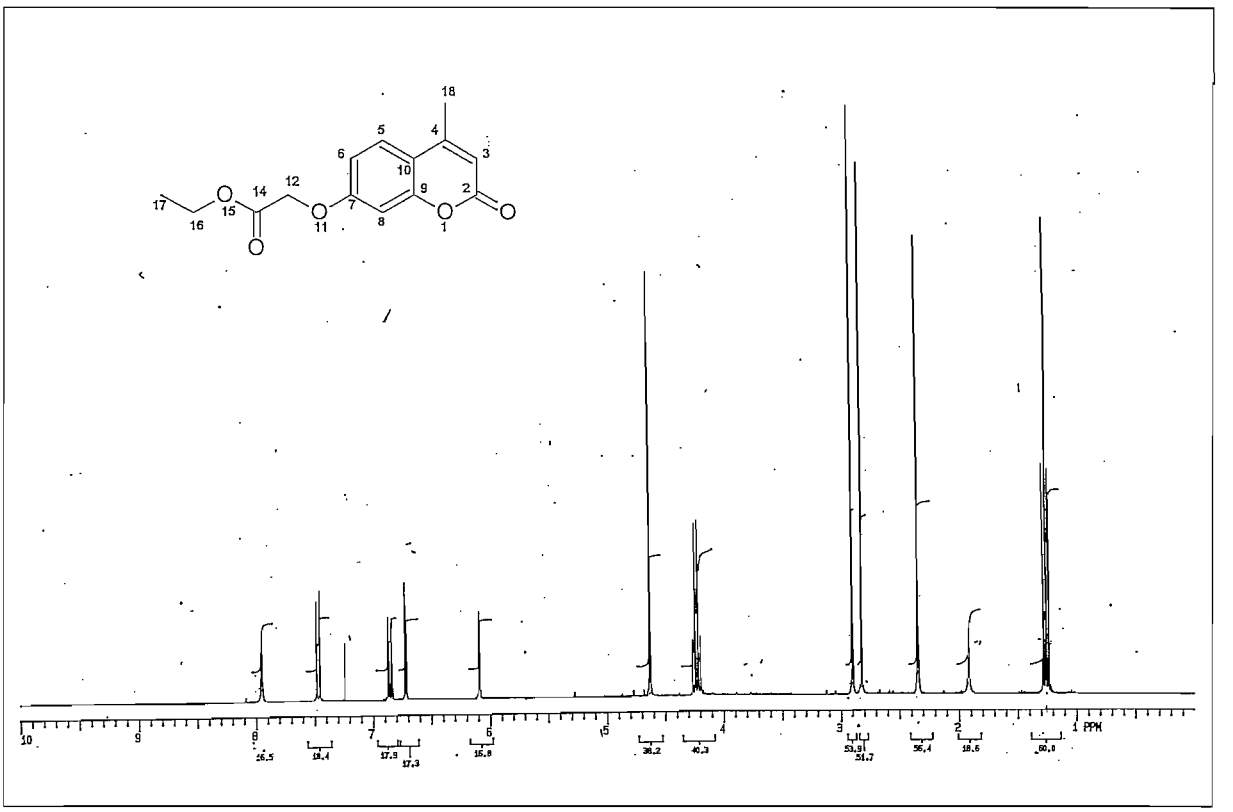

Spectrum 2

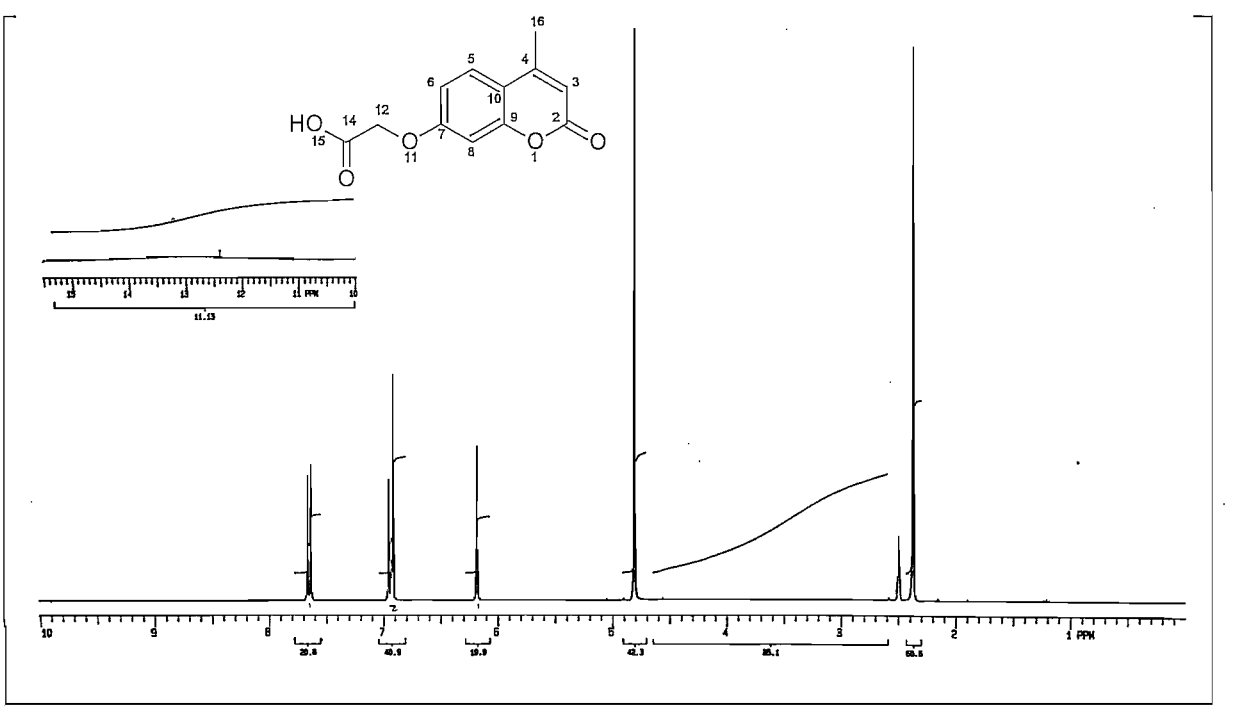

Spectrum 3

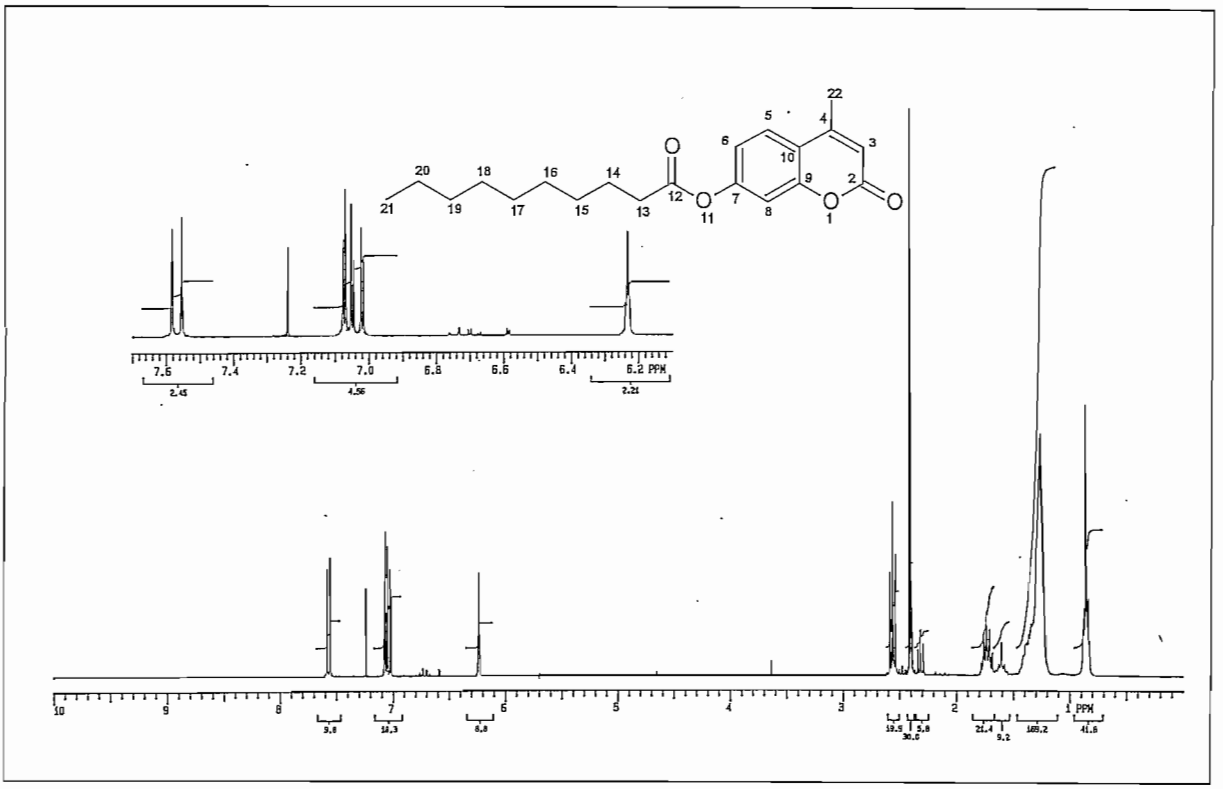

Spectrum 4

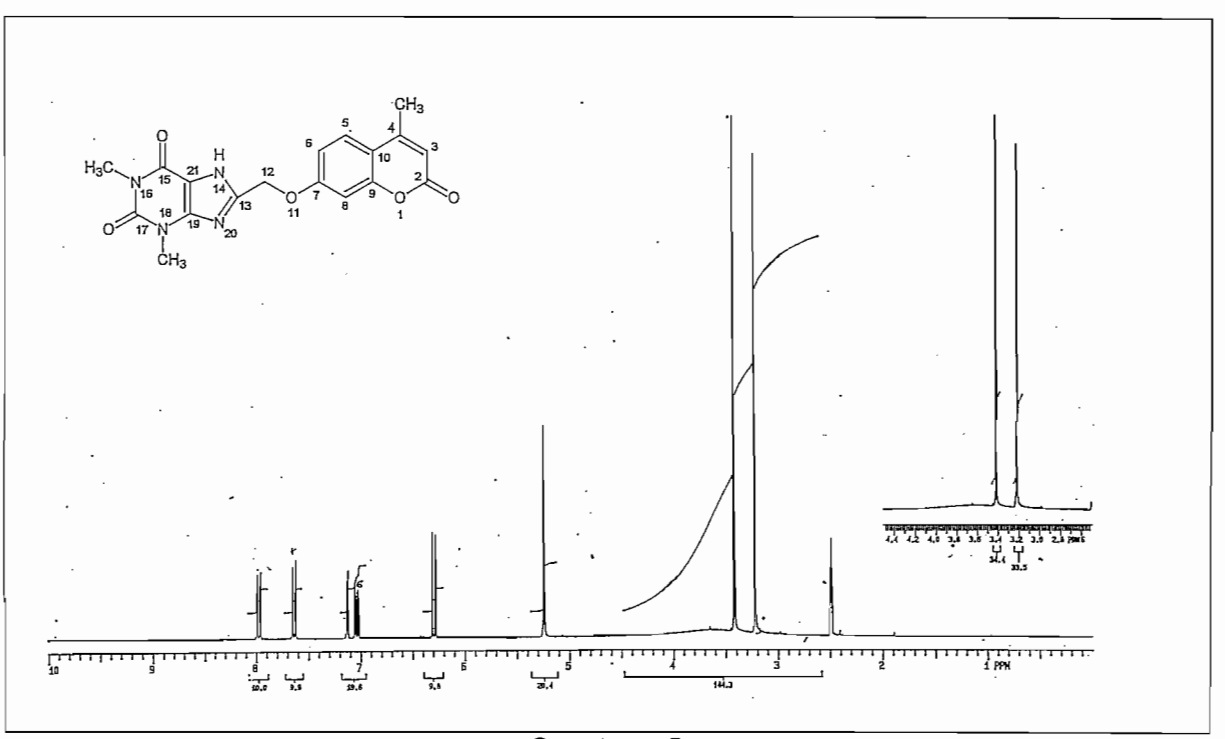

Spectrum 5

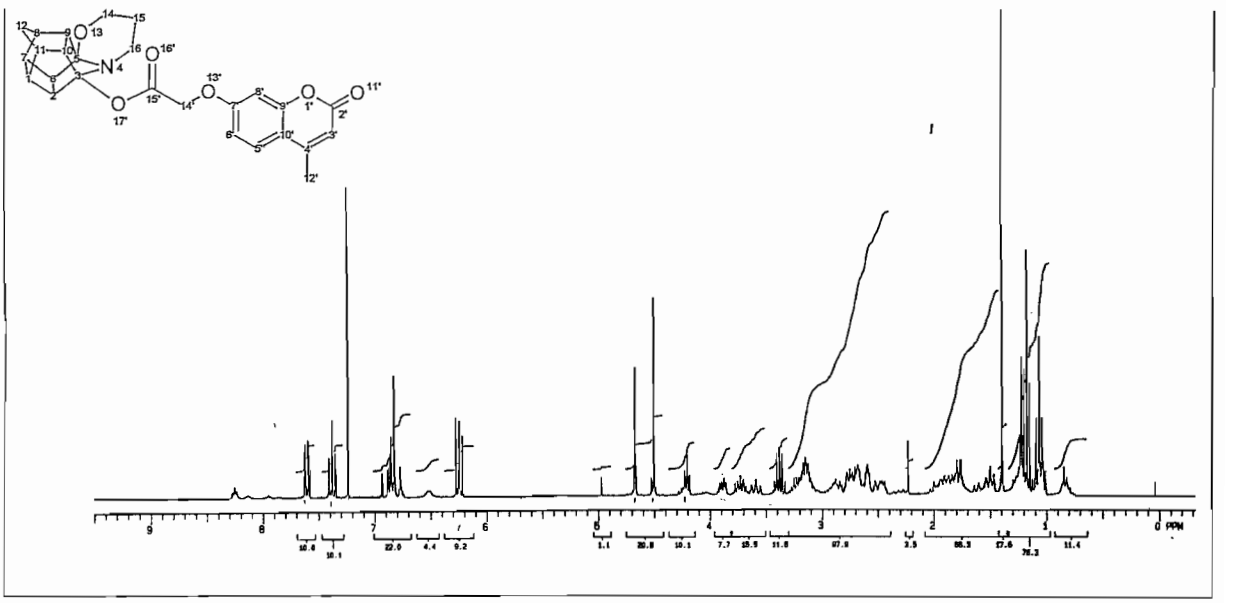

Spectrum 6

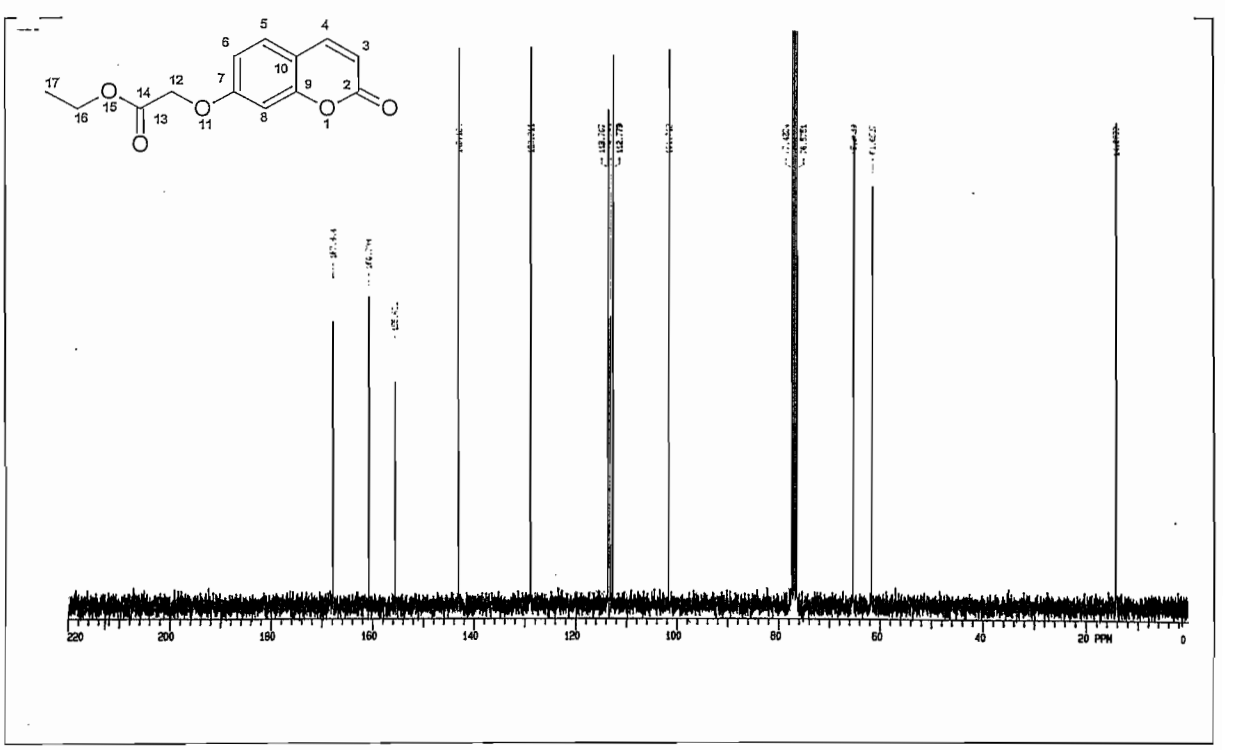

Spectrum 7

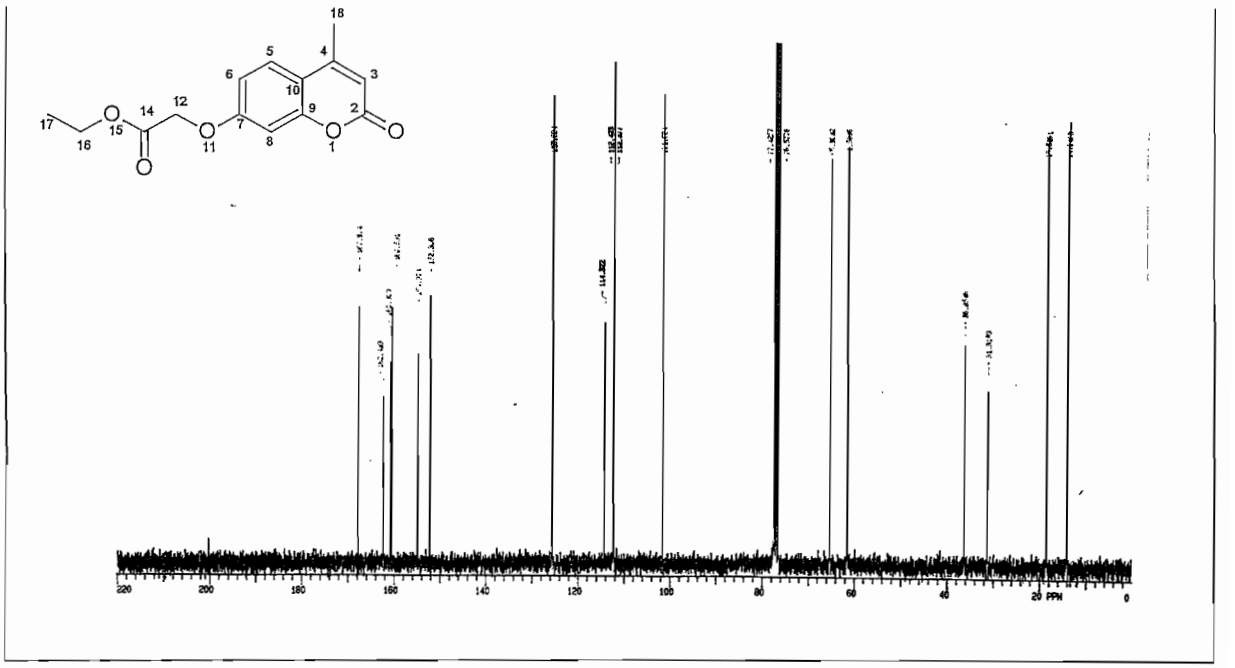

Spectrum 8

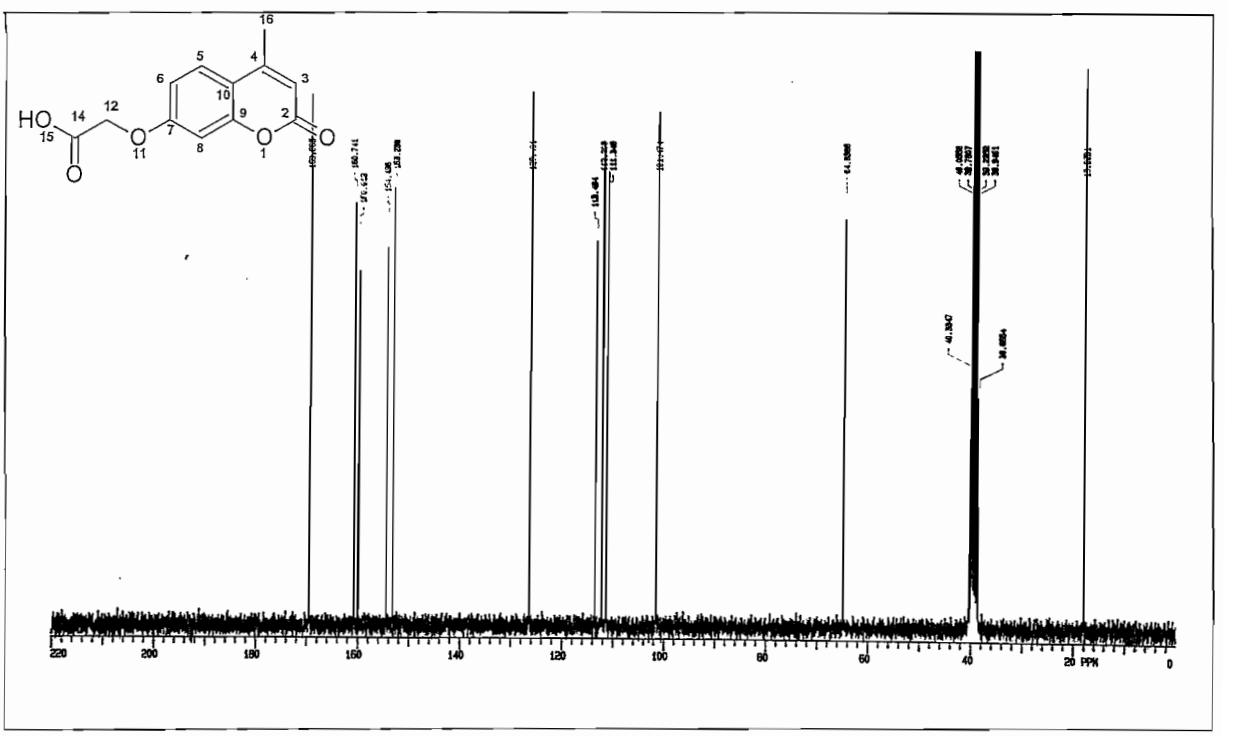

Spectrum 9

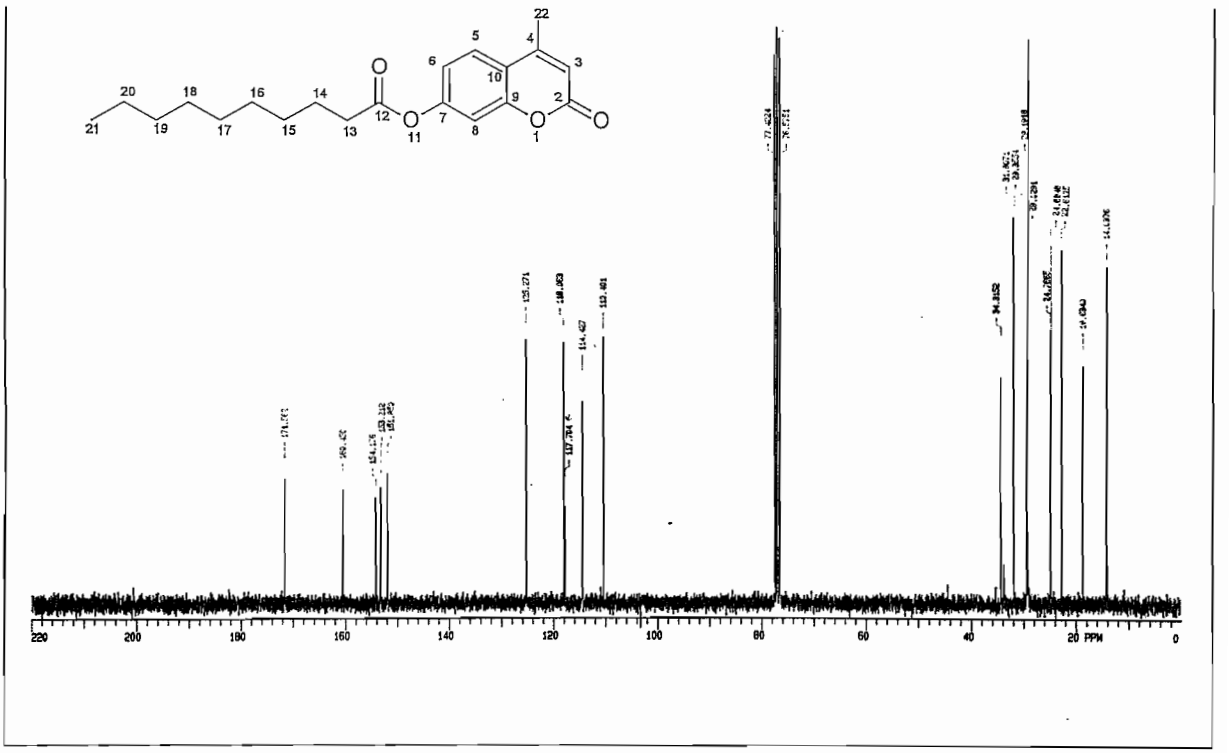

Spectrum 10

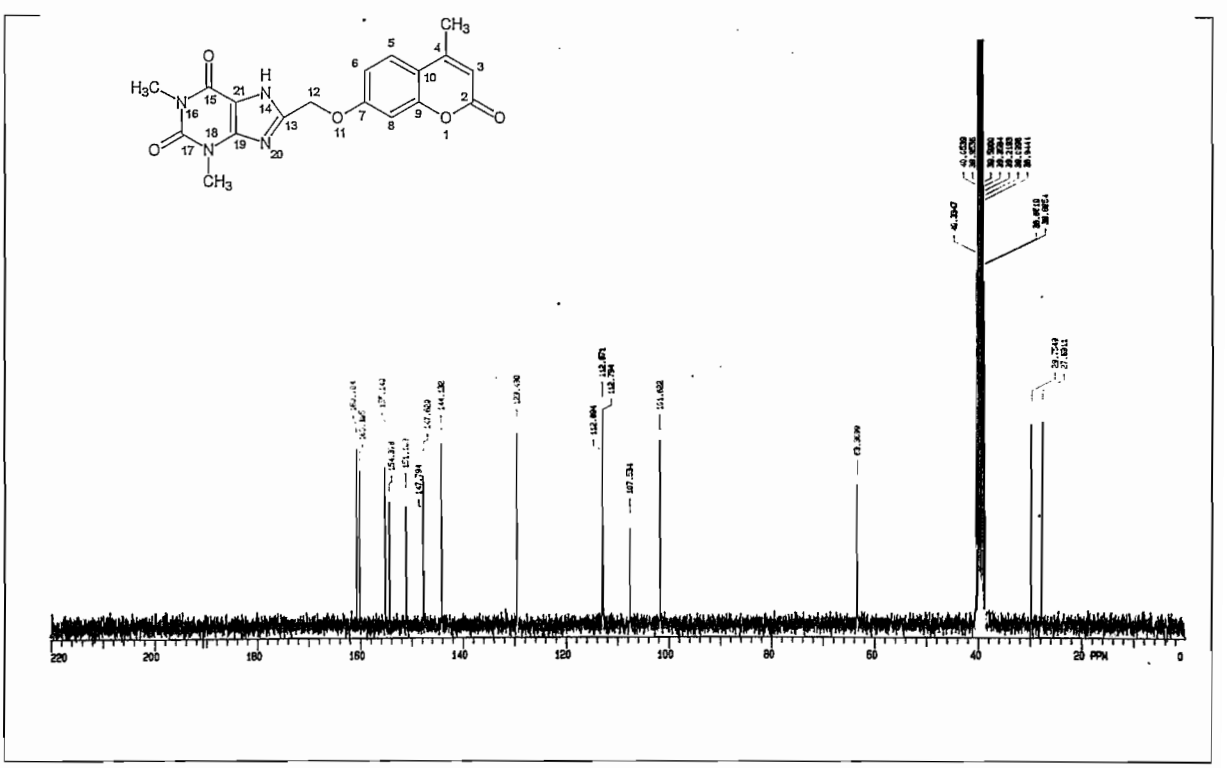

Spectrum 11

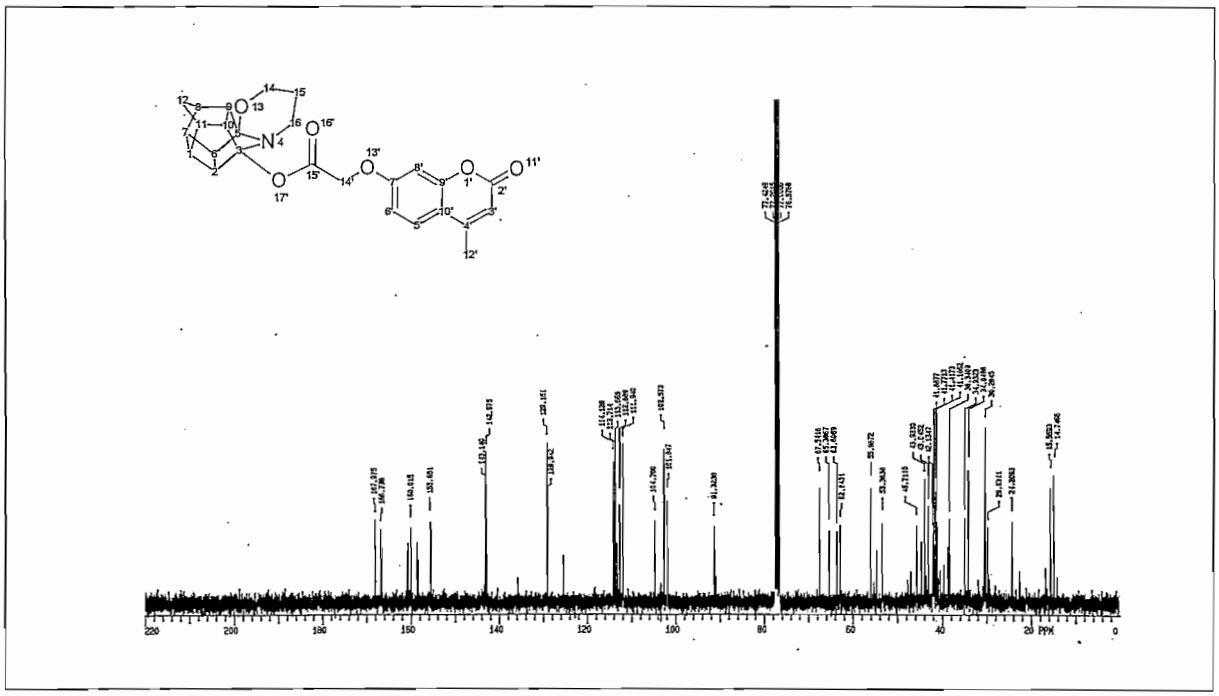

Spectrum 12

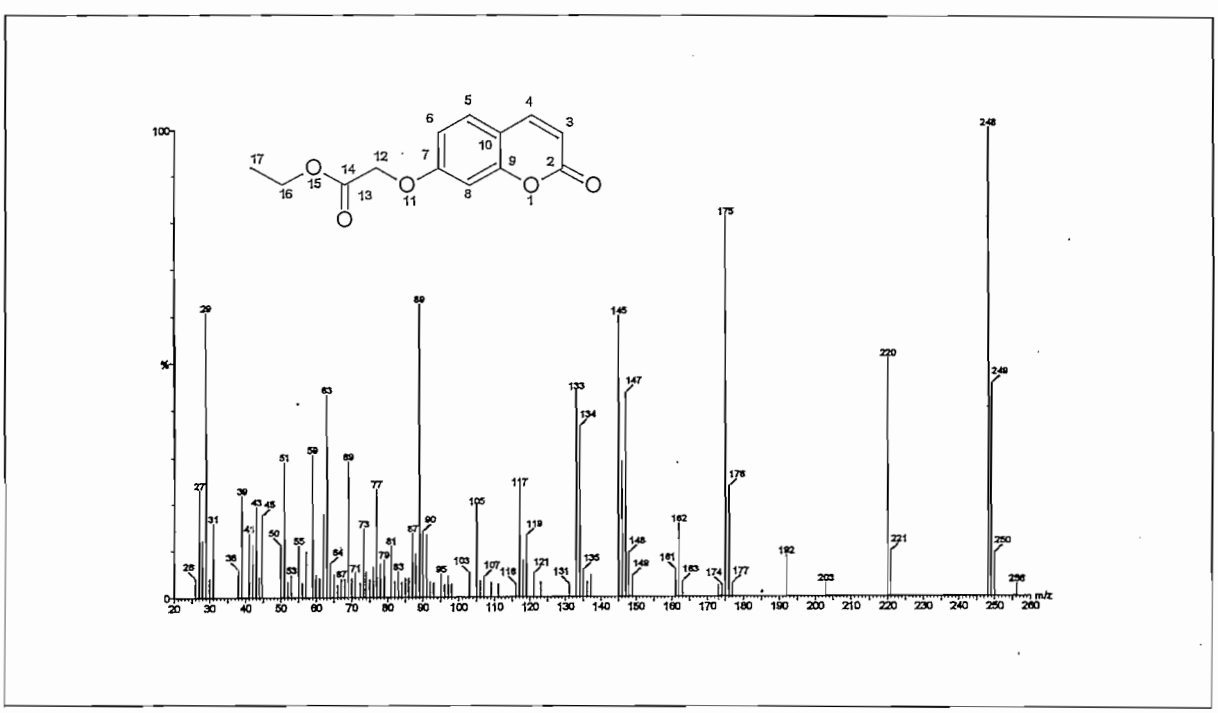

Spectrum 13

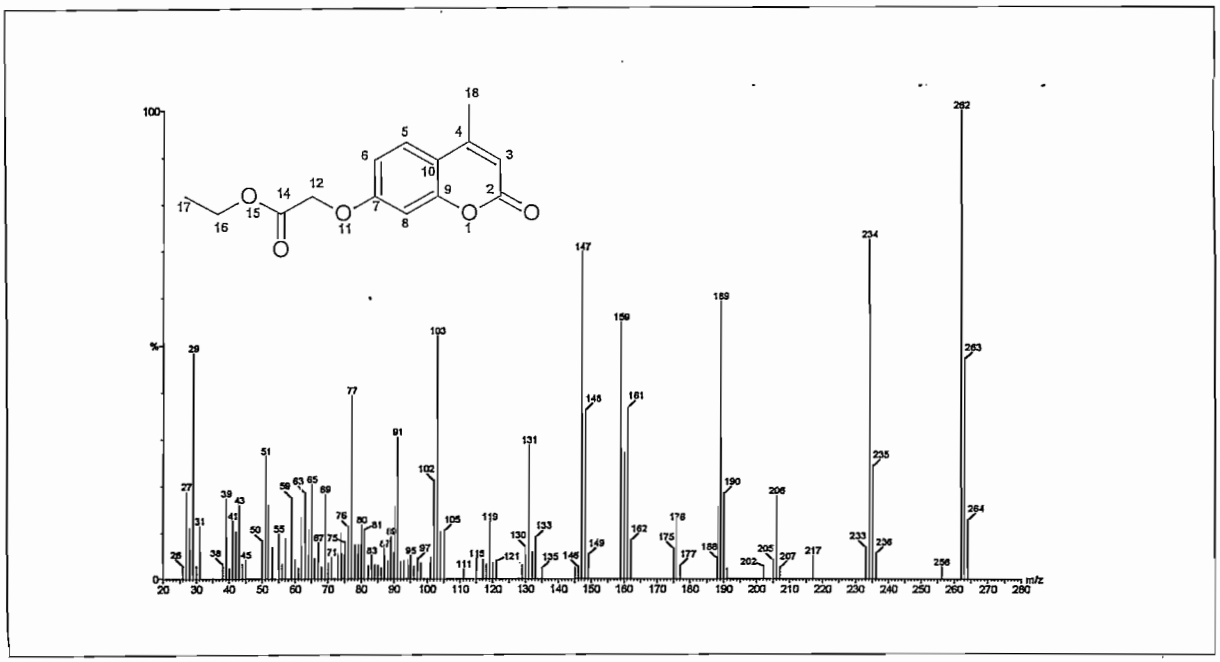

Spectrum 14

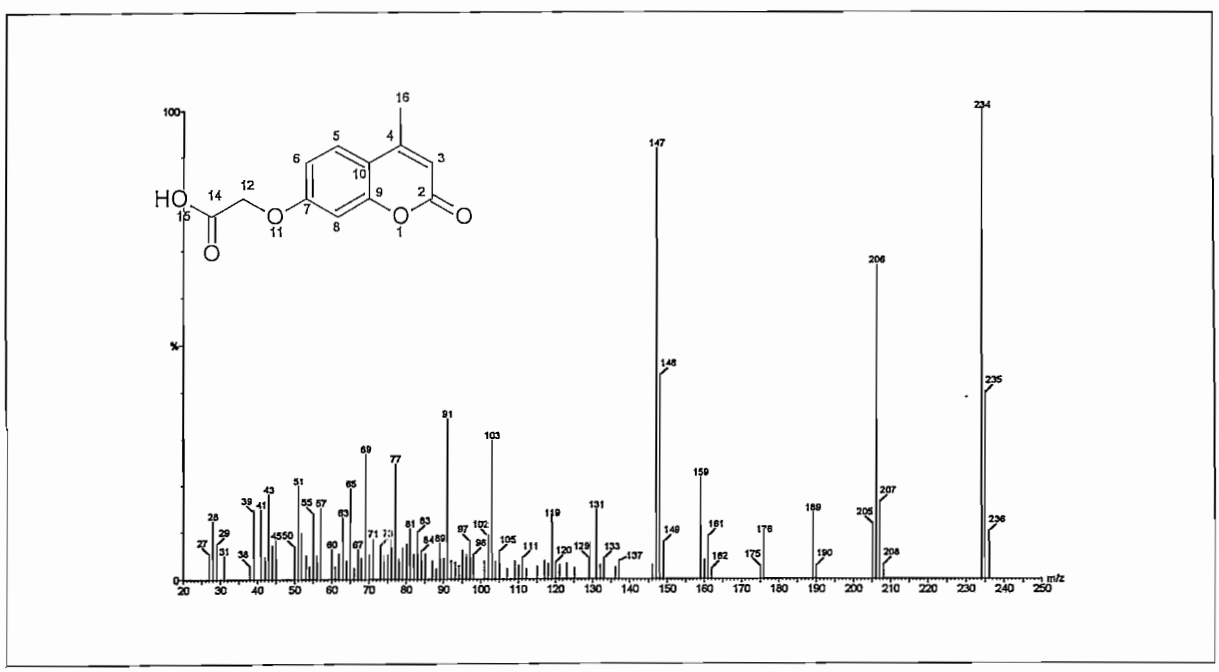

Spectrum 15

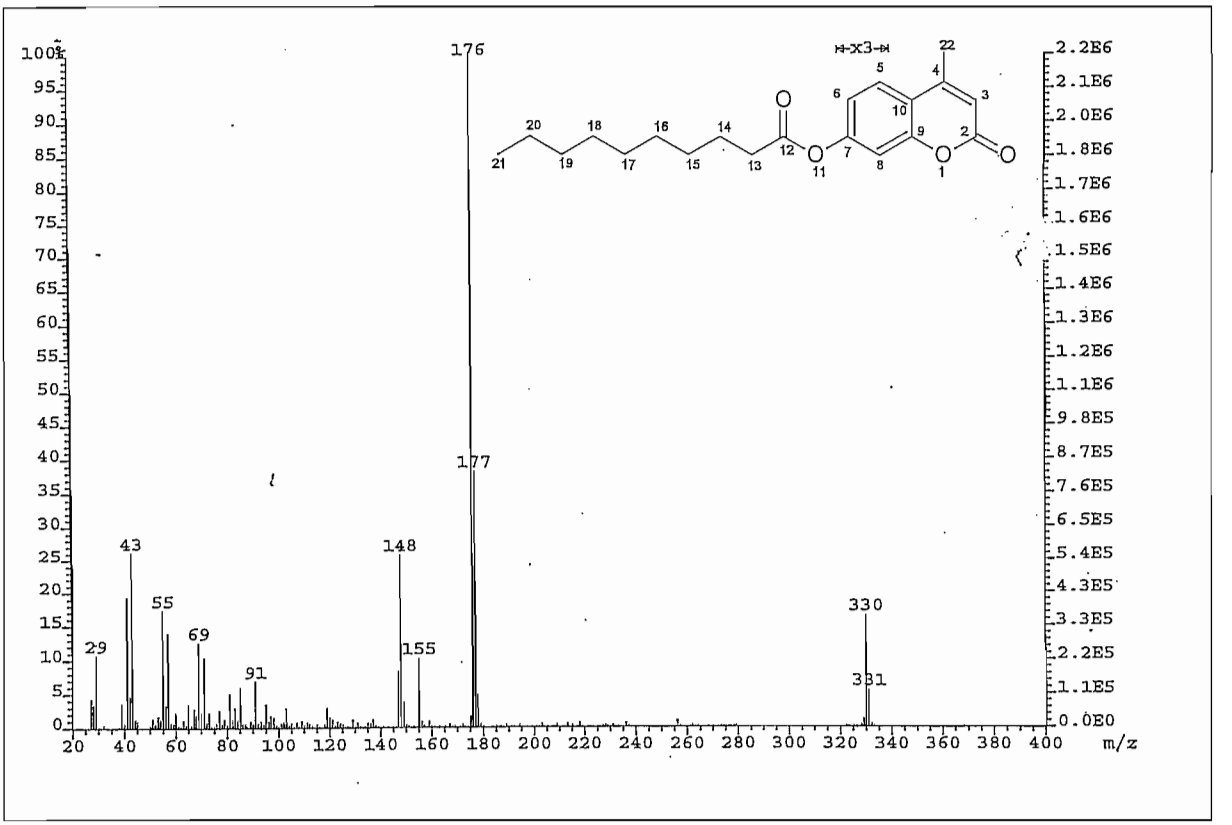

Spectrum 16

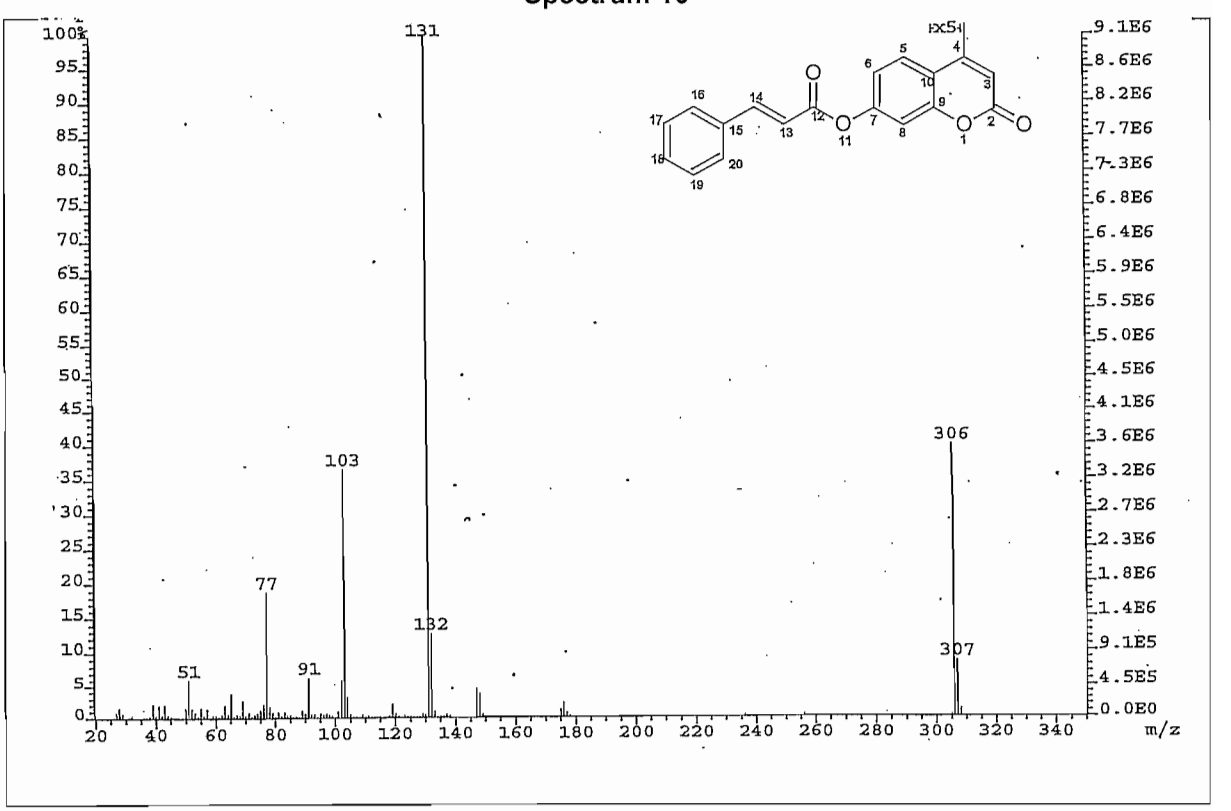

Spectrum 17

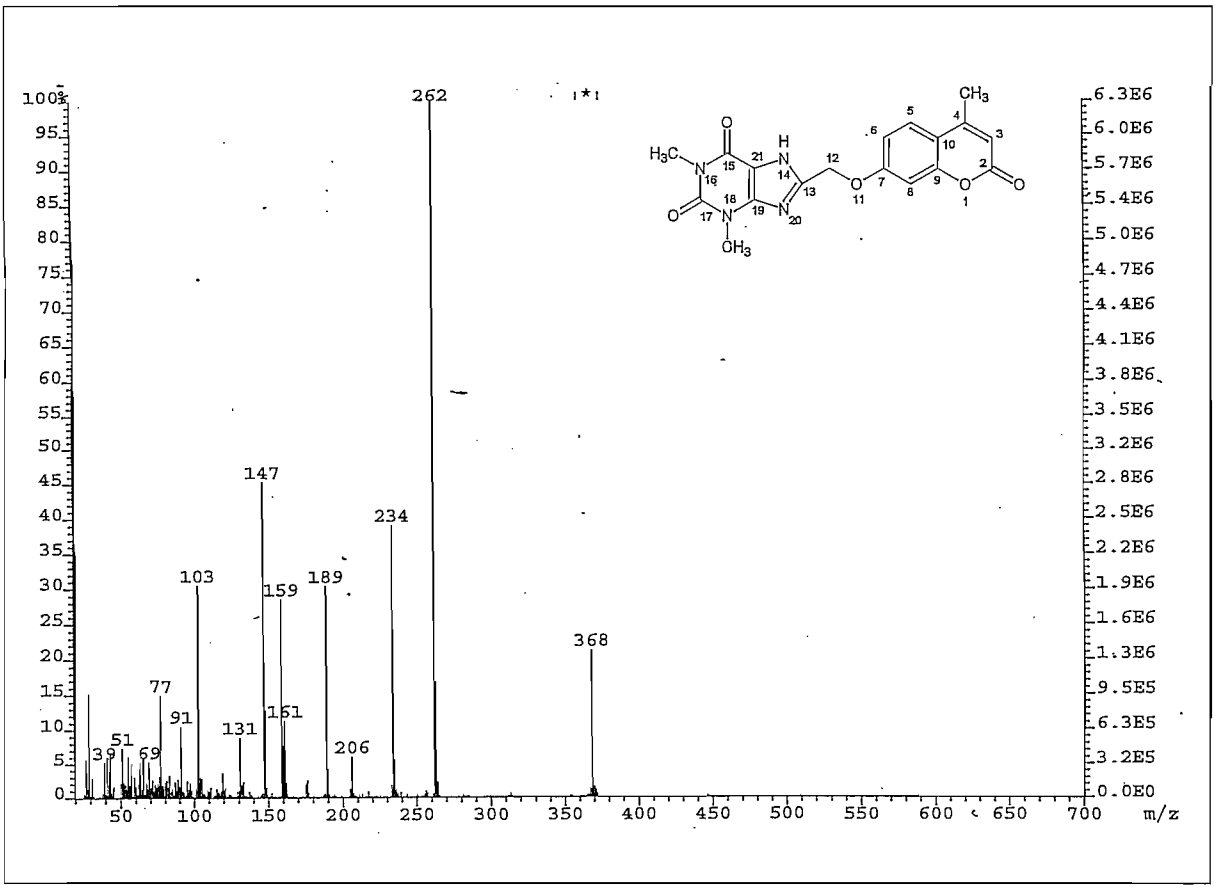

Spectrum 18

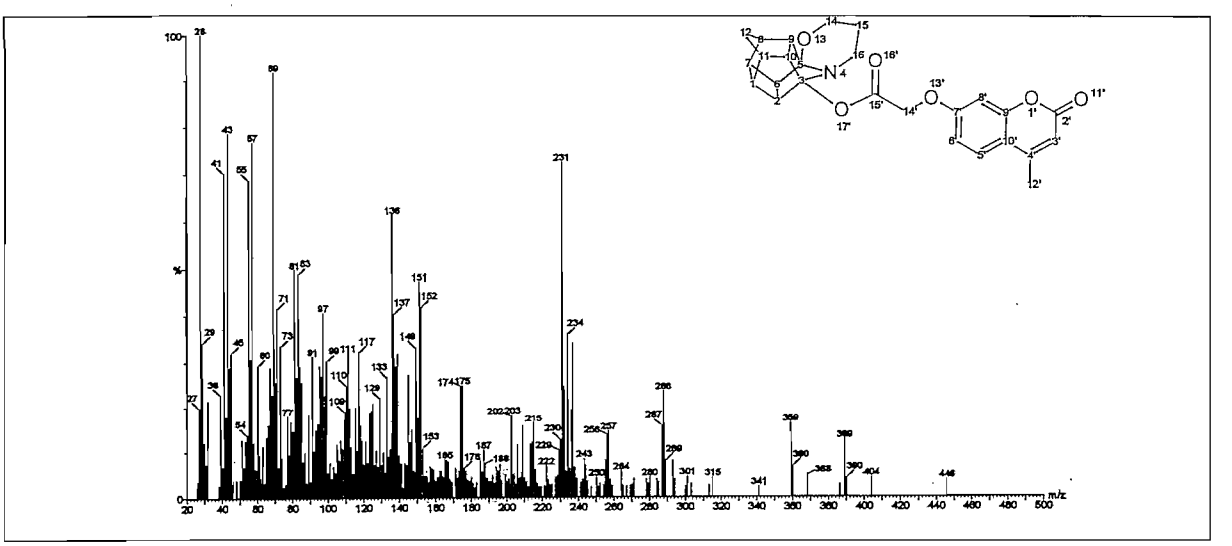

Spectrum 19